Photodynamic Antimicrobial Chemotherapy Activities of Modified Carbocyanine-Zinc Oxide Nanoparticle- and Nanoflower-based Nanoconjugates

By

MPHO GIFT KHORAE

Dissertation submitted in accordance with the requirements for the degree of

MASTER OF SCIENCE

in the subject

CHEMISTRY

at the

UNIVERSITY OF SOUTH AFRICA

SUPERVISOR   : Dr. Kutloano Edward Sekhosana

CO-SUPERVISOR   : Professor Titus Alfred Makudali Msagati

                               : Dr. Unathi Thembakazi Sidwaba

February 2023

DECLARATIONS

Name: Mpho Gift Khorae

Student number: 67152252

Degree: Master of Science in Chemistry

The exact wording of the title of the dissertation as appearing on the electronic copy submitted for examination:

Photodynamic Antimicrobial Chemotherapy Activities of Modified Carbocyanine-Zinc Oxide Nanoparticle- and Nanoflower-based Nanoconjugates

I declare that the above dissertation is my own work and that all the sources that I have used or quoted have been indicated and acknowledged by means of complete references.

I further declare that I submitted the dissertation to originality-checking software and that it falls within the accepted requirements for originality.

I further declare that I have not previously submitted this work, or part of it, for examination at Unisa for another qualification or at any other higher education institution.

(The dissertation will not be examined unless this statement has been submitted.)

_____   17/02/2023

SIGNATURE   DATE

DEDICATIONS

This work is dedicated to my parents, Mr O.A. Khorae and Mrs N.L. Khorae; my siblings, Lebogang Khorae and Kelegadi Khorae; my supportive partner; and my late loved one.

ACKNOWLEDGEMENTS

Psalm 32:8 The LORD says, "I will guide you along the best pathway for your life. I will advise you and watch over you."

First and foremost, I want to thank my supervisor, Dr. K. E. Sekhosana, for his important guidance, unwavering support, and patience during my Master's studies. His vast knowledge and expertise have inspired me in both my academic research and my daily life. Second, I'd like to express my appreciation to my co-supervisors, Prof. T. A. M Msagati and Dr U. T. Sidwaba (R.I.P), for their contributions to this project; without them, this work would be incomplete.

I would also like to thank Dr M. E. Managa for her great help in taking me through part of my project, and for that, I will always be grateful. Also, I want to thank the laboratory technicians in particular.

I would like to send special gratitude to my late brother, a laboratory technician, and an advisor, Mr Kagiso Mokalane. May God be with you and your soul as it continues to rest in peace. I would also like to express my deepest appreciation to all those who supported me through this journey.

My deepest gratitude goes to my parents and my spouse. It would have been difficult for me to finish my studies without their wonderful understanding and encouragement throughout the last few years.

PUBLICATIONS

1. Mpho Gift Khorae[a], Muthumuni Managa[a], Tshifhiwa Tambani[b], Tracy Masebe[b], Titus Alfred Makudali Msagati [a], Kutloano Edward Sekhosana[a]. Photodynamic Antimicrobial Activities of ZnO Nanoparticle- and Nanoflower-Carbocyanine Nanoconjugates against *E. coli*. (**Sent for publication in the journal: Materials Chemistry and Physics**)

ABSTRACT

The continuously rising cases of antibiotic resistance and pathogenic bacterial mutations pose a serious medical problem. Microorganisms are ubiquitous because they can adapt to conditions in any environment. They can colonize all types of environments, including water, air, soils, and the bodies of plants and animals. When pathogenic microorganisms are prevalent in such situations, they are harmful because they promote degeneration and degradation of the matrix, which harms the ecosystem and humans by harming individual health. This calls for environmental decontamination efforts to protect the ecology and human health.

Several chemical and physical methods have been applied for the treatment of different environments where pathogenic microbes have been contaminated. The use of physical methods includes the employment of heat and filtrations, whereas chemical methods include chlorination, antibiotics and photocatalyst. Although these methods have been used more often, they are associated with limitations, including a lack of effectiveness that contributes to the problem of the development of antimicrobial-resistant strains. Furthermore, using physical agents does not eradicate all the microbes since some are suitably adapted to extreme conditions through mutation phenomena.

Due to these drawbacks, scientists and researchers have embarked on research to find alternative methods and approaches that can eliminate the microbes while avoiding mechanisms that can develop resistance within the strains.

However, photodynamic antimicrobial chemotherapy (PACT) has been reported to be an attractive alternative method that can be employed to counter the limitations of the classical approaches for dealing with microbial contaminants in the environment. Among the pathogenic bacteria are Gram-negative bacteria. These Gram-negative bacteria are less likely to be denatured by chemical treatment because of the intricate construction of their bacterial cell membrane, it functions as an efficient barrier to the penetration of many photosensitizing compounds like dyes. For them to be effectively

Abstract

denatured, only cationic dyes can cause effective photo-induced inactivation of Gram-negative bacteria. In addition, nanostructures have been used as drug delivery platforms for photodynamic therapy (PDT) and as strategies to improve photosensitizers' efficiency in producing reactive oxygen species (ROS) when exposed to light. Thus, in this dissertation, photodynamic antimicrobial chemotherapy has been employed to study the photodynamic antimicrobial chemotherapy activities of functionalized zinc oxide-based nanomaterials and nanoconjugates against *E. coli*.

This dissertation, thus, reports on the fabrication of zinc oxide nanoparticles (ZnO-NPs) and nanoflowers (ZnO-NFs), their functionalized forms (GSH-ZnO-NPs and GSH-ZnO-NFs), as well as the modified carbocyanine (SHBS-IR-791 iodide). It also reports on the conjugations of GSH-ZnO-NPs and GSH-ZnO-NFs with SHBS-IR-791 iodide, labelled as follows: GSH-ZnO-NPs-SHBS-IR-791 iodide and GSH-ZnO-NFs-SHBS-IR-791 iodide conjugates. The analysis of the materials mentioned above using various instruments is also presented in this dissertation. The resulting GSH-ZnO-NPs, GSH-ZnO-NFs and SHBS-IR-791 iodide, as well as GSH-ZnO-NPs-SHBS-IR-791 iodide and GSH-ZnO-NFs-SHBS-IR-791 iodide conjugates, were used for PACT against *E. coli*. The PACT activities of the as-prepared materials show that the ranking of photo-inactivation depends on the attentiveness of the complex and the presence of light. The results show that GSH-ZnO-NFs-SHBS-IR-791 iodide has higher phototoxicity against *E. coli* than the other complex, with the trend observed as follows: GSH-ZnO-NFs-SHBS-IR-791 iodide > ZnO-NPs-SHBS-IR-791 iodide > SHBS-IR-791-iodide > GSH-ZnO-NFs> GSH-ZnO-NPs.

TABLE OF CONTENTS

LIST OF ACCRONYMS AND ABBREVIATIONS

- *E.coli*   *Escherichia Coli*
- *MNEC*   *Meningitis-Associated E. Coli*
- *UPEC*   *Uropathogenic E. Coli*
- *EHEC*   *Enterohaemorrhagic E. Coli*
- TDP   Thermal Death Point
- TDT   Thermal Death Time
- HEPA   High-Efficiency Particulate Air
- GAC   Granular Activated Carbon
- RO   Reverse Osmosis
- AMR   Antimicrobial Resistance
- PACT   Photodynamic Antimicrobial Chemotherapy
- PDT   Photodynamic Therapy
- PSs   Photosensitizers
- ROS   Reactive Oxygen Species
- Cys   Carbocyanines
- Cy   Carbocyanine
- NMs   Nanomaterials
- PS-NM   Photosensitizer-Nanomaterial Nanoconjugate
- SOC   Spin-Orbit Coupling
- ZnO   Zinc Oxide
- ZnO-NMs   Zinc Oxide Nanomaterials
- ZnO-NPs   Zinc Oxide Nanoparticles
- ZnO-NFs   Zinc Oxide Nanoflowers
- ISC   Intersystem Crossing
- P   Phosphorescence
- LPS   Lipopolysaccharide
- EDTA   Ethylenediaminetetraacetic Acid
- ICG   Indocyanine Green
- MC540   Merocyanine 540
- PNA   Peptide Nucleic Acid

List of accronyms and abbreviations

- MONs — Metal Oxides
- GSH — Glutathione
- DMSO — Dimethyl Sulfoxide
- DMF — Dimethylformamide
- A/Abs — Absorbance
- iNanoWS — Institution for Nanotechnology and Water Sustainability
- IR — Infrared
- UV-Vis — Ultraviolet/Visible
- XRD — X-Ray Diffraction
- FT-IR — Fourier-Transform Infrared
- PSD — Position-Sensitive Detector
- SEM — Scanning Electron Microscope
- EDX — Energy Dispersive X-Ray
- ISC — Inter system crossing
- SHBS — Sodium salt, 4-hydroxybenzenesulfonic acid

LIST OF FIGURES

List of figures

LIST OF TABLES

LIST OF SCHEMES

LIST OF SYMBOLS

- $^3O_2$ Triplet oxygen molecule
- S_0 initial/ ground state
- S_1 singlet excited state
- $*T_1$ triplet excited state
- P phosphorescence
- $^1O_2$ singlet oxygen
- O_2^- superoxide radical
- $^•OH$ hydroxyl radical

CHAPTER 1

1.   Background of the study

1.1.   Microorganisms

Microorganisms are acellular organisms that can only be seen through microscopes (1,2). Various microorganisms include fungi, algae, protozoa, archaea, and bacteria. Some microbes, such as certain species and strains of bacteria, are gaining attention as they play essential roles in daily human life; for example, *Lactobacillus acidophilus* is beneficial in biological processes such as digestion, neutralizing toxins, and in the defence against infections by invading pathogens (3,4).

Bacteria are grouped based on various criteria (5). Among the criteria for classifying bacteria include their shapes, such as *streptococcus* and other spherical bacteria are classified as cocci, while rod-shaped ones are classified as bacilli, and an example of rod-shaped bacteria is *Escherichia coli (E. coli)*. A spiral shape characterises another bacterial type; thus, they are classified as spirillas, for example, *Campylobacter jejuni* (6,7). Another way of classifying the bacteria is by grouping them based on their reaction to Gram staining, with some classified as Gram-negative while others as Gram-positive depending on the reaction to the Gram stain (8,9).

1.1.1.   The Gram-positive and Gram-negative bacteria

The chemical and physical features of bacteria's cell walls determine their Gram classification. Gram-positive bacteria have thicker cell walls than Gram-negative bacteria due to the presence of several peptidoglycan layers (approximately 40 layers), whereas Gram-negative bacteria have a single peptidoglycan layer, as shown in **Figure 1.1**. An example of Gram-negative bacteria includes *E. coli,* while an example of Gram-positive bacteria includes *Staphylococcus aureus.*
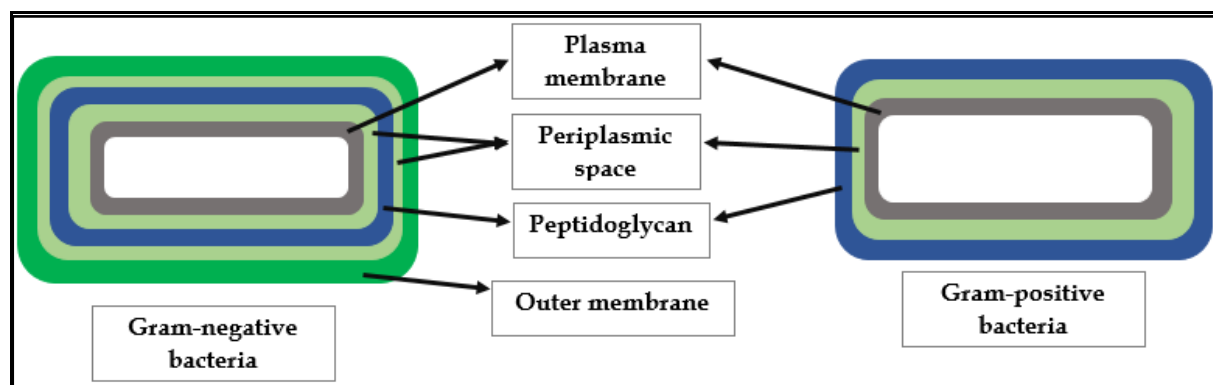
Figure 1.1: Gram-negative and Gram-positive bacterial cell envelope (10).

Moreover, the Gram-negative and Gram-positive can be differentiated by colour using a microscope (8,9,11,12). **Table 1.1** depicts the difference between the Gram-negative bacteria and the Gram-positive bacteria.

Table 1.1: The difference between Gram-negative and Gram-positive bacteria

Gram-negative-bacteria	Gram-positive bacteria
Outer membrane present	No outer membrane
Double Plasmic space present	Single Plasmic space
They appear to be pink under the microscope after the Gram stain	They appear to be purple under the microscope after the Gram stain
They are less susceptible to anionic detergents	They are more susceptible to anionic detergents

1.1.1.1.   The pathogenicity of bacteria

Despite the many beneficial roles bacteria play in human life, some species and/or strains of bacteria are very pathogenic. Most pathogenic bacteria are capable of causing illnesses, diseases and infections through air, food and water contamination (13,14). In recent years, there has been a global increase in the incidence of illnesses caused by Gram-negative bacteria, with diseases caused by these organisms frequently being more widespread than Gram-positive infections (15).

The diseases and infections caused by Gram-negative bacteria include bloodstream infections, wound or surgical site infections, pneumonia, and meningitis in healthcare

settings (16). *E. coli* is one of the Gram-negative bacteria that has become a great concern in health premises (17). Thus, it is important to develop systems that can help to eradicate these pathogenic microbes.

The pathogenicity of *Escherichia coli* (*E. coli*)

E. coli is a member of the Enterobacteriaceae family, a widespread part of the normal intestinal bacterial microflora in humans, and is thought to be a harmless commensal in the caecum and colon mucous layer. This bacteria can also live in a variety of biological niches, including abiotic ones, making it a very adaptable species. Although *E. coli* persists as a harmless commensal, some of its strains have evolved into pathogenic strains capable of causing different human diseases (17–19).

The pathotype of *E. coli* can be classified based on the clinical manifestation of diseases such as *meningitis-associated E. coli (MNEC),* which is known to be the cause of meningitis, particularly during the neonatal period. *Uropathogenic E. coli (UPEC)* is the primary cause of urinary tract infections (UTIs), while *Enterohaemorrhagic E. coli (EHEC)* is one of the *E. coli* strains that cause severe intestinal infections in humans (19).

Since the spread of reports that microorganisms have the potential of becoming pathogenic, there has been a campaign the awareness that controlling the bacteria will help to reduce and prevent unwanted microbial contamination, the transmission of diseases, and infection (20). In addition to the awareness campaign, scientists and researchers have developed several methods to control infectious bacteria, especially Gram-negative bacteria, to safeguard human health (21).

1.2. Strengths and weaknesses of methods to treat a bacteria-contaminated environment

The methods developed for the treatment of environments contaminated by pathogenic bacteria can be separated into two different types of groups, namely physical and chemical-based methods. Physical-based methods refer to the methods

used for microbial control that does not have specificity for controlling microbes and include the employment of temperature (22), filtration (23), and radiation (24). On the other hand, chemical-based methods imply the employment of disinfectants (25), antibiotics (26), and chemotherapeutic antimicrobial chemicals (27).

1.2.1. Physical methods

For the past decades, humans have been applying physical methods to control and minimize microbial contamination, and these methods have been applied in settings such as laboratory experiments, water treatments, and food preservation. There is a strong belief that applying physical methods kills microbial cells by changing the membrane permeability and disrupting their membranes (24). Section **1.2.1.1** presents the strength of physical methods.

1.2.1.1. Strength of the physical methods

Physical methods, such as temperature, lead to the damage of microbial proteins and nucleic acids by denaturation, degradation, or chemical modification (28). Temperature, filtration, and desiccation (drying) are still used as today's most common physical methods (29).

a. Temperature

Employing high temperatures is one of the oldest and most common forms of microbial control, such as boiling water, cooking, and direct heat. These methods lead to the alteration of microbial membranes and the denaturation of their proteins. Higher temperatures have been demonstrated and reported to indicate that the thermal death point (TDP) of microbes is low and that different microbial species respond differently to temperature, such as thermophiles, which are high-temperature tolerant microbes (30,31). Also, it has been mentioned that the thermal death time (TDT) is determined by the period of microbial exposure to the given

temperature (30). Moreover, applying temperature, such as direct heat, is one of the most used laboratory sterilisation methods.

In the same way, applying high temperatures is effective, and similarly, employing lower temperatures, such as refrigerators, has also been reported to be effective. Several studies have reported that applying lower temperatures inhibits microbial metabolism and delays their growth (32,33). This method is applied in households, laboratories, and health premises. In places such as laboratories, this method is used when culturing bacteria and medical specimens, which are normally frozen at an ultra-low temperature of up to -10 °C degrees Celsius for long-term storage or transportation. **Figure 1.2** presents the application of both high and lower temperatures (22,29,34–36).
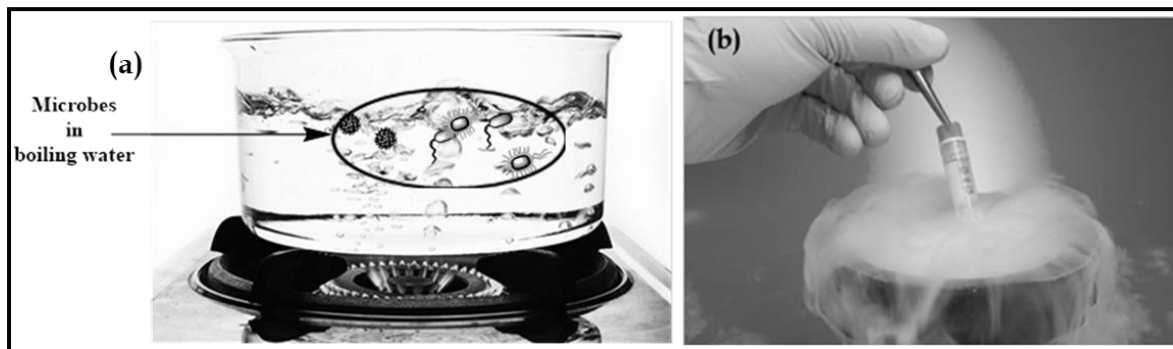
Figure 1.2: The application of both high and lower temperatures for microbial control. **(a)** Illustration of the application of high-temperature and **(b)** presentation of the application of lower temperature (29).

b. Filtration and desiccations

Filtration is among the physical methods that separate microbes from samples. This method is mostly applied in water treatment sites, and airborne prevention through high-efficiency particulate air (HEPA) filters with effective pore sizes of 0.3 µm (37,38). The pores are reported to be small enough to capture and trap bacterial cells and many viruses. HEPA is used mostly in clinical settings, laboratories, vacuum cleaners, and aeroplanes (29).

On the other hand, sand and soil have been employed as particulate entities to separate bacteria in water treatment. The current development of platforms such as sediment filtration, activated carbon block (ACB) filtration, granular activated carbon (GAC) filtration, reverse osmosis (RO) filtration, etc, is attracting more interest (39–41). **Figure 1.3** presents HEPA and sediment filtration as two of the filtration methods that are mostly applied. This method is still considered among the most effective and is still being researched; most reports state that filtration is effective and help reduce pathogenic microbes (42).
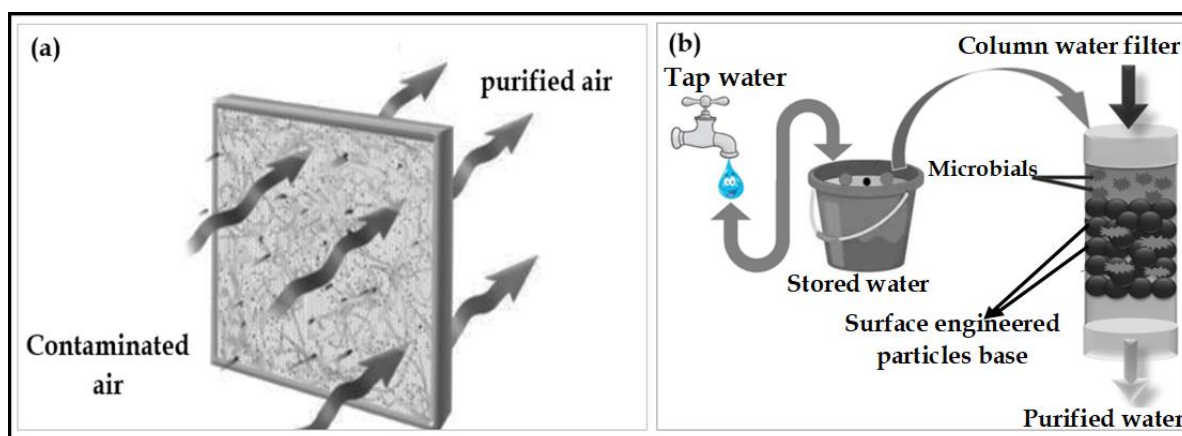
Figure 1.3: The application of both air and water filtration for microbial control. **(a)** Illustration of the application of HEMA for air filtration (b) illustration of sedimentation filtration for water treatment (29).

Also, desiccation is one of the well-known and often utilized physical processes, particularly in biology and ecology. This method involves drying out the microorganisms to inhibit their growth and multiplication. This method involves drying out the microorganisms to inhibit their growth and multiplication (43). Other businesses, such as pharmaceutical corporations, are using desiccation in the form of freeze-drying instruments to extend the shelf life of items such as vaccines and other injectables (44).

1.2.1.2. Shortcomings of physical methods

Although the above-mentioned types of physical methods have been employed up to this date, there are a few reservations about them, such as temperature, filtration, and desiccation. Few reports have presented the shortcomings of physical methods, such as the lack of microbial eradication.

a. Temperature

A few studies have criticized the use of warm temperatures, such as boiling water, to destroy endospores, claiming that it is less effective since endospores may survive the temperature of boiling water. Moreover, the water will evaporate if it is cooked for an extended period (45). In addition, lower temperatures, such as the use of refrigerators, have also been criticized for failing to denature bacteria such as psychrophiles, which prefer and tolerate cold temperatures (29).

b. Filtrations and desiccations

The effectiveness of filtration and desiccation has also been questioned. Some single-celled microorganisms, such as bacteria, are too small to pass through some filters; thus, filtration does not completely remove bacteria but rather reduces their numbers because some bacteria pass through the filter. (46).

On the other hand, as desiccation is recognized as one of the most often utilized physical processes, it does not provide sterilization or eliminate microbials. It merely keeps them from multiplying and growing. Bacteria such as Escherichia coli (*E. coli*) can survive for extended periods in desiccating and osmotically difficult settings, particularly sterile faces (44). Desiccation does not eradicate all the microbes and their endospores. Thus, favourable conditions can resume microbial growth (29).

1.2.2. Chemical-based methods

Just as with the physical methods, some methods are classified as chemical-based methods and are used as disinfectants or antiseptics. Unlike the physical method, chemical-based methods are chosen based on the type of microbes being targeted.

1.2.2.1. Strength of chemical methods

The use of chemical methods is mostly in the laboratories and clinical premises. They are also applied in households. The application of chemical methods such as disinfectants has been favored because of their safety for the environment, animals, and humans, their expense, and their ease of use (47). Disinfectants are chemicals extensively used for microbial control in hospitals, laboratories, and other healthcare settings for topical and hard surface applications (48,49). Disinfectants used frequently include phenols, alcohols, halogens, and heavy metals, which include Hg and Ag metals (42). These agents are mostly used for cleaning the surface areas of operation wounds and different types of equipment (25,50). Some of the most applied chemotherapeutic agents are antimicrobials, such as antibiotics (51).

a. Antibiotics

Antibiotics are one of the chemotherapeutic agents under the chemical method. Antibiotics were first discovered in 1928 by the Scottish bacteriologist Alexander Fleming at St. Mary's Hospital laboratory. Alexander Fleming noticed that a germ-free zone formed in one of the Petri dishes containing the bacterium *Staphylococcus aureus*, which led to the conclusion that mould must produce an antibacterial agent since there was inhibition of the *staphylococci* growth (27,52). Later, Alexander Fleming named the form penicillin. After the test and the trial, pure penicillin was produced in America, and the era of antibiotics commenced in 1945 (27,53). Since then, several books and articles have been published about the discovery of penicillin and antibiotics, which have made ground-breaking progress in the history of microbial treatment and medicine. This discovery transformed the world by making earlier incurable illnesses and infections treatable and allowing medical procedures such as

operations and chemotherapy to be performed safely (26,27,51,53,54). Antibiotics were then used to treat or prevent some types of bacterial infection including strep throat, urinary tract infections, and *E. coli* (55–57).

1.2.2.2. Shortcomings of antibiotics

Although the aforementioned chemical-based techniques, such as antibiotics, are still in use, there are some reservations about them, and a few publications have increased awareness about the issue of antibiotic use. The use of antibiotics is measured as a quick and easy technique for treating microbes and infections, but few reports reveal that their misapplication lead to the generate of widespread antimicrobial resistance (AMR) (58,59). Antimicrobial resistance occurs when microorganisms, such as bacteria, develop the ability to defeat or block the drug designed to kill or denature them (60). Antibiotic defence mechanisms can be developed through mutation.   The Gram-negative bacteria are the most concerning, as they have discovered a way to develop resistance to many antimicrobial drugs, resulting in the spread of AMR. *E. coli* is one of the bacteria that have been reported to have gained antibacterial resistance (61).

The concern about the development of AMR among Gram-negative bacteria stems from the difficulty of treating them, as they can also pass along genetic components that allow other bacteria to become drug-resistant. This pattern results in limited treatment options (51,58,59,62–64). With such a call, the emphasis is considerably more on the strategy that promises to reduce the drug-resistant epidemic. Considering the rapid evolution of pathogens and the variety of pathogens encountered, photodynamic antimicrobial chemotherapy (PACT) has received much attention from researchers as a promising alternative method (65,66).

1.2.3. Photodynamic antimicrobial chemotherapy (PACT)

Recently, the light-dependent method known as photodynamic antimicrobial chemotherapy (PACT) has been developed and is favoured due to its advantages and

promises for treating microbes, such as antimicrobial-resistant species. This method utilizes oxygen, light at a specific wavelength, and photosensitizing agents (66–68). PACT has been applied in treating infections such as gingivitis, periodontitis, and root canal biofilm infections (69,70). Based on the results obtained from the treatment mentioned above, this method has been found to provide numerous advantages more than other chemotherapeutics with less chances of emerging resistance.

1.2.4. Photosensitizers (PSs) applied in PACT

Photosensitizers (PSs) are light-absorbing molecules that change the cause of the photochemical reaction; they generate reactive oxygen species when exposed to a specific wavelength of light. Several molecules have been used as photosensitizers (PSs) for treating microbes such as bacteria (71). Ideal molecules should have characteristics that include a strong absorption band, substantial triplet quantum yield, producing Reactive Oxygen Species (ROS), no dark toxicity, ideal solubility, and killing microorganisms sufficiently without affecting the surrounding environment. PSs should also have high stability under storage conditions (72–74). Compounds with tricyclic, heterocyclic, or porphyrin-like ring structures, such as phthalocyanines, carbocyanines (Cys), and porphyrins, have been verified to reach a triplet state and result in good production of ROS, which plays a key role in destroying a wide spectrum of pathogens. (75,76).

The results obtained from the PACT studies that have been conducted using phthalocyanine and carbocyanine dyes as PS agents against the bacterial treatment show a sign of promise that the molecules have the required properties. However, some shortcomings still exist. The shortcomings that are experienced with the currently used PSs include the formation of low triplet state quantum yields, low generation of ROS, and target specificity (73). To address these issues, PS molecules have been combined with nanomaterials (NMs) to construct nanoconjugates for PACT (77,78).

1.2.4.1.   **Metal nanomaterials and their possible use together with PACT**

Nanomaterials are known as the cornerstone of Science. They play the most significant role in the medical field, such as in drug delivery. The most interesting properties of nanomaterials include their smaller size with large surface area-to-volume ratio, bio-detection of pathogens, detection of proteins, and strategies to enhance the efficiency of photosensitizers in generating ROS upon irradiation (79,80). Nanomaterials such as metal nanomaterials are reported to be potential carriers of photosensitizers due to their advantages, which include structural stability, well-organized delivery to pointed cells, high singlet oxygen, and enhance the photosensitivity. Moreover, metal nanomaterials possess essential properties to upgrade the effectiveness of photosensitizers by preventing aggregation even at high concentrations, providing selective antimicrobial activity at the local-aimed sites, and increasing bacterial cell wall permeability (81,82). Different nanostructured materials, such as inorganic NMs, micelles, and liposomes, have been used to conjugate with PSs (79,83).

The association of NMs with PSs to form photosensitizer-nanomaterial nanoconjugate (PS-NM) has been done to enhance the properties of the currently used PSs, such as their solubility, triplet state quantum yield, and production of ROS (79,80,84). Most of the used NMs are semiconductor nanomaterials composed of heavy metals, which promote the intersystem crossing (ISC) and result in a high triplet quantum yield through spin-orbit coupling (SOC) (85,86). The heavy atomic effect promotes the production of a high triplet state quantum yield by decreasing the fluorescence quantum yield (77,78).

1.3.   Summary of the Aim and Objectives of this Dissertation

1.3.1.   Aims of the study

This study focuses on designing the GSH-ZnO-NMs-SHBS-IR-791 iodide nanoconjugates using zinc oxide nanomaterials (ZnO-NMs) as drug delivery vehicles for modified carbocyanine (SHBS-IR-791 iodide). The designed nanoconjugates were

used as photodynamic antimicrobial chemotherapy-photosensitizer (PACT-PS) agents against *Escherichia coli* (*E. coli*) in the aquatic environment.

1.3.2. Objectives

To achieve the aim of the study, the following objectives were pursued:

- ⬜ To synthesis of zinc oxide nanomaterials (zinc oxide nanoparticles (ZnO-NPs) and zinc oxide nanoflowers (ZnO-NFs)).
- To functionalize as-synthesized ZnO-NPs and ZnO-NFs.
- To modify IR-780 iodide to SHBS-IR-791 iodide.
- To conjugate GSH-ZnO-NPs and GSH-ZnO-NFs with SHBS-IR-791 iodide.
- To Characterize all the prepared complexes
- To experimentally simulate the potential of as-prepared materials in PACT against *E. coli*.

Chapter 2

2.   Literature review

This chapter surveys the literature on the various treatment methods for pathogenic bacteria using the PACT method. This alternative microbial treatment method (PACT) has been given more attention due to its quality properties such as showing the effectiveness in the denaturation of microbes and enhancing performance such as increasing the capacity of denatured microbes.

2.1.   Photodynamic antimicrobial chemotherapy (PACT)

PACT refers to approaches that use non-toxic light-sensitive dyes as a photosensitizer (PS) in conjunction with visible light of the suitable wavelength from the power source to match the PS's absorption spectra in the presence of triplet state molecular oxygen ($^3O_2$) (10). The activated PS enters a triplet state, capable of reacting with $^3O_2$, resulting in the formation of reactive oxygen species (ROS) that will be responsible for denaturing the targeted microbe (87) (**Figure 2.1**). PACT has been classified as a great alternative method for microbial treatment due to its advantage of having broad-spectrum activity against Gram-negative bacteria, Gram-positive bacteria, yeast, and fungi, with no bacterial resistance being produced (88,89).
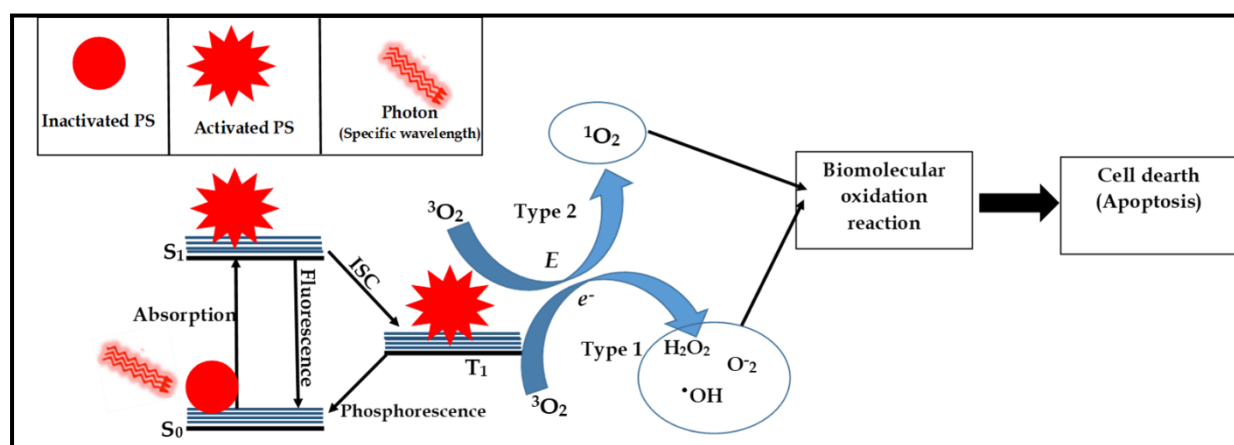
Figure 2.1: The photochemical mechanism operating in PACT (90).

2.1.1.   Background and working principle of the PACT method

The discovery of the photodynamic therapy (PDT) technique was made in 1897–1898 by Oscar Raab, who worked under the supervision of Hermann Von Tappeiner when studying the toxicity of acridine towards paramecia (91). Oscar Raab observed that *Paramecium* spp. protozoans were inhibited after staining with acridine orange and subsequent exposure to bright light. When Raab and the group further investigated the phenomena, they concluded that the toxicity of acridine orange against *Paramecia caudatum* depended on the light intensity (92,93). Further studies were conducted by von Tappeiner and Jodlbauer, who invented the term "photodynamische Wirkung", which translates as "photodynamic therapy" (PDT) after they had noticed that the inactivation requires the presence of oxygen. Since then, this technique has been clinically applied to treat various malignancies (93). In the year 1907, Alfred Bertheim and Paul Ehrlich applied the PDT technique to treat *syphilis* using arsphenamine, and it was then labelled as photodynamic antimicrobial chemotherapy (PACT) (94). The principles and mechanisms of PACT are similar to those of PDT.

Initially, PS is in the ground state (S_0), and when the light at a specific wavelength is applied, the PS will absorb the energy (hv) and undergo the electronic transition to the excited singlet state (S_1). When the PS is at the excited singlet state, it will relax to a longer-lived triplet excited state (*T_1) via intersystem crossing (**ISC**). **ISC** is a rapid process favoured by non-fluorescent PS molecules. Furthermore, the PS at the triplet state will either transfer energy or an electron to the triplet ground state molecular oxygen ($^3O_2$) through phosphorescence (**P**) relaxation, resulting in type I and or type II reactive oxygen species (**ROS**). These ROS include singlet oxygen ($^1O_2$), superoxide radical (O_2^-), hydroxyl radicals ($^\bullet OH$), and hydrogen peroxide (H_2O_2) (17).

In type I, an electron transfer from the triplet excited state PS, leads to the formation of O_2^-, $^\bullet OH$, and H_2O_2. In type II, an energy transfer from the triplet excited state PS to $^3O_2$ helps to convert it to $^1O_2$. Therefore, the generated ROS will then either directly kill the bacteria by producing oxidative damage to bio-compounds or indirectly by driving pathogen elimination through a variety of non-oxidative methods depending

on the localization of the excited PS in bacterial cell walls or lipid membranes, resulting in bacterial apoptosis. Consequently, the PS will return to its initial state (ground state) and restart the mechanical cycle as explained above. The PACT method has been tested in-vitro against antimicrobial-resistant bacteria, viruses, and protozoa and is more effective compared to the above-mentioned methods.

PACT has been used to treat pathogenic microbes and infections such as gingivitis, periodontitis, and canal biofilm. Moreover, the use of PACT in dentistry is increasing, primarily in periodontal and mucosal diseases, but also for other purposes, such as accelerating tooth movement (95). However, the emphasis of this research is on microscopic organisms.

2.1.2. Inactivation of Microorganisms using PACT

There is a persistent increase in AMR in bacteria, which makes them the main targeted microorganisms, particularly Gram-negative bacteria (96). Unlike Gram-positive bacteria, Gram-negative bacteria possess a single layer of peptidoglycan surrounded by an outer membrane composed of lipopolysaccharide (LPS), phospholipids, and unique components, as shown in **Figure 1.1** above (10).

Gram-negative bacteria, such as *E. coli*, consume an additional layer on their outside cells known as the outer membrane, which Gram-positive bacteria do not have.. The extra layer in Gram-negative bacteria leads to the highly negatively charged surface, making it difficult for the photosensitizers to penetrate the cell wall, while Gram-positive bacteria allow the easy penetration of the PS and readily undergo photo-inactivation (97). In the case of less photo-inactivation of PSs in Gram-negative bacteria, numerous neutral or anionic PSs are effective against Gram-negative bacteria when pre-conditioned with cationic agents such as ethylenediaminetetraacetic acid (EDTA) or $CaCl_2$. Also, more research has been conducted using positively charged PSs against Gram-negative bacteria (98). Photosensitizers are classified into three categories based on their charge. Neutral photosensitizers, positively charged photosensitizers (99), and negatively charged photosensitizers . Photosensitizers with

cationic charges are referred to as positively charged photosensitizers; photosensitizers with anionic charges are referred to as negatively charged photosensitizers; and photosensitizers with no charged ions are referred to as neutral photosensitizers (99,100). Examples of photosensitizers include phthalocyanines, cyanines, phenothiazines, acridines and others. To this date, several PSs, along with Acridines, cyanines, phthalocyanines, chlorins, and phenothiazines, have been investigated for usage as PACT PS agents (101).

2.1.3. The photosensitizers (PSs) applied in PACT

In PACT, porphyrins and other tetrapyrrole compounds including as chlorins, phthalocyanines (Pcs), and carbocyanines (Cys), are desirable photosensitizers in PACT (80,102,103). They are exceptional ROS generators due to their aptitude to engross strongly in the UV-Vis-IR region of the electromagnetic spectrum near the IR region and generate a significant triplet quantum yield (87). Section **2.1.3.1** below will briefly overview carbocyanine and its potential as a photosensitizer.

2.1.3.1.   Carbocyanine dyes (Cys)

Carbocyanines (Cys) is the cyanine dye that contain two nitrogen-containing heterocyclic entities joined by an alkene group (**Figure 2.2**). The number of carbon atoms in the molecular structure and the nature of the end groups containing nitrogen atoms can vary based on the molecule of interest (104).
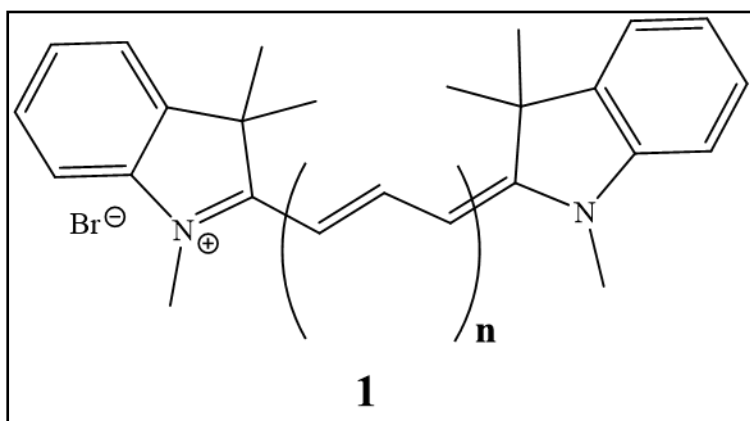
Figure 2.2: General structure of carbocyanine dyes **1**.

Carbocyanine was first synthesized by C. H. G. Williams in 1856 through heating quinolone with N-amyl lepidinium iodide in the presence of ammonia (105). The resulting compound produced had a "magnificent blue colour," so the general carbocyanine dye name was derived from the Latin word *cyanos*, which means "blue" (104–106). Carbocyanine molecules are referred to as dyes because they have extremely strong absorption bands in the visible region of the electromagnetic radiation spectrum, as illustrated in **Figure 2.4.** They have narrow absorption bands and high extinction coefficients. The position (wavelength) and strength (absorption coefficient) of the carbocyanines are dependent on the length of the carbon chain (number of methine groups) between the nitrogen atoms and the changes in the heterocyclic unit of the structure. Increasing the number of carbon atoms in the polymethine chain that connects the heterocyclic units or expanding the aromatic parts of the terminal heterocyclic units may result in red shifting towards longer wavelengths. The addition of two carbon atoms to the polymethine chain shifts the absorption band by 100 nm bathochromically, whereas fusing the benzo ring as the terminal indole moiety shifts the absorption band by about 30 nm (107). **Figure 2.4** depicts carbocyanine's electronic absorption spectra based on the molecular structure's length (108,109).
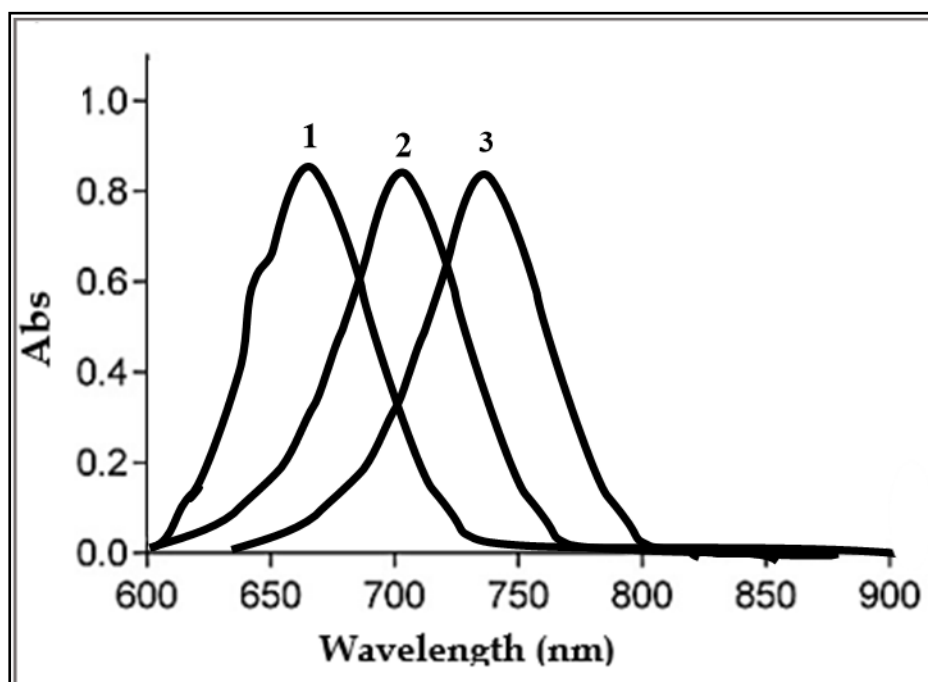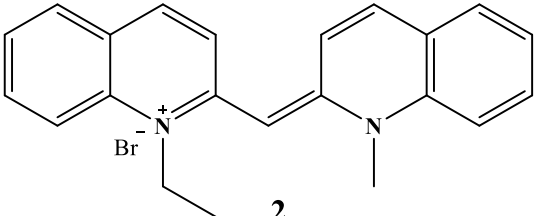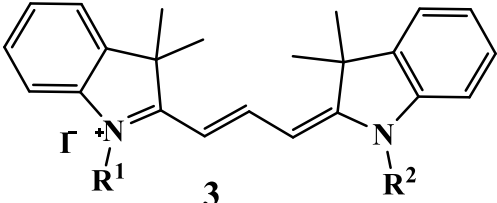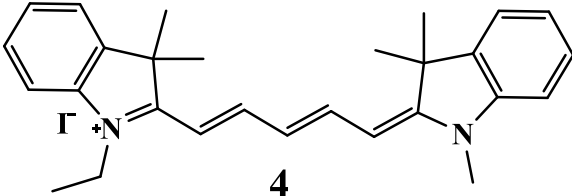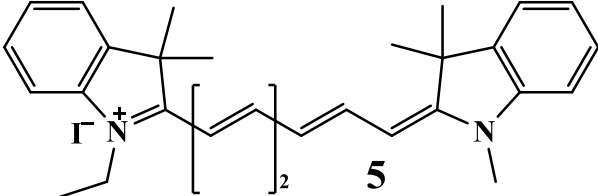
Figure 2.4: Different spectra of different carbocyanines based on the length of the structure and the modification (108,109).

Although it has been previously mentioned that the general carbo-cyanine dye name was derived from the Latin word cyanos, which means "blue", their family encompasses the whole electromagnetic spectrum from near infrared to ultraviolet. However, because to their extraordinary light sensitivity, the incredible utility of carbocyanine dyes was not identified until recently when H.W. Vogel utilised them to increase the sensitivity of the photographic plate (110). Since its first application by H.W. Vogel, carbocyanine has been used in a wide range of applications, including in the optical method (to monitor membrane electrical potential difference in cells) (111), pH sensors (112), in-vivo fluorescence imaging (111), and medicines (113). These compounds were initially used in photographic emulsions, but they were later discovered to be good photosensitizers and have been investigated for diagnostic and therapeutic purposes (110,114,115).

Carbocyanine dyes and their derivatives have been extensively studied recently for their cytotoxic activity against a wide range of tumours (116). The name and the structure of the Cy-molecules vary based on the number of carbons in the alkene structure and the modification of the molecules such as follows: Dyes containing n = 0, 1, 2, and 3, are classified as mono- **2**, tri- **3**, Penta- **4**, and heptamethine **5**, respectively (115). Also, the structure presented in **Table 2.1** shows different carbocyanines (Cys).

Table 2.1: The structures of Cy-molecules and their name based on the methine group (114).

Carbocyanine molecules	The structural molecules
Monomethine (n=0)	

Trimethine dye (n=1)	
Pentamethine dye (n=2)	
Heptamethine dye (n=3)	

2.1.3.1.1. The modification of carbocyanines

Most carbocyanines have short absorption spectra (absorption spectra around 300 nm to 500 nm), which leads to less formation of ROS as the PS struggles to reach the triplet state (107). They are often altered to modify their absorption maxima, solubility, and hydrophobic-hydrophilic characteristics, as well as to incorporate reactive groups that allow for further coupling to biomolecules and target-specific carriers. Incorporating heavy elements such as iodine into organic dyes is known to boost PDT and PACT performance, which is ascribed to increased spin-orbit coupling and triplet state population, which results in greater rates of reactive species formation (117). This effect has recently been observed with cyanine dyes, among other things. **Figure 2.3** presents some of the modified carbocyanines.
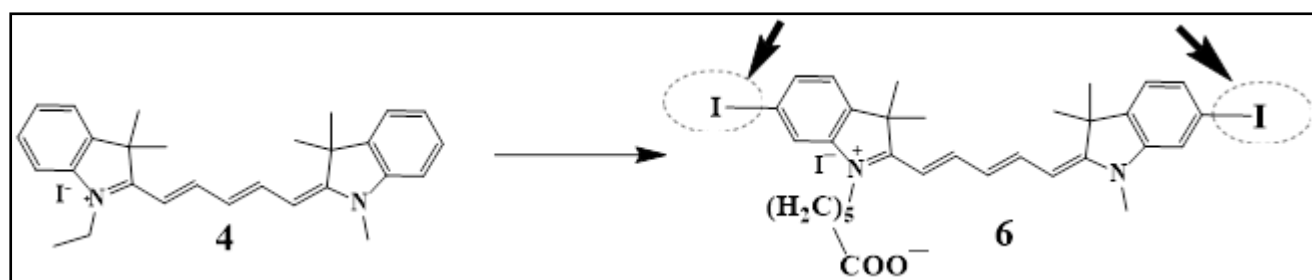
Figure 2.3: Modified carbocyanine (Cy) dyes. Cy-**6** presents the modified Cy with iodine atoms on both sides of the indole group (109,118).

The molecular structures are presented in **Table 2.1.** In addition, the absorption spectra of the modified carbocyanine have been analysed, and the results are shown in **Table 2.2**.
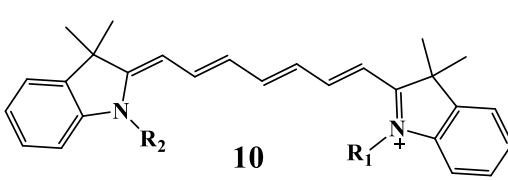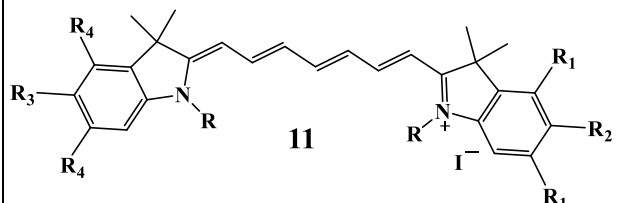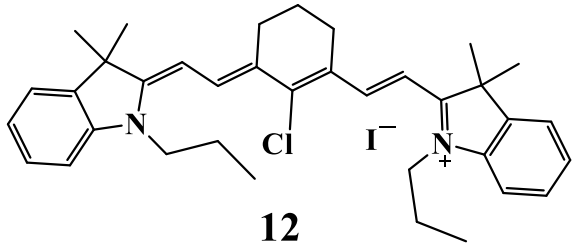
Table 2.2: The absorption spectra of the iodide-modified carbocyanines (109).

Dye	Structure	λ_{max} Ab (nm)	0.7% DMSO in saline
Cy7		753	739
ICy7		759	746
I₂Cy7		766	754
I₃Cy7		760	677

One of the most known carbocyanines used as PS is Indocyanine Green (ICG). This molecule and methylene blue are the only carbocyanine members reported to be approved by the Food and Drug Administration (FDA) (119). ICG has been reported

to express toxicity towards various cancerous cells (120,121). Also, heptamethine cyanine dye (Cy7) was reported to be an effective PS molecule (116). **Table 2.3** presents examples of carbocyanines together with their structures. All the carbocyanine molecules presented in **Table 2.2** have been applied as PSs in photodynamic antimicrobial chemotherapy (PACT) against *E. coli,* S. *aureus,* and *P. aeruginosa* (122).

Table 2.3: The type of carbocyanines that have been applied as photosensitizers (PSs).

Cyanine molecules	Chemical structures	Applications	References
Indocyanine green dye (ICG)		photodynamic treatment of several kinds of cancer	(116)
Iodide heptamethine cyanine dyes		photodynamic eradication of Gram-positive and Gram-negative pathogens	(118)
IR-780 iodide Dye		Combatting the Multidrug-Resistant Bacterial Infections	(123)

Ming Guan et al. (124) combined cyanine with Carbomer gel (Cy-CBMG hydrogel) to improve its antibacterial characteristics. The results demonstrated that the created Cy-

CBMG gel exhibited reduced photodegradation when exposed to laser light, and so could effectively increase ROS formation in bacteria. In vitro, the synthesised Cy-Cy-CBMG gel also shown exceptional ROS-induced killing effectiveness against methicillin-resistant Staphylococcus aureus and extended-spectrum b-lactamase-manufacturing *E. coli*.

PACT activity of cyclohexene-based cyanine dyes with two and three terminal end-groups of indolenine, benzothiazole, and benzoselenazole against *S. aureus* and *E. coli* bacteria was examined by Arjun Veliyil Prakash et al. (125). Both di-substituted benzothiazole and benzoselenazole cyanines have been shown to effectively kill *S. aureus* and *E. coli* at nanomolar and micromolar dye concentrations.

2.1.4. The synthetic route of carbocyanine

In general, the synthesis of carbocyanine dyes is primarily determined by the type of molecule of interest, which is determined by the heterocycles and metals present, as well as the length of the molecule. One method of synthesizing carbocyanine, such as heptamethine cyanine, is through a condensation reaction between two quaternary ammonium salts and a dianil-linker (109,114,126). **Figure 2.6** below presents the synthesis of meso-substituted heptamethine cyanines (127). The other method for synthesising carbocyanine is known as the aldehyde method, and the synthesis mechanism is presented in **Figure 2.6**.
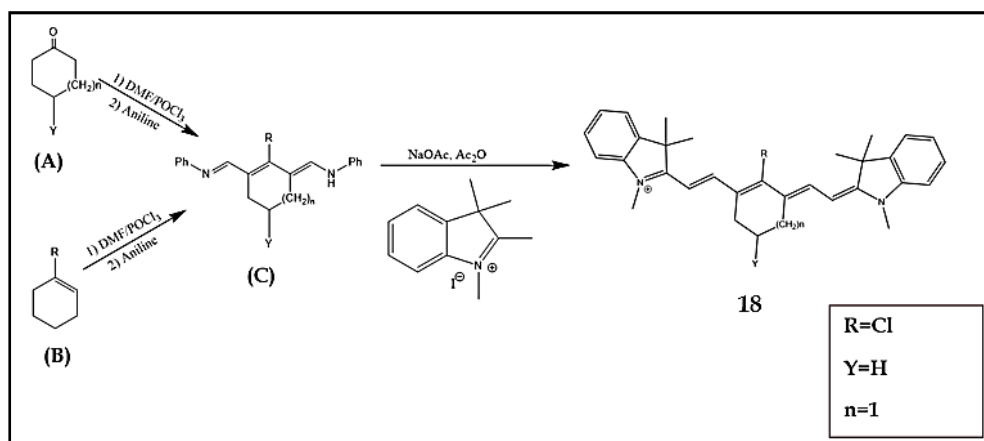
Figure 2.6: The chemical synthesis of meso-heptamethine carbocyanine dye **18** (127).

The key step in the synthetic procedure for heptamethine, as in **Figure 2.6,** is the formation of dianil linkers via the reaction of a substituted cycloketone **(A)** or 1-substituted cycloalkene **(B)** with the Vilsmeier-Haack reagent, which is generated from phosphorous oxychloride and N, N-Dimethylformamide, resulting in dialdehyde. The following step is to cap the molecule with aniline for stability to produce dianil linkers (**C**). Finally, the product **(C)** is condensed with quaternary ammonium salts in acetic anhydride in the presence of sodium acetate and purified by precipitation using ether or column chromatography (1–5% methanol/DCM). All these steps result in product **18**.

The aldehyde method is an alternative for producing one carbocyanine molecule (114). In brief, the quaternary ammonium salt (i) will be converted to a Fischer base (ii) under basic conditions. The Fischer base **(ii)** will then be reacted with chloromethylene, dimethylammonium chloride, and dichloromethane before being dissolved in an aqueous K_2CO_3 solution to form the aldehyde **(iii)**. The aldehyde **(iii)** is cleaved to form a carboxylic acid, which will be used to attach a molecule **(iv)** to one of the strands of peptide nucleic acid (PNA), and the molecule **(v)** to the other. These two strands are combined to form a molecule as a final product **19**. **Figure 2.7** presents the synthesis of carbocyanine using the aldehyde method (114).
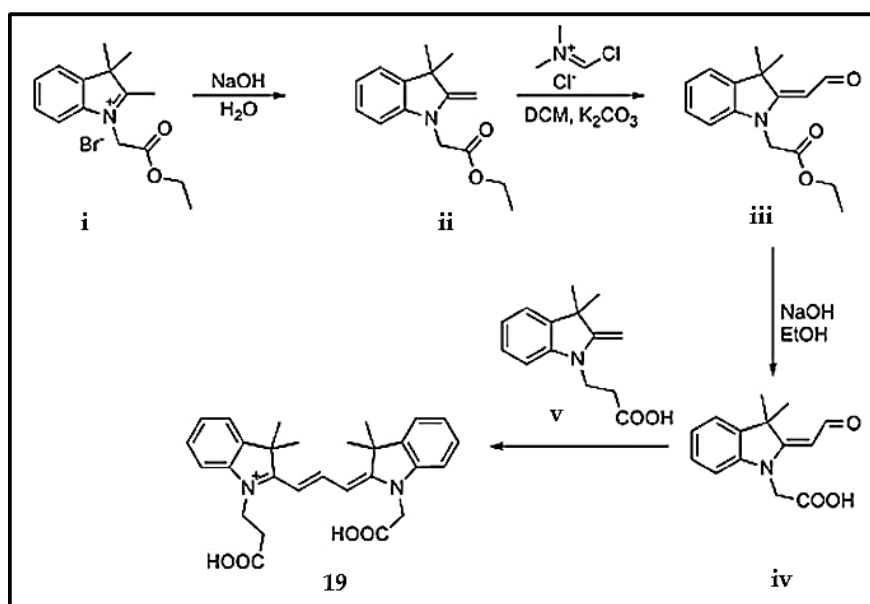
Figure 2.7: The Synthesis of carbocyanine following the aldehyde method (114).

The other method common for synthesizing pentamethine and heptamethine carbocyanine molecules is presented in **Figure 2.8**.
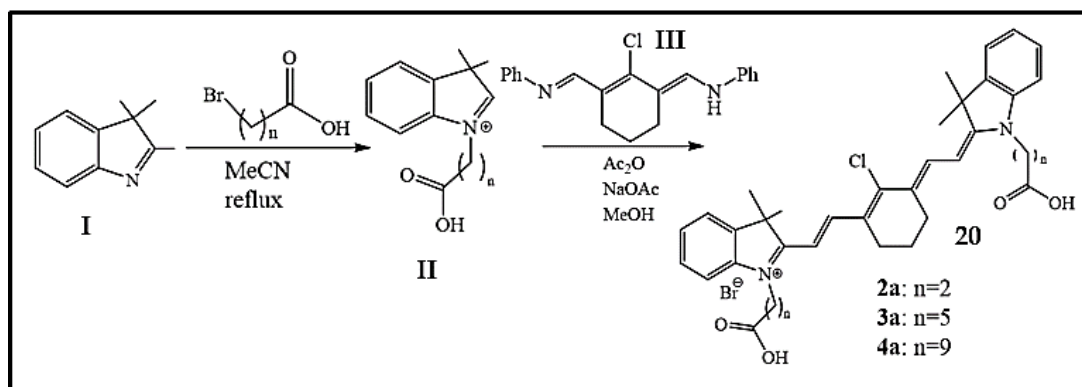
Figure 2.8: Alternative method for the preparation of carbocyanine **20** (128).

Refluxing reagent-**I** in acetonitrile with different chain-length carboxylic acids, 3, 6, or 10-bromopropionic acid in a nitrogen environment, followed by the addition of Vilsmeier-Haack reagents **II** in acetic anhydride under basic conditions. The reaction mixture was quenched with methanol once it had cooled to room temperature. To remove unreacted sodium acetate, the crude material was treated in dichloromethane and filtered. Column chromatography on silica gel eluting with methanol can be used to separate the components.

2.2. Nanomaterials (NMs)

Nanomaterials have become the cornerstone of nanoscience and nanotechnology due to their potential to revolutionize the ways materials and products are fabricated. Moreover, nanomaterials can also offer a wide range of functionalities. Nanomaterials are substances with at least one dimension of fewer than 100 nanometers. Several types of nanomaterials are synthesized or fabricated to suit different types of applications. Some nanomaterials occur naturally, but engineered nanomaterials (EN) are of particular interest because they are designed for and are already used in a wide range of commercial products and processes (129,130). **Figure 2.9** presents the

commonly known types of nanomaterials. Nanomaterials are characterised by their unique optical, magnetic, electrical, and other properties.
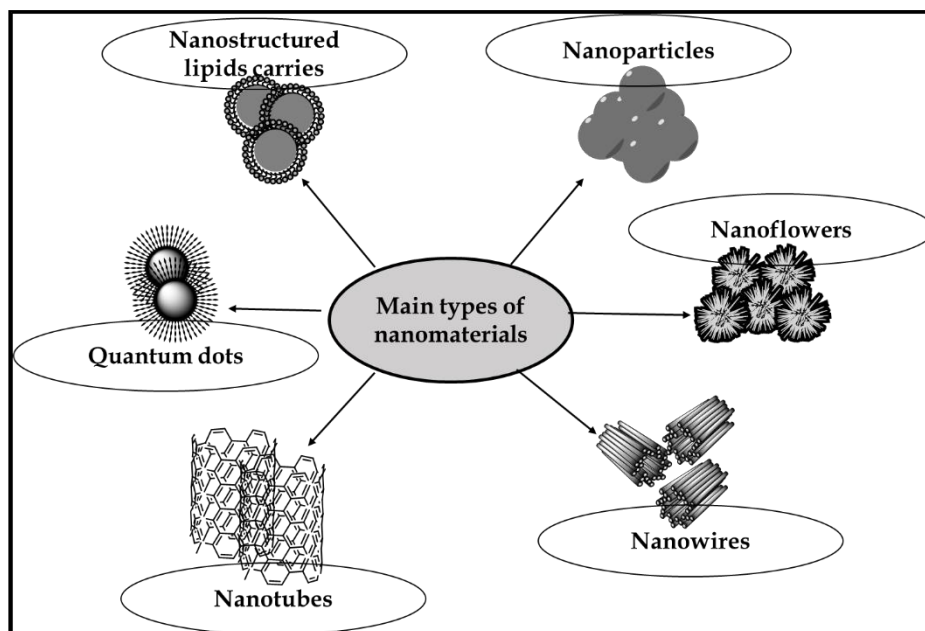
Figure 2.9: A variety of nanomaterials (131).

2.2.1. Metal oxide nanomaterials (MONs)

Metal oxide nanomaterials (MONs) are among the nanomaterials that have shown potential in various fields, including chemistry, materials science, physics, and biotechnology (132,133). Nanomaterials' conductor, semiconductor, and insulator properties are determined by their unique electronic structure. MONs, mainly copper(II) oxide (CuO), zinc oxide (ZnO), nickel oxide (NiO), indium oxide (In$_2$O$_3$), and tungsten oxide (WO$_3$), are potential sensing materials with high sensitivity, fast response and recovery time, excellent replicability and photostability (132). Furthermore, Because of their excellent photostability, large extinction coefficient, high emission quantum yield, and simplicity of surface modification, MONs have found exciting biological applications for fluorescent labelling. Silver oxide and zinc oxide are two metal oxide nanomaterials with the most promise (134,135). Among the two most promising nanomaterials, the study will focus on zinc oxide nanomaterial as a drug carrier for PSs in the PACT study. Zinc oxide materials have been described to be antibacterial, anticancer, immunomodulatory, sunscreen, and antioxidant, or

they can be used as an adjuvant treatment to chemotherapy drugs to lessen their side effects (136). Furthermore, zinc oxide has been revealed to promote the generation of reactive oxygen species (ROS) when exposed to UV light.

2.2.1.1.   Properties and application of zinc oxide nanomaterials (ZnO-NMs)

Zinc oxide (ZnO) nanomaterials are white semiconductor compounds that are nearly insoluble in water. They are also known as II-VI semiconductors because they have a large band gap energy of 3.3 eV and high excitation energy of 60 eV. Because of their high band gap energy, these compounds can accommodate large electric fields, high temperatures, and high power operations (137). ZnO compounds have crystalline wurtzite (B4) crystal structure at room temperature, composed of hexagonal unit cells with two lattice parameters (a and c) belonging to the C^4_{6v} or $P6_3$ *mc* space group. **Figure 2.10** presents the crystalline wurtzite of zinc oxide compounds. Low toxicity and biodegradability are two of the most important properties of ZnO nanomaterials (138).
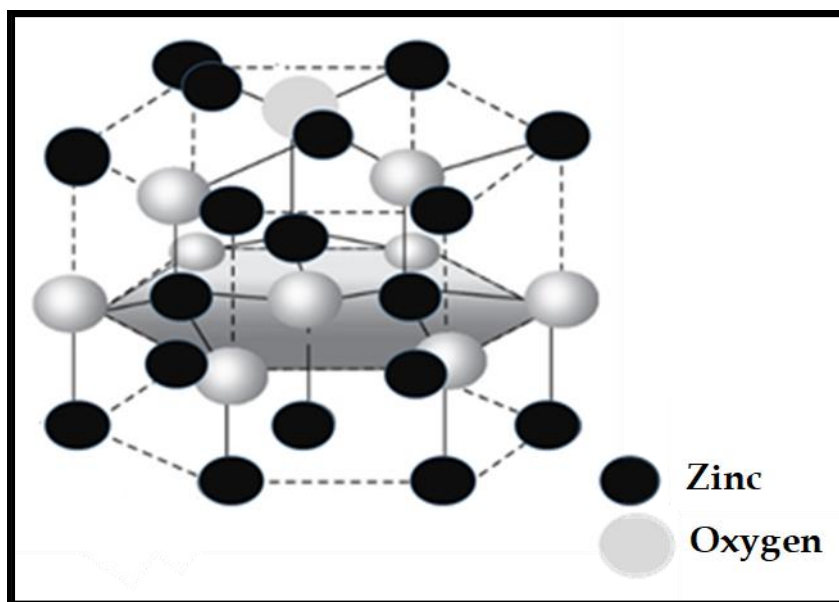
Figure 2.10: The hexagonal wurtzite structure model of ZnO (138).

These nanomaterials have been favoured in applications and products, including biomedical imaging (including fluorescence, magnetic resonance, positron emission

tomography, and dual-modality imaging) (139), drug delivery (140), gene delivery (141), and biosensing of various molecules of interest. ZnO-NMs have also been used in photodynamic therapy due to their ability to generate reactive oxygen species (ROS) when exposed to light, and they have demonstrated great potential and efficiency in killing cancer cells (138,142).

2.2.1.2.   Synthetic routes of zinc oxide nanoparticles and nanoflowers

ZnO nanomaterials or nanostructures can be synthesized using a variety of techniques such as vapour deposition (143), precipitation method, hydrothermal synthesis (144), the sol-gel process (145), precipitation from micro-emulsions (146), and mechano-chemical processes (147). The methods for obtaining zinc oxide nanomaterials are summarized in **Table 2.4** below.

Table 2.4: Method for the synthesis of ZnO-Nanomaterials.

Method	Precursors	Synthesis conditions	Properties	Ref
Mechanochemical Process	▫ $ZnCl_2$ ▫ Na_2CO_3 ▫ $NaCl$	Room temperature, Calcination: 2 h, 600 °C	Hexagonal structure; particles diameter: 21–25 nm	(148–150)
		Room temperature, Calcination at 400–800 °C	Hexagonal structure; particles diameter: 18–35 nm	
Precipitation process	$Zn(NO_3)_2$, NaOH	Synthesis: 2 h; drying: 2 h, 100 °C	Spherical particles; size of around 40 nm	(131)
	$Zn(CH_3COO)_2$, NaOH	Synthesis: 30 min, 75 °C; drying: overnight, room temperature	Hexagonal structure; flower shape (L: >800 nm);	(151)
Sol-gel	$Zn(CH_3COO)_2$, oxalic acid, ethanol and methanol	Reaction temperature: 60 °C; drying: 24 h, 80 °C; calcination: 500 °C	Zincite structure; aggregate particles: ~100 nm; the shape of the rod; particles L: ~500 nm, D: ~100 nm;	(152)

	Zn(CH$_3$COO)$_2$, oxalic acid (C$_2$H$_2$O$_4$), ethanol	Reaction: 50 °C, 60 min; dried of gel: 80 °C, 20 h; calcined: under flowing air for 4 h at 650 °C	Hexagonal wurtzite structure; uniform, spherically shaped particles	(153)
Solvothermal hydrothermal and microwave techniques	Zn(CH$_3$COO)$_2$, Zn(NO$_3$)$_2$, ethanol, imidazolium tetrafluoroborate ionic liquid	Reaction: 150–180 °C; drying: 80 °C in vacuum oven; calcinations: 500 °C	Hexagonal (wurtzite) structure, hollow microspheres (2–5 µm) consisted of nano-sized particles and contained channels (10 nm); hollow microspheres consisted of nanorods (~20 nm); flower-like microspheres (2.5 µm)	(144)

The green synthetic approach and the chemical method are two of the most widely used ways of producing ZnO-NMs. The green synthetic approach includes using plants to synthesize nanomaterials (155). The term "chemical synthetic, on the other hand, refers to procedures that employ non-aqueous liquid (polyol) as a solvent and reducing agent, with the goal of minimizing surface oxidation and agglomeration (156). Although the green synthetic pathway offers advantages such as lower costs and less pollution, chemical procedures are preferred because they may be conducted with a range of precursors and variables such as temperature, time, and reactant concentration (157). **Figure 2.11** depicts the most commonly used chemical process for producing ZnO-NMs.
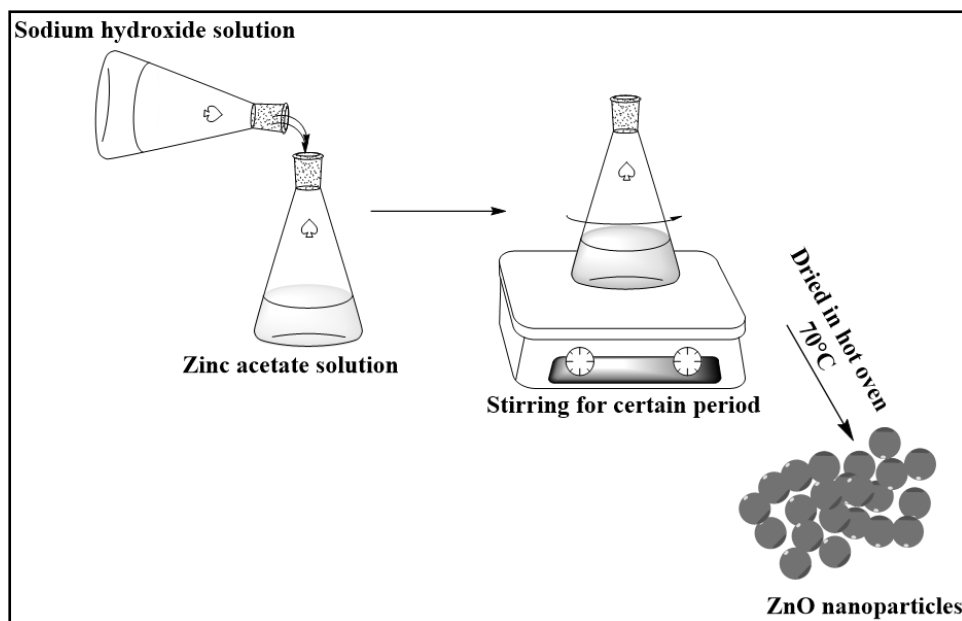
Figure 2.11: Chemical steps of ZnO nanoparticles (ZnO-NPs) synthesis (158).

Briefly, the synthesis of ZnO-NMs, such as nanoparticles, involves the preparation of two reactant solutions (zinc acetate and sodium hydroxide solution). The sodium hydroxide solution is then added drop by drop into the zinc acetate solution to achieve a pH scale range of 12 –13. Then the mixture is then stirred for a predetermined amount of time until the precipitate is visible, which represents the ZnO nanoparticles. The precipitation is washed with deionized water, filtered, and dried overnight in a hot air oven (158).

2.3.   Functionalization of MNs

Nanomaterials are functionalized lately to enhance their properties and characteristics including surface modification, which enable them to play a major role in medicine. The term "functionalization" refers to the surface modification of NPs, which includes the conjugation of chemicals or biomolecules on the surface, such as folic acid, biotin molecules, oligonucleotides, peptides, antibodies, and so on, to improve the properties and hit the target with high precision. Moreover, functionalization plays an important role in improving nanomaterials' physical and chemical properties, including anticorrosion, anti-agglomeration, and non-invasive properties.

Functionalization of nanomaterials also allows researchers to inculcate properties that they specifically like to incorporate into NPs (129,159).

2.3.1. Functionalization of NPs

The functionalization of NPs impacts the interaction of the nanoprobe with the biological environment and the imaging modality technique. Various approaches to the functionalization of NPs are investigated, depending on the molecular imaging applicability, efficiency, and other requirements. **Figure 2.12** depicts a summary of molecules of interest that can be attached to the NPs via secondary linkers. The conjugation of molecules on the surface of NPs is the process by which they are functionalized. Because of the high surface-to-volume ratio, particles can be efficiently functionalized to meet our needs. Understanding the chemistry of conjugation is critical because it allows us to assess the feasibility of various functionalization approaches (160,161).
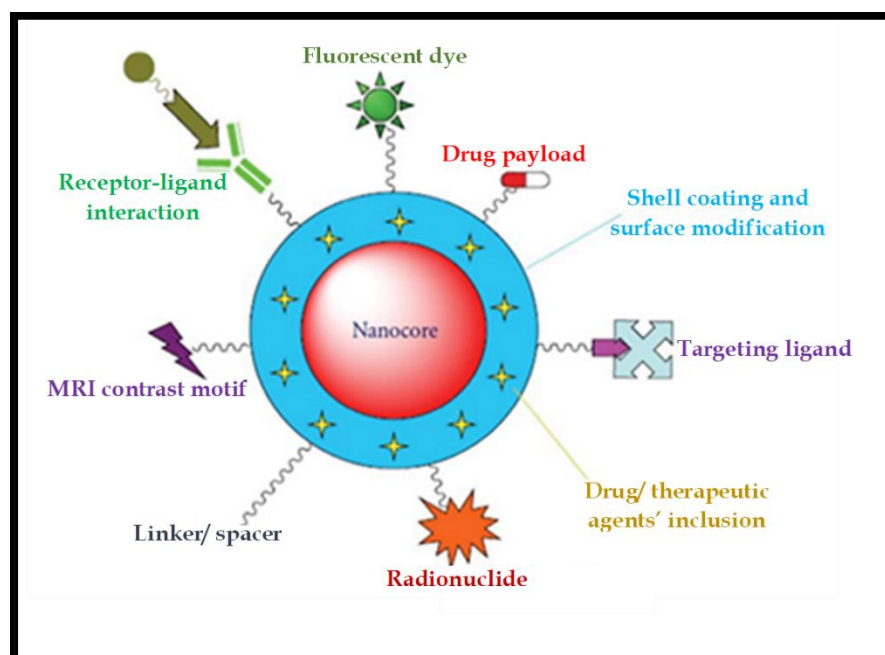
Figure 2.12: A variety of functionalizations in nanomaterials for a variety of applications (162).

Noncovalent binding can be used to functionalize nanomaterials by attaching specific secondary ligands. Functionalization can also occur through covalent binding, which

involves the direct binding of molecules by the interaction between the functional groups and the surface of the NPs. In terms of functionalization stability, this method involves a linkage reaction aided by a catalyst and is generally preferred over unspecific physisorption (162). Glutathione is one of the known substances for functionalizing metal and magnetic nanomaterials, especially for drug delivery purposes (163).

Glutathione is defined as a substance formed from the amino acids glycine, cysteine, and glutamic acid. It possesses many functional groups, including -SH, -NH2, and -COOH, and has strong abilities for coordinating with metal ions. More intriguing, because of the thiol group, it is soluble in water and may be easily absorbed into the surface of metal nanoparticles (164). In this study, glutathione will be employed in the functionalization of zinc oxide nanomaterials (ZnO-NMs), primarily for making the synthesized materials water-soluble.

2.4. The impact of NMs in PACT and PSs

The use of nanomaterials in PSs has recently gained popularity in improving PS properties. Metals such as titanium dioxide (TiO_2), for example, have been complexed with meso-tetrakis (p-sulfonatophenyl) porphyrin, and the subsequent developments have demonstrated the enhanced photostability and fluorescence into nanoparticles (165). Few studies have demonstrated the use of nanoparticles in PACT. In PACT, nanoparticles have been used in a variety of ways, including as an adjunct to a PS, as PSs themselves, as capsules containing a PS, and as particles that a PS has attached and bound to its surface (166).

Chen et al. (2012) investigated the effectiveness of chitosan (CS) nanoparticles in PACT. Using an ion gelation technique, they loaded CS nanoparticles with erythrosine(167). They tested the antimicrobial efficiency of CS-erythrosine using planktonic cells and biofilm from three different strains of *S. mutans, P. aeruginosa*, and *Candida albicans*. Shrestha and Kishen (2014) conducted an in-vitro study to assess the antibacterial efficacy of a newly developed PS, RB-functionalized CS nanoparticles,

against an *E. faecalis* biofilm and a multispecies biofilm. Using atomic force microscopy, they observed PS adherence to bacteria, surface roughening, and cell disruption (168). Moreover, they discovered that the new PS was more effective in terms of biofilm penetration, affinity toward the cell membrane, cellular disruption, and eradicating viable bacteria. Up to this date, there has been no study that expresses the employment of nanoflowers in PACT. Nonetheless, nanoflowers have so far been employed for drug delivery and in PDT. **Table 2.5** below shows a few applications of nanoflower as a drug carrier. They concluded that nano-PS could be used as an antibacterial measure to control root canal infections (169).

Table 2.5. The employment of nanoflowers

Nanoflowers	Preparation method	functions	References
Titanium dioxide nanoflower	One-step hydrothermal technique	Photo anode for dye sensitized solar cells	(170)
Manganese oxide (MnO2) nanoflowers	mild in-situ self-collapse method	as a multifunctional nano-platform for photodynamic therapy and MR imaging	(171)
gold nanoflowers	Microbial synthesis	Drug delivery, photo imaging and diagnosis	(172)

Chapter 3

3. Experimental

This chapter describes all the procedures used in the experiments of this work. This includes the synthesis, characterisation, and analytical instrumentation used in this work for all nanomaterials.

3.1. Materials

3.1.1. Solvents used in this study

Methanol (99.8%), ethanol (96%), acetonitrile (C_2H_3N) (99%), dimethyl sulfoxide (DMSO) (99.9%), and dimethylformamide (DMF) (99.8%) were purchased from Sigma Aldrich (Johannesburg, South Africa). Ultra-pure water (0.055uS/cm at 25°C) was obtained from a Milli-Q Water System (Merck, Johannesburg, South Africa) available in the laboratories for the Institution for Nanotechnology and Water Sustainability (iNanoWS) at the University of South Africa.

3.1.2. Organic molecules and reagents for the synthesis of Zinc oxide nanomaterials (ZnO-NMs)

IR-780 iodide, Zinc acetate dihydrate ($Zn(CH_3COO)_2 \cdot 2H_2O$), and Sodium hydroxide (NaOH) were purchased from Sigma Aldrich. ZnO-NFs were synthesized with a similar method followed in the literature (173), and the synthesis of ZnO-NPs and the functionalizations of ZnO-nanomaterials were done following the methods in the literature (174) and (175), respectively. The 3-Bromo-1-propanesulfonic acid sodium salt, 4-hydroxybenzenesulfonic acid, potassium carbonate (K_2CO_3), and glutathione (GSH) were purchased from Sigma Aldrich.

3.1.3. Reagents for bacterial work

Agar bacteriological BBL Mueller Hinton broth (HG000C24.500) and nutrient agar (HG0000C1.500) broth and nutrient agar were purchased from MERCK Chemical Ltd. *E. coli* (ATCC 8739) were purchased from Anatech.

3.2.   Equipment

The PerkinElmer Lambda 650s UV/VIS Spectrometer was used to record the UV-Visible absorption spectra of all prepared sample solutions. The prepared molecules' infrared (IR) spectra were recorded using the Perkin Elmer- Frontier FT-IR Spectrometer. The structural patterns of nano-sized materials were investigated using X-ray diffraction (XRD) (SmartLab X-Ray Diffractometer), a technique in which the sample remains stationary while the x-ray tube and detector move towards each other at a regulated pace of °θ/min. The XRD was programmed to measure intensities in the 2 = 5° to 100° range, scanning at 1° min-1 with a filter time constant of 2.5 s per step and a slit diameter of 6.0 mm. **Figure 3.1** below presents the set-up of XRD. D1 and D2 represent the position-sensitive detector (PSD), while ND represents the sample stage with a specimen.
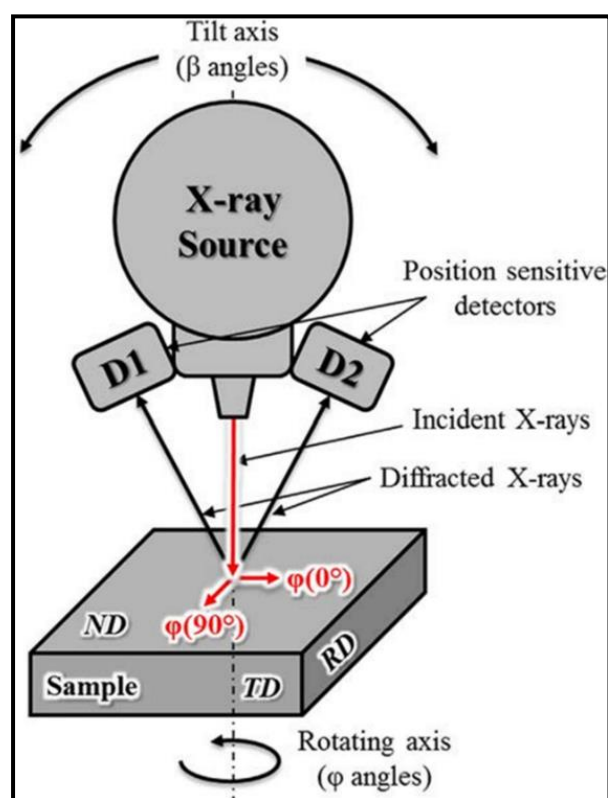
Figure 3.1: Schematic diagram of X-ray diffraction (XRD) set-up.

The overall morphology of ZnO-NFs was studied using a field emission scanning electron microscope (ZEISS FE-SEM) set to 5,00 kV, whereas ZnO-NPs were studied using scanning electron microscopy (JEOL SEM IT 300) set at 15 kV to 20 kV.

PACT experiments were conducted with the use of a General Electric lamp (230 W, light intensity = 8.27 x 1020 photons s^{-1} cm^{-2}). All plate readings (Optical density) for the antimicrobial investigations were collected using the LEDETECT 96 microplate reader for in vitro diagnostics from LABXIM PRODUCTS. To remove infrared radiation, a water filter was used, as shown in **Figure 3.2**.
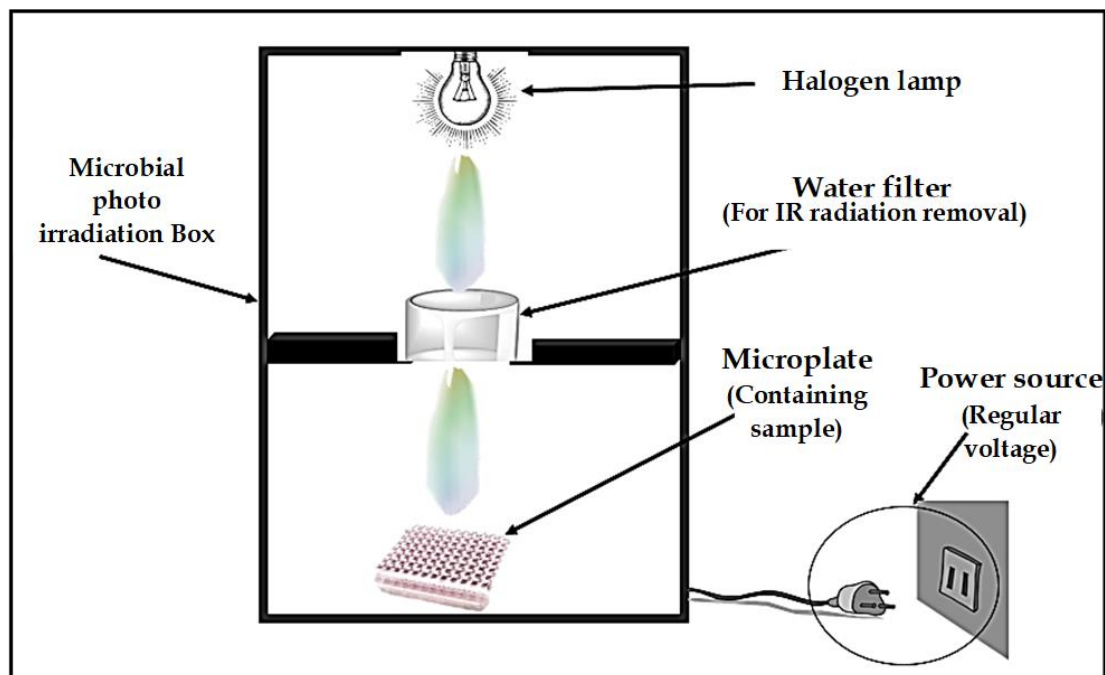
Figure 3.2: Schematic diagram of a microbial photo-irradiation photochemical set-up in a box.

3.3.   Synthesis

3.3.1. Synthesis and functionalization of ZnO-NPs and ZnO-NFs

ZnO-NPs and ZnO-NFs were synthesized using a combination of the titration method and the Sol-gel method. **Figure 3.3** depicts the schematic methods used to synthesize both nanoflowers and nanoparticles. The chemical steps of producing ZnO from zinc acetate dihydrate and sodium hydroxide are outlined in **Scheme 3.1.1** below. The chemical reaction for the synthesis of zinc oxide nanomaterials is divided into three mechanical steps, which includes two temporary products in the whole mechanical reaction. The initial step is the reaction of zinc acetate dihydrate and sodium hydroxide which lead to the formation of ashoverite and zinc hydroxide with the

presence of dihydrate. The second step is the chemical reaction of zinc hydroxide with dihydrate to result in the imbalance product of zincate ion and dihydrogen. Lastly, imbalance product of zincate ion results to the formation of zinc oxide, hydroxide in the presence of dihydrate. The method for the functionalization of as-prepared ZnO-NMs was adopted from the literature (175).
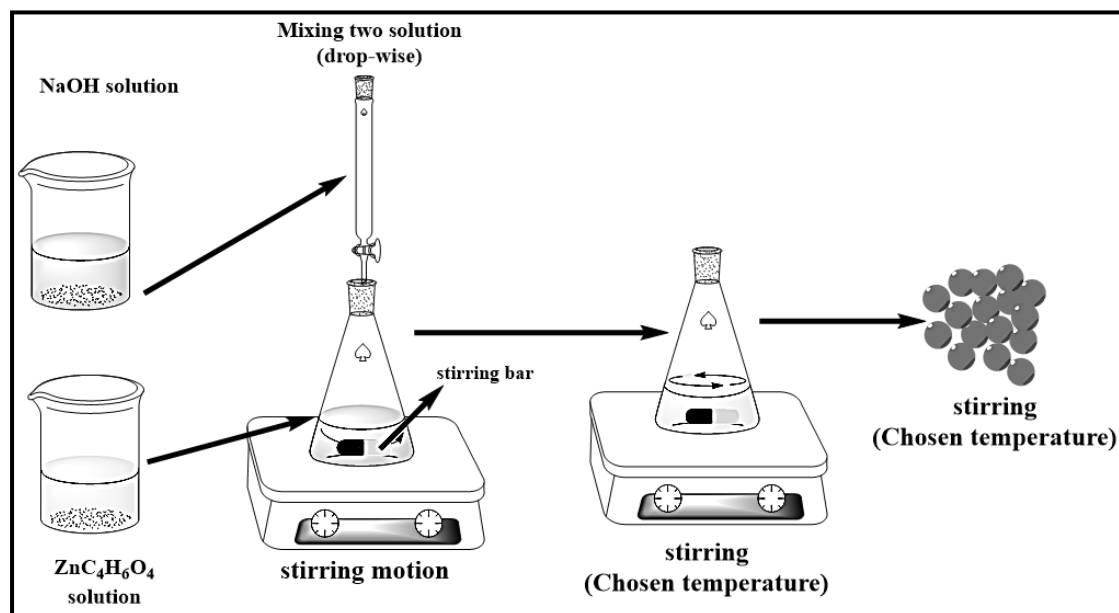
Figure 3.3: The schematic illustration of the Sol-gel method combined with the titration method.

3.3.2. Synthesis of Zinc oxide nanoparticles (ZnO-NPs)

The synthesis of ZnO-NPs was carried out according to the literature method (174). Briefly, aqueous zinc acetate dihydrate (1.7 M) and sodium hydroxide (1.5 M) solutions were prepared in methanol separately. The sodium hydroxide solution was added dropwise to the zinc acetate dihydrate solution (50mL) under magnetic stirring at room temperature. The resulting solution was homogenized by magnetic stirring for 2 hrs and 30 min and stirred for the next 24 hrs at room temperature. The product was harvested through centrifugation with the speed of 3500 rpm at room temperature, followed by washing with a 1:1 methanol–Milli-Q water mixture, and dried in the oven at 60 °C overnight. IR [KBr, υ, cm^{-1}]: 535, 688, 1377, 1496 [ZnO structure]. UV-Vis (λ_{max} nm) (solid state), 367 nm.

3.3.2.1.   Synthesis of Zinc oxide nanoflowers (ZnO-NFs)

Briefly, zinc acetate dihydrate (0.2 mol) and sodium hydroxide (1.45 mol) standard solutions were accurately prepared. The pH of the zinc acetate dihydrate solution (50 mL) was adjusted by sodium hydroxide dropwise under magnetic stirring. The reaction mixture was heated to reflux temperatures at constant stirring for 3 hrs and 30 min and then cooled to room temperature. The precipitate was harvested through centrifugation with the speed of 3500 rpm at room temperature and washed with Milli-Q water and ethanol. The product was dried in the oven at 60 °C overnight. IR [KBr, υ, cm^{-1}]: 541, 688, 1377, 1496, 3355 [ZnO structure]. UV-Vis (λ_{max} nm) (solid state), 368 nm. **Scheme 3.1.1:** The chemical reaction process for the formation of zinc oxide.

$$Zn(CH_3COO)_2 \cdot 2H_2O + 2NaOH \longrightarrow Zn(OH)_2 + 2CH_3COONa + 2H_2O \quad [1]$$

$$Zn(OH)_2 + 2H_2O \longrightarrow Zn(OH)_4^{2-} + 2H^+ \quad [2]$$

$$Zn(OH)_4^{2-} \longrightarrow ZnO + 2OH + 2H_2O \quad [3]$$
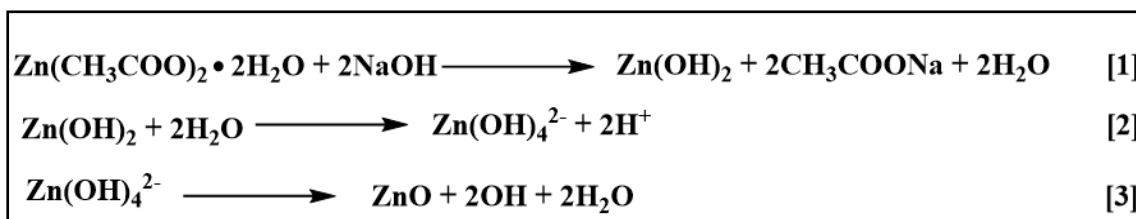
Scheme 3.1.1: The chemical reaction mechanism for the formation of ZnO from zinc acetate and sodium hydroxide

3.3.2.2.   Functionalization of Zinc oxide nanoparticles (ZnO-NPs) with glutathione

For the preparation of GSH-coated ZnO nanoparticles (GSH-ZnO-NPs), ZnO-NPs (75 mg, 0.92 mmol) and glutathione (100 mg, 0.325 mmol) were each dispersed in methanol (6 mL). Both solutions were sonicated for 30 min. The Glutathione solution was then added to the zinc oxide solution dropwise while the solution was stirred. The mixture was then stirred for 72 hrs at room temperature. Later, the solution was centrifuged with the speed of 3500 rpm at room temperature to harvest the product which was then washed with methanol and then dried in the oven overnight at 60 °C. The obtained sample was labelled as GSH-ZnO-NPs. IR [KBr, υ, cm^{-1}]: 849 [Zn-O]. UV-Vis (λ_{max} nm) (solid state), 349 nm.

3.3.2.3.   Functionalization of Zinc oxide nanoflowers (GSH-ZnO-NFs) with glutathione

For the preparation of GSH-coated ZnO nanoflowers (GSH-ZnO-NFs), ZnO-NFs (75 mg, 0.92 mmol) and glutathione (100 mg, x 0.325mmol) were each dispersed in methanol (6 mL). Both solutions were sonicated for 30 min. Glutathione solution was then added to the zinc oxide solution drop wisely while the solution was in the stirring motion. The mixture was then stirred for 72 hrs at room temperature. Later, the solution was centrifuged with the speed of 3500 rpm at room temperature to harvest the product, washed with methanol, and then dried in the oven overnight at 60 °C. The obtained sample was labelled as GSH-ZnO-NFs. IR [KBr, υ, cm^{-1}]: 600, 840 [Zn-O]. UV-Vis (λ_{max} nm) (solid state), 368 nm.

3.3.2.4.   Modification of IR-780 iodide to SHBS-IR-791 iodide

Briefly, IR-780 iodide (300 mg, 0.45 mmol), sodium 4-Hydroxybenzenesulfonic acid (80 mg, 0.459 mmol), and potassium carbonate (15 mg, 0.108 mmol) were dissolved in methanol (20 ml), and the reaction mixture was stirred for 24 hrs at a temperature of 60 °C under nitrogen gas. After the time had elapsed, the solvent was evaporated. The second step was purification, whereby a mixture of methanol and acetone with a ratio of 1:7 was prepared and then dissolved the obtained product in it. The solvent was evaporated again, and lastly, the product was washed with methanol and allowed to dry at 40 °C. The obtained sample was labelled as SHBS-IR-791 iodide. IR [KBr, υ, cm^{-1}]: 500-1088cm^{-1} (=C-H), 1404 (C-H scissoring) UV-Vis (λ_{max} nm) (DMF): 791 (log ε): 5.0613.

3.3.3. Conjugation of functionalized nanomaterials and modified organic dyes

3.3.3.1.   Synthesis of GSH-ZnO-NFs-SHBS-IR-791 iodide nanoconjugate

GSH-ZnO-NFs-SHBS-IR-791 iodide nanoconjugate was prepared by mixing SHBS-IR-791 iodide and GSH-ZnO-NFs (1:1 mass ratio (55 mg each)) in NaOH (10 mL, 1 M) in a glass vial. DMSO (5 mL) was then added to the solution mixture and subjected to ultrasonification for 30 min, followed by stirring for 72 hrs at room temperature. After this period, the product was obtained through precipitation in methanol and washed several times using the same solvent. The product was harvested through centrifugation and dried in the oven at 40 °C. IR [KBr, v, cm^{-1}]: UV-Vis (λ_{max} nm) (DMF): 368, 778.

3.3.3.2.   Synthesis of GSH-ZnO-NPs-SHBS-IR-791 iodide nanoconjugate

GSH-ZnO-NPs-SHBS-IR-791 iodide nanoconjugate was prepared by mixing SHBS-IR-791 iodide and GSH-ZnO-NPs (1:1 mass ratio (55mg each)) in NaOH (10mL, 1 M) in a glass vial. DMSO (5mL) was then added to the solution mixture and subjected to ultrasonification for 30 min, followed by stirring for 72 hrs at room temperature. After this period, the product was obtained through precipitation in methanol and washed several times using the same solvent. The product was harvested through centrifugation and dried in the oven at 40 °C. IR [KBr, v, cm^{-1}]: UV-Vis (λ_{max} nm) (DMF): 362, 787.

3.3.4. Antimicrobial activity

The antimicrobial activity of five drug samples (drug **1** denotes GSH-ZnO-NFs-SHBS-IR-791 iodide, drug **2** denotes GSH-ZnO-NPs-SHBS-IR-791 iodide, drug **3** denotes SHBS-IR-791 iodide, drug **4** denotes GSH-ZnO-NPs, and drug **5** denotes GSH-ZnO-NFs) was studied against E. coli. The study was carried out using 96-well plates, as demonstrated below in **Figure 3.5**. Four 96-well-cell plates were used to cover all the drug samples and the antimicrobial study. Each plate was divided into four parts. Plate **1** carried the activities of drugs **1**, **2**, and **3**, whereas plate **2** carried the activities

of drugs **4** and **5**. Another two plates were copies of plates **1** and **2**. Plates **1** and **2** were for the light exposure study; plates **3** and **4** were for the dark place study.

100 µl of *E. coli* was inoculated into (**X mL**) Luria nutrient broth and placed in a shaking incubator with a speed of 68 rpm for 37 °C for 24 hrs. The microbial culture's optical density (OD) at 600 nm was adjusted to around 0.8 by letting the bacteria grow until the OD reached 0.8, followed by drug sample preparation in which each drug sample was dissolved in a 1:4 distilled water and DMF solution (75% distilled water and 25% DMF).

The inactivation of E. coli was carried out by placing aliquots of 100 µL of the bacteria culture in a 96-well plate, followed by pipetting 50 µL of drug samples. The prepared four-96-well-celled plates were placed in an incubator for 24 hrs at 37 °C. After the time had elapsed, Plates **1** and **2** were taken out for irradiation, whereas plates **3** and **4** were left in the dark place. During the irradiation, the lightbox was used, and each plate (Plates **1** and **2**) was exposed to the light with an optical filter for 5 min.
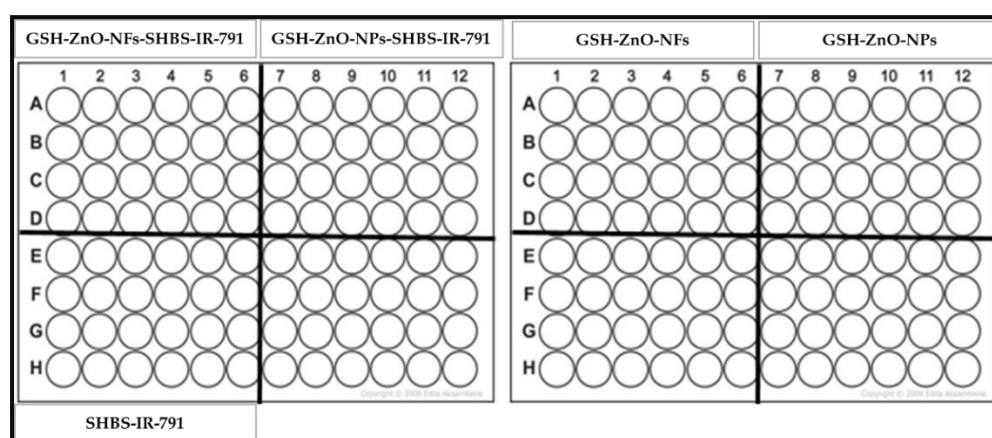
Figure 3.4: The representation of the 96-well-celled plated divisions.

Chapter 4

4. Results and discussion

This chapter reports on all the discussed results from the experiments carried out in this thesis. This begins with all the synthetic routes, followed by the results for all complexes used in this project.

4.1. Synthesis

4.1.1. Zinc oxide nanoparticles (ZnO-NPs) and zinc oxide nanoflowers (ZnO-NFs)

The sol-gel method was employed to synthesize two types of zinc oxide nanomaterials (ZnO-NMs) which are zinc oxide nanoparticles (ZnO-NPs) and nanoflowers (ZnO-NFs). Zinc acetate and sodium hydroxide were employed for the synthesis of ZnO-NPs and ZnO-NFs. **Scheme 4.1** depicts the synthesis of the zinc oxide nanomaterials using zinc acetate and sodium hydroxide. Both samples (ZnO-NPs and ZnO-NFs) were white powders.
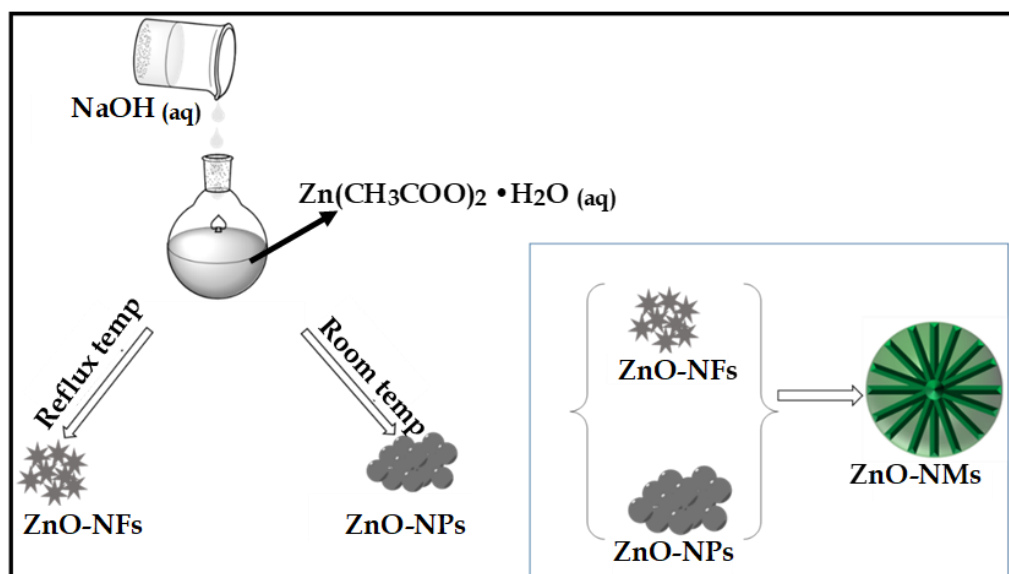
Scheme 4.1: The synthesis of Zinc oxide complex from zinc acetate and sodium hydroxide.

4.1.2. Functionalization of zinc oxide nanoparticles and nanoflowers (ZnO-NPs and ZnO-NFs) with glutathione

Glutathione was used to functionalize ZnO-NPs and ZnO-NFs (GSH-ZnO-NPs and GSH-ZnO-NFs), which binds to metal-rich nanomaterials via the thiol group. This method was carried out in basic aqueous media while stirring for several hours in the open air (**Scheme 4.2**). Methanol precipitation and centrifugation were used to purify the GSH-functionalized ZnO-NPs and ZnO-NFs, followed by oven drying at 60 °C. These substances were discovered to be highly soluble in water.
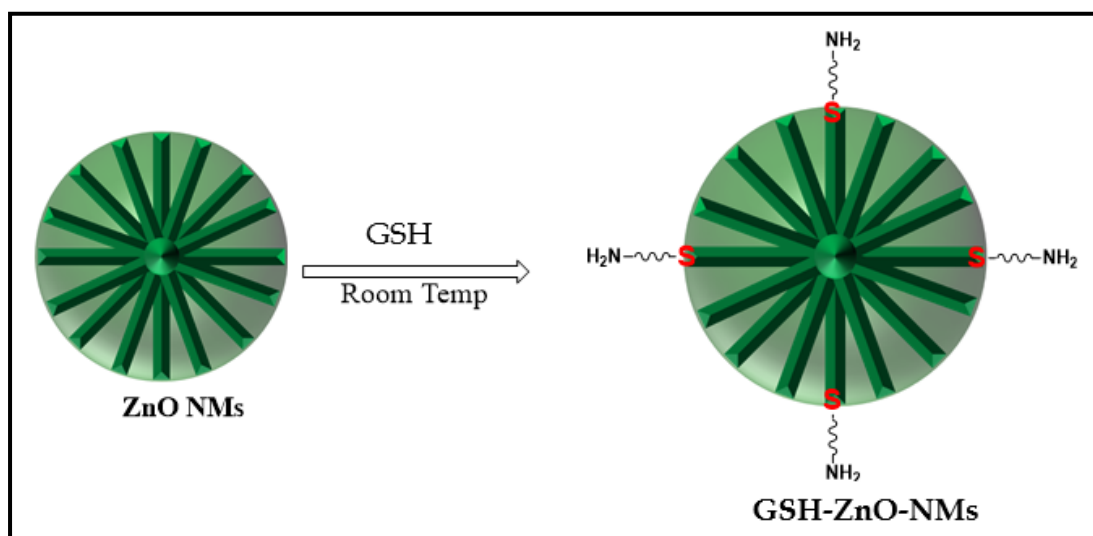
Scheme 4.2: Schematic representation of the synthesis of GSH-ZnO-NPs and GSH-ZnO-NFs.

4.1.3. Modification of IR-780 iodide complex to SHBS-IR-791 iodide Complex

The synthesis of benzenesulfonic acid sodium-modified IR-780 iodide (SHBS-IR-791 iodide) was performed with the use of IR-780 iodide and 4-Hydroxybenzenesulfonic acid sodium salt. The chemical reaction mechanism is presented in **Scheme 4.3**. This reaction resulted in the chloride ion on IR-780 iodide being displaced by the benzoxysulfonic acid sodium entity. The product is herein presented as SHBS-IR-791 iodide. The final product was green in colour and slightly soluble in water.
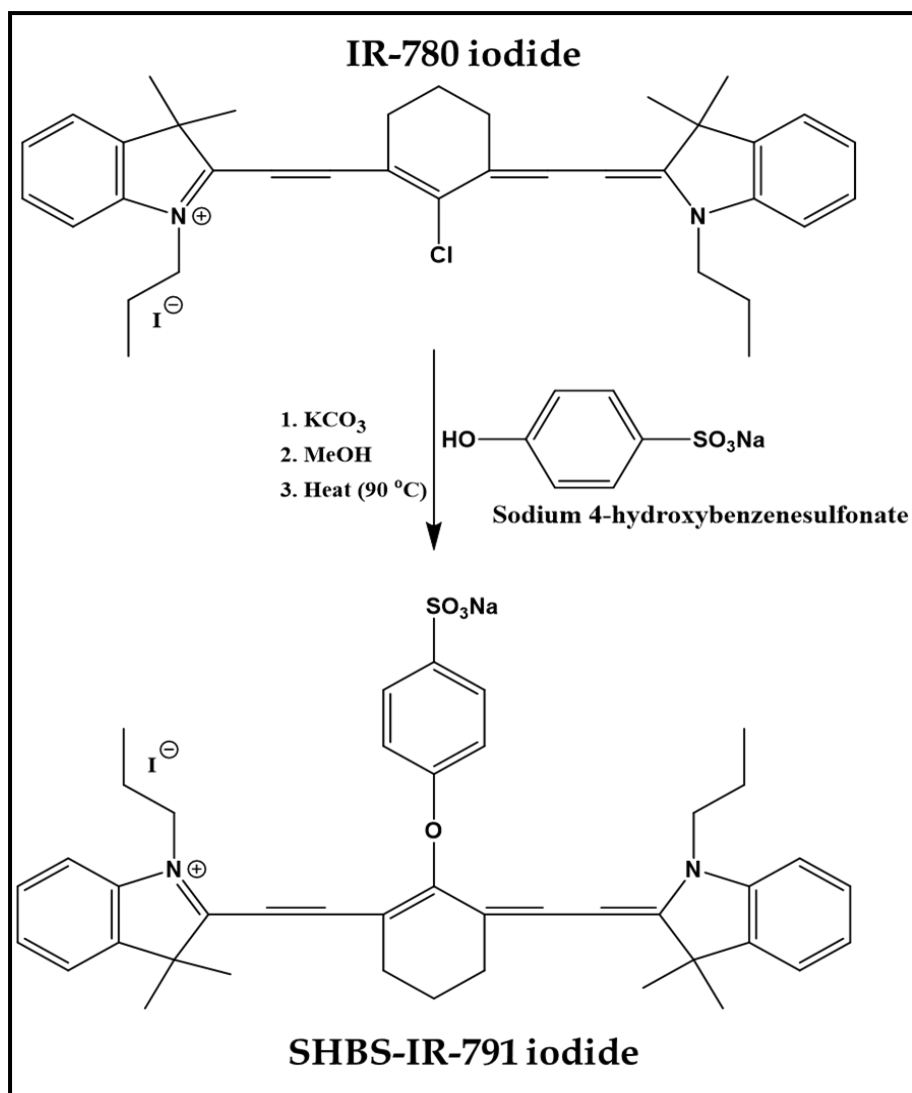
Scheme 4.3: Schematic representation synthesis of SHBS-IR-791 iodide.

4.1.4. Synthesis of GSH-ZnO-NPs-SHBS-IR-791 iodide and GSH-ZnO-NFs-SHBS-IR-791 iodide

GSH-ZnO-NPs-SHBS-IR-791 iodide and GSH-ZnO-NFs-SHBS-IR-791 iodide were synthesized by conjugating GSH-ZnO-NPs and SHBS-IR-791 iodide, as well as GSH-ZnO-NFs and SHBS-IR-791 iodide, respectively, as shown in **Scheme 4.4** below.
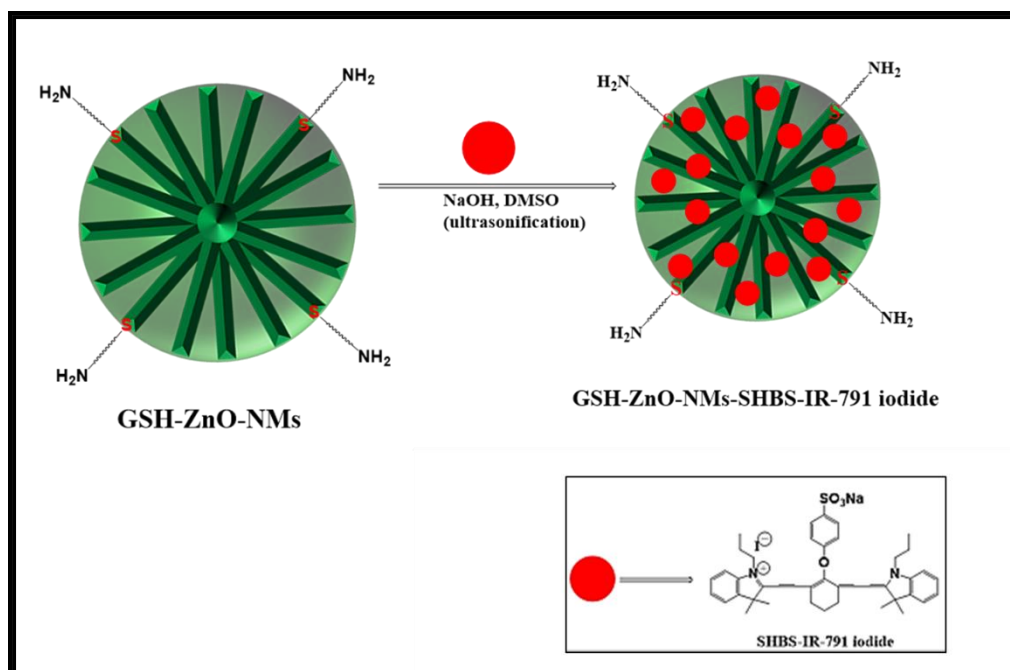
Scheme 4.4: Schematic representation of the synthesis of GSH-ZnO-NPs-SHBS-IR-791 iodide and GSH-ZnO-NFs-SHBS-IR-791 iodide.

4.1.5. Loading studies of the nanoconjugates

The nanoconjugates (GSH-ZnO-NPs-SHBS-IR-791 iodide and GSH-ZnO-NFs-SHBS-IR-791 iodide) were designed by individually incorporating SHBS-IR-791 iodide into GSH-ZnO-NPs and GSH-ZnO-NFs. The number of SHBS-IR-791 iodide complexes bonded to GSH-ZnO-NPs and GSH-ZnO-NFs was estimated using the following literature method, but absorption was used rather than fluorescence studies (176). Estimates are made by comparing the absorbance intensity of SHBS-IR-791 iodide in the conjugate with the absorbance of SHBS-IR-791 iodide before the conjugation. The obtained absorbance are shown in **Table 4.1**. The number of SHBS-IR-791 iodide bonded to GSH-ZnO-NPs were estimated as SHBS-IR-791 iodide: GSH-ZnO-NPs-SHBS-IR-791 iodide ratio, to be: 1:5 and the number of SHBS-IR-791 iodide bonded to GSH-ZnO-NFs were estimated as SHBS-IR-791 iodide: GSH-ZnO-NFs-SHBS-IR-791 iodide ratio, to be: 1:3.

Table 4.1: The absorbance used for loading estimation.

Complexes	λ$_{max}$ **absorbance**
SHBS-IR-791 iodide	1.87
GSH-ZnO-NPs-SHBS-IR-791 iodide	0.39
GSH-ZnO-NFs-SHBS-IR-791 iodide	0.55

Table 4.2. The optical parameters (UV-Vis and molar extinction coefficient) for all the complexes.

Complexes	λ$_{Abs.}$ (nm)	Molar extinction coefficients (ε)
ZnO-NPs	367	-—
ZnO-NFs	368	-—
GSH-ZnO-NPs	349	-—
GSH-ZnO-NFs	368	-—
IR-780 iodide	780	5.0613
SHBS-IR-791 iodide	791	5.0594
GSH-ZnO-NPs-SHBS-IR-791 iodide	363, 787	-—
GSH-ZnO-NFs-SHBS-IR-791 iodide	367, 777	-—

4.2.   Characterisation

4.2.1.   Ultraviolet-Visible spectroscopy of ZnO-NPs and ZnO-NFs

UV-vis spectroscopy was performed at room temperature to determine the optical properties of as-synthesized ZnO-NPs and ZnO-NFs, and the results are shown in **Figure 4.1.** The two obtained graph lines denote ZnO-NFs and ZnO-NPs. All samples were studied in solid powder form with an absorption detection range of 300-800 nm.
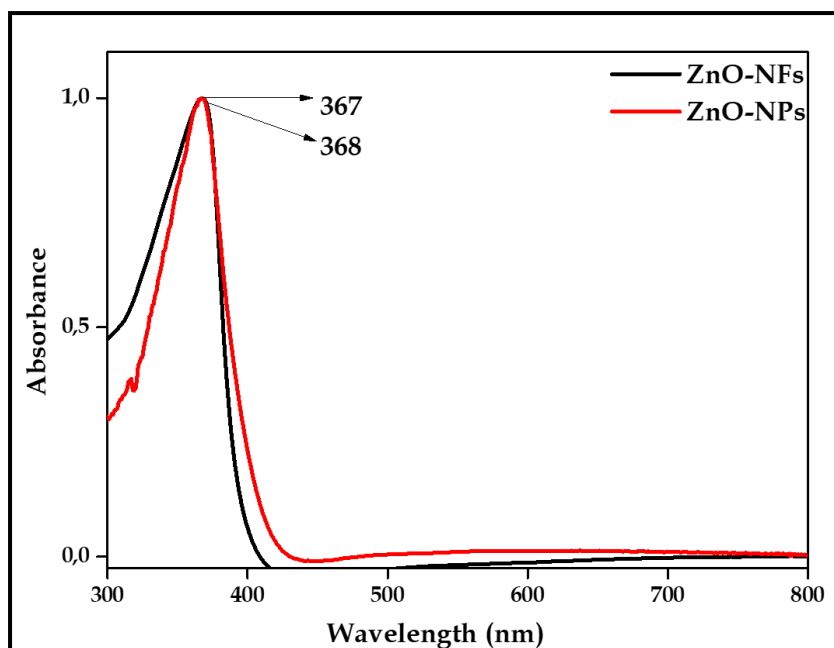
Figure 4.1: UV-Vis spectra of ZnO-NPs and ZnO-NFs.

The UV-Vis spectra obtained showed an exciton absorption peak at 367 and 368 nm for ZnO-NPs and ZnO-NFs, respectively. The presence of only one peak on each line graph indicated that the ZnO nanostructures were pure and could have good optical properties (177).

4.2.2. UV-Vis spectra of ZnO-NPs, ZnO-NFs, GSH-ZnO-NPs and GSH-ZnO-NFs

The optical properties of as-synthesized ZnO-NPs, ZnO-NFs GSH-ZnO-NPs and GSH-ZnO-NFs were determined using UV-vis spectroscopy at room temperature, and the results are shown in **Figure 4.2.** All samples were studied in powder form, with a detection range of 300-800 nm for absorption.
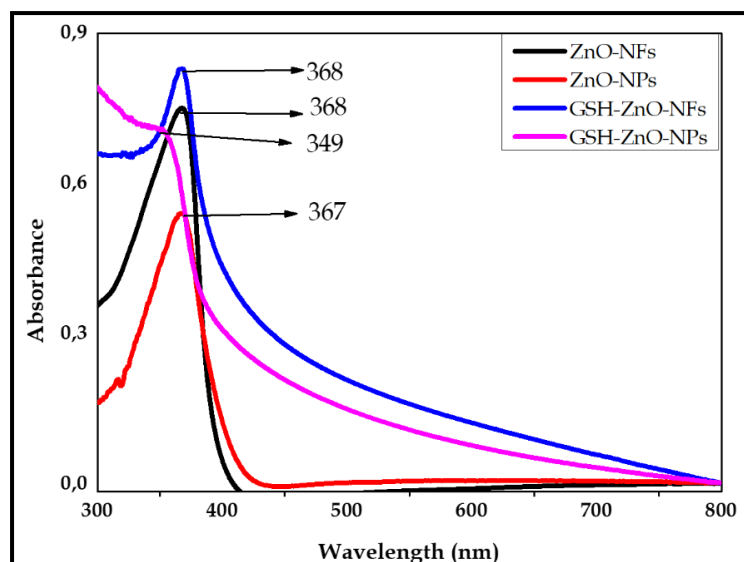
Figure 4.2: UV-Vis spectra of zinc oxide nanoparticles (ZnO-NPs) and zinc oxide nanoflowers (ZnO-NFs) and their functionalized materials (GSH-ZnO-NFs and GSH-ZnO-NPs).

The obtained UV-Vis spectra show an exciton absorption peak at 349, 367, 368 and 368 nm for GSH-ZnO-NPs and ZnO-NPs, GSH-ZnO-NFs and ZnO-NFs, respectively. The presence of only one peak on each line graph indicated that the ZnO nanostructures were pure and had the potential for good optical properties (174,177). The data displayed in **Figure 4.2** reveal that all of the complexes (ZnO-NPs, ZnO-NFs, GSH-ZnO-NFs, and GSH-ZnO-NPs) have just one band between 300 nm and 400 nm. However, the outcomes reveal that GSH-ZnO-NFs and GSH-ZnO-NPs have comparable bands that are broader than ZnO-NPs and ZnO-NFs. Therefore, it can be concluded that the change in absorbance is introduced by the presence of GSH in GSH-ZnO-NFs and GSH-ZnO-NPs since it is the only component that makes the GSH in GSH-ZnO-NFs and GSH-ZnO-NPs vary from ZnO-NPs and ZnO-NFs. Moreover, similar results were obtained in the literature (175) during the capping of ZnO.

4.2.3. Ultraviolet-Visible spectroscopy of IR-780 iodide and SHBS-IR-791 iodide complexes

The optical studies of SHBS-IR-791 iodide were performed at room temperature with the samples dissolved in DMF. The UV-Vis absorption detection measurement range is 300-900 nm, and the results are presented in **Figure 4.3.** The presented findings are the optical properties of IR-780 iodide and SHBS-IR-791 iodide.
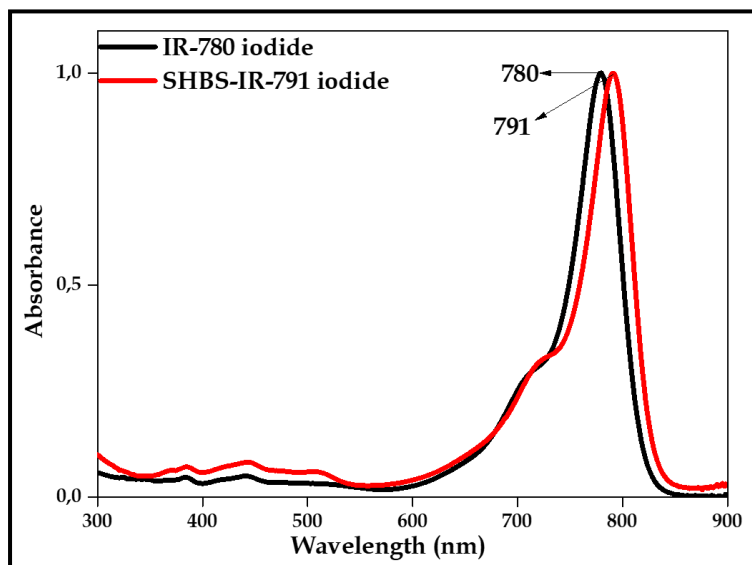
Figure 4.3: UV-Visible spectra of IR-780 iodide and SHBS-IR-791 iodide.

The absorption spectra of IR-780 iodide and SHBS-IR-791 iodide show exciton absorption peaks at 780 and 791 nm, respectively. The SHBS-IR-791 iodide spectra present a slight red shift as compared to IR-780 iodide. Red-shift is described as the movement of spectral lines towards longer wavelengths (the red end of the spectrum), and the opposite of red-shift is blue-shift, which is defined as the displacement of spectral lines towards shorter wavelengths. Referring to the literature (107), the extension of aromatic groups in dyes induces a bathochromic shift and significant strengthening of the long-wavelength absorption band (red shift).

4.2.4. The molar extinction coefficient of IR-780 iodide and SHBS-IR-791 iodide

Figure 4.4 below presents the concentration dependence of the IR-780 iodide using DMSO as a solvent. The results show the UV-Vis electronic spectra of IR-780 iodide for a sequence of concentrations in the range from 6×10^{-6} M to 16×10^{-6} M.
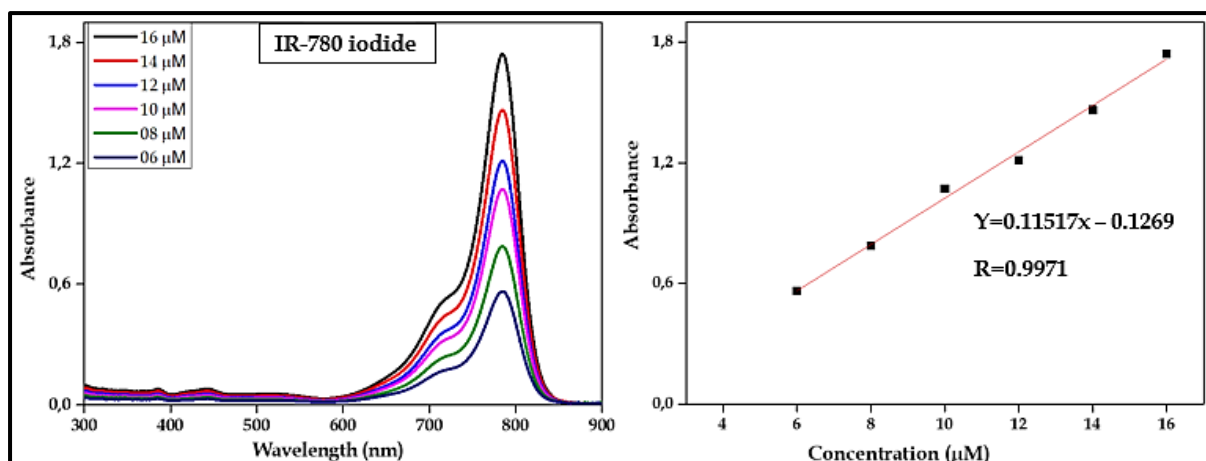
Figure 4.4: Variation of the absorption vs wavelength and absorption vs concentration of IR-780 iodide in DMSO as a function of concentration. The concentrations range from 6-16 µM.

The observed IR-780 iodide results show that the concentration is directly proportional to the absorbance. From the obtained outcomes, for the IR-780 iodide, the greatest absorption wavelengths and accompanying molar extinction coefficients are shown. Y=0.11517x – 0.1269 formulate the coefficient of IR-780 iodide and R=0.9971 is the molar extinction coefficient for IR-780 iodide. **Figure 4.5** below presents the concentration dependence of the SHBS-IR-791 iodide using DMSO as a solvent. The results show the UV-Vis electronic spectra of SHBS-IR-791 iodide for a sequence of concentrations in the range from 6×10^{-6} M to 16×10^{-6} M.
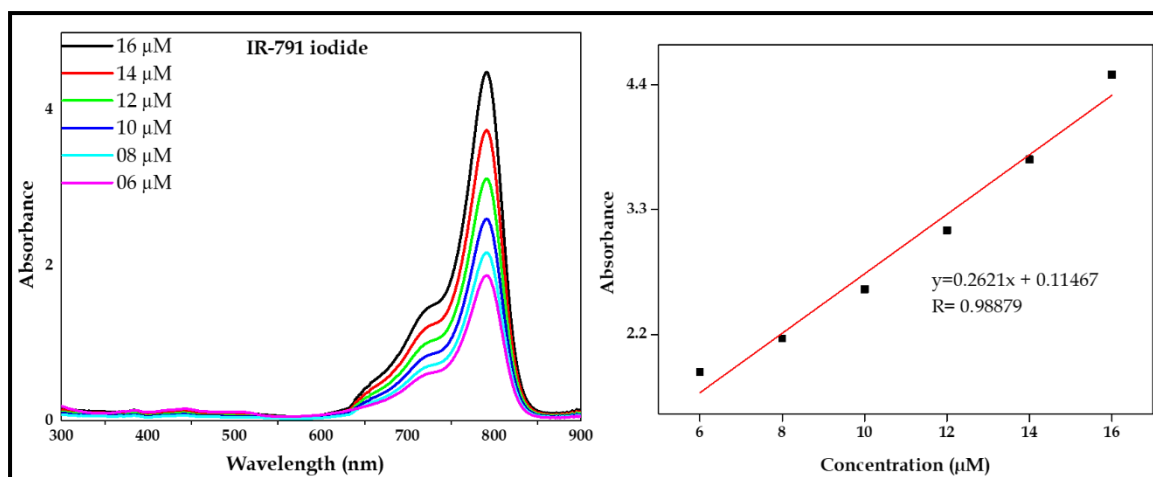
Figure 4.5: Variation of the absorption vs wavelength and absorption vs concentration of SHBS-IR-791 iodide in DMSO as a function of concentration. The concentrations range from 6-16 µM.

The observed SHBS-IR-791 iodide data reveal that concentration is directly related to absorbance, and absorbance reflects redshift. Based on the results, the wavelengths of maximum absorption and related molar extinction coefficients for the SHBS-IR-791 are displayed in **Figure 4.5**.

4.2.5. UV-Vis spectra of GSH-ZnO-NPs-SHBS-IR-791 iodide and GSH-ZnO-NFs-SHBS-IR-791 iodide

The optical properties of the GSH-ZnO-NPs-SHBS-IR-791 iodide and GSH-ZnO-NFs-SHBS-IR-791 iodide were carried out using UV-vis spectroscopy at room temperature, and the obtained results are shown in **Figure 4.6.** All the samples were dissolved in DMF for ground-state absorption studies, and the wavelength ranged from 300-900 nm.
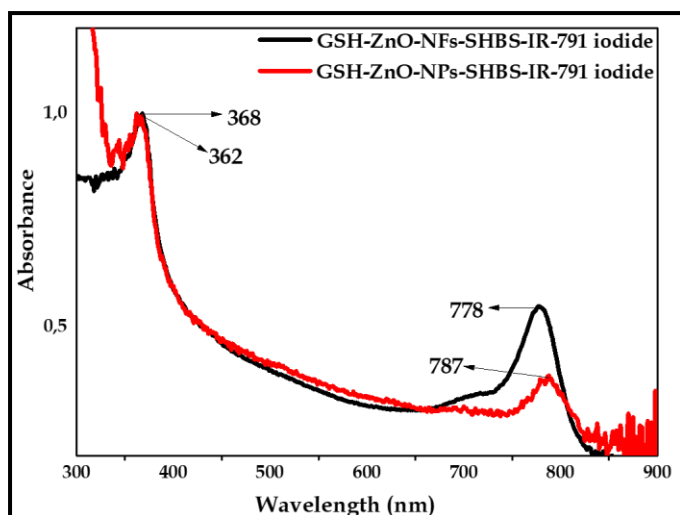
Figure 4.6: UV-Visible spectra for GSH-ZnO-NPs-SHBS-IR-791 iodide and GSH-ZnO-NFs-SHBS-IR-791 iodide nanoconjugates.

The GSH-ZnO-NFs-SHBS-IR-791 iodide and GSH-ZnO-NPs-SHBS-IR-791 iodide line graphs display the blue shift in the absorbance as compared to the outcomes of SHBS-IR-791 iodide presented in **Figure 4.6.** Interestingly, the absorbance can be noticed at 362 and 368, which tells that there is a detection of GSH-ZnO-NPs and GSH-ZnO-NFs in GSH-ZnO-NPs-SHBS-IR-791 iodide and GSH-ZnO-NFs-SHBS-IR-791 iodide complexes. As a result, it is possible to conclude that the conjugations are obtained.

4.3. Fourier transform infrared spectroscopy

4.3.1. Infrared spectra of ZnO-NPs and ZnO-NFs

FTIR analysis was performed on generated ZnO-NPs and ZnO-NFs to observe the numerous distinctive functional groups associated with the nanomaterials. The infrared spectra were recorded at room temperature between 500 and 4000 cm^{-1}. The obtained results are shown in **Figure 4.7.**
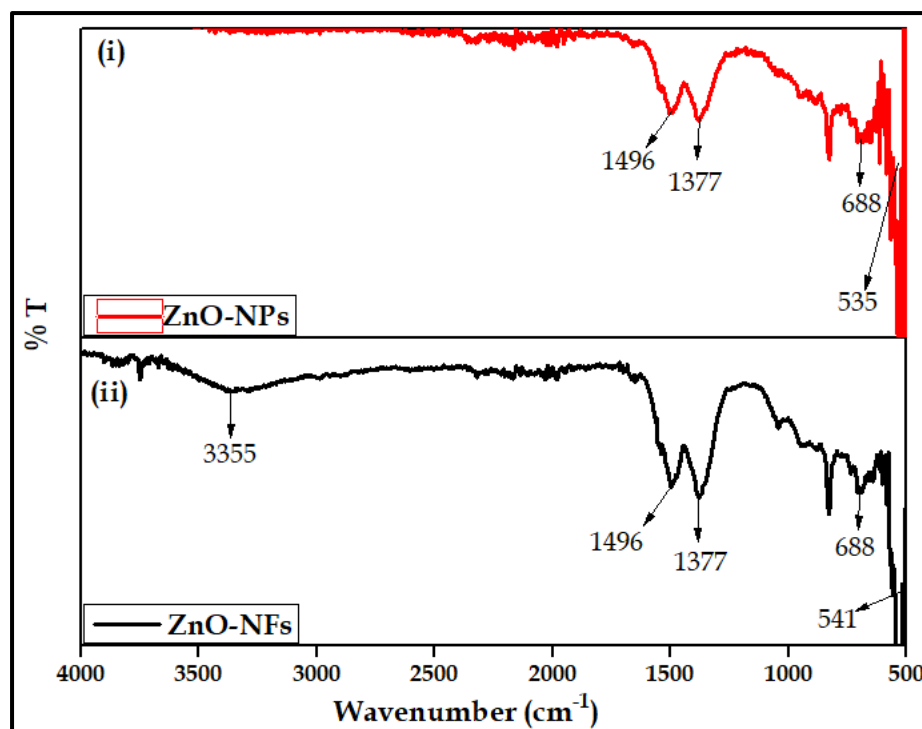
Figure 4.7: Fourier transforms infrared spectroscopy of ZnO-NPs and ZnO-NFs.

The characteristic peaks observed at 535 cm^{-1} and 688 cm$^{-1,}$ are attributed to the stretching vibration metal oxide which in this study, they are attributed to Zn-O. Two bands at 1377 cm^{-1} and 1496 cm^{-1} can be attributed to the stretching vibration mode of C—O and C=O. the broad absorption peak at 3355 cm^{-1} corresponds to the characteristic absorption of O—H (178).

4.3.2. Infrared spectra of GSH-ZnO-NPs and GSH-ZnO-NFs

FTIR instrument was used to detect the various characteristics of functional groups associated with the GSH-ZnO-NPs and GSH-ZnO-NFs. The obtained results are shown in **Figure 4.8**.
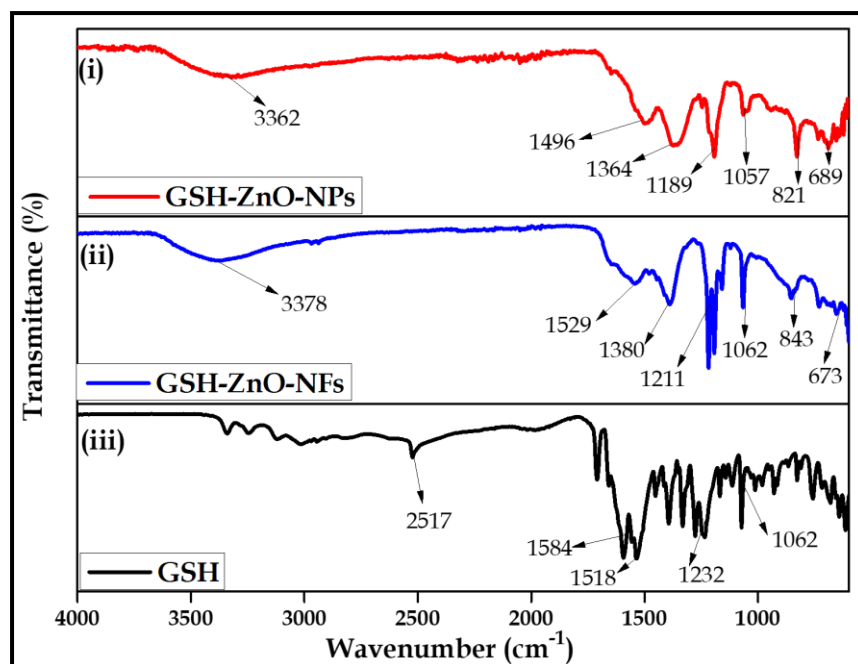
Figure 4.8: Fourier transforms infrared spectroscopy of GSH-ZnO-NPs and GSH-ZnO-NFs.

A band at 2525 cm^{-1} in the pure GSH spectrum corresponds to the -S-H stretching vibration of GSH. However, it vanished in the spectrum of GSH-ZnO-NPs and GSH-ZnO-NFs. The disappearance of this band indicated that the thiol group was deprotonated and coordinated the structures of ZnO-NPs and ZnO-NFs, for the formation of GSH-ZnO-NPs and GSH-ZnO-NFs, respectively (179). Thiol groups R-SH form of chemical moieties, and when subjected to deprotonation (loss of H$^+$), they form charged thiolates with distinct properties and reactivities compared with thiols when in R-SH form (180). Thus, the disappearance of the band indicates that thiol has undergone deprotonation and taken part in interaction with the surface of ZnO-NPs and ZnO-NFs to form GSH-ZnO-NPs and GSH-ZnO-NFs. The C=O and C-O stretching frequencies at 1540 cm^{-1} and 1375 cm^{-1} in glutathione are assigned to asymmetric and symmetric carboxylate group stretching modes, respectively. In GSH-ZnO-NPs, asymmetric and symmetric carboxylate group stretching modes shifted to 1496 cm^{-1} and 1364 cm^{-1}, respectively, but were observed at 1529 and 1380 cm^{-1} for GSH-ZnO-NFs. Due to Zn-O-Zn stretching modes, the main absorption peaks of ZnO are in the 850-550 cm^{-1} range.

4.3.3. Infrared spectra of IR-780 iodide and SHBS-IR-780 iodide

IR-780 iodide and SHBS-IR-780 iodide were subjected to FTIR analysis to establish the various characteristic functional group associated with the benzoxysulfonic acid sodium salt-modified IR-780 iodide. The spectra of the complexes are presented in **Figure 4.9**.
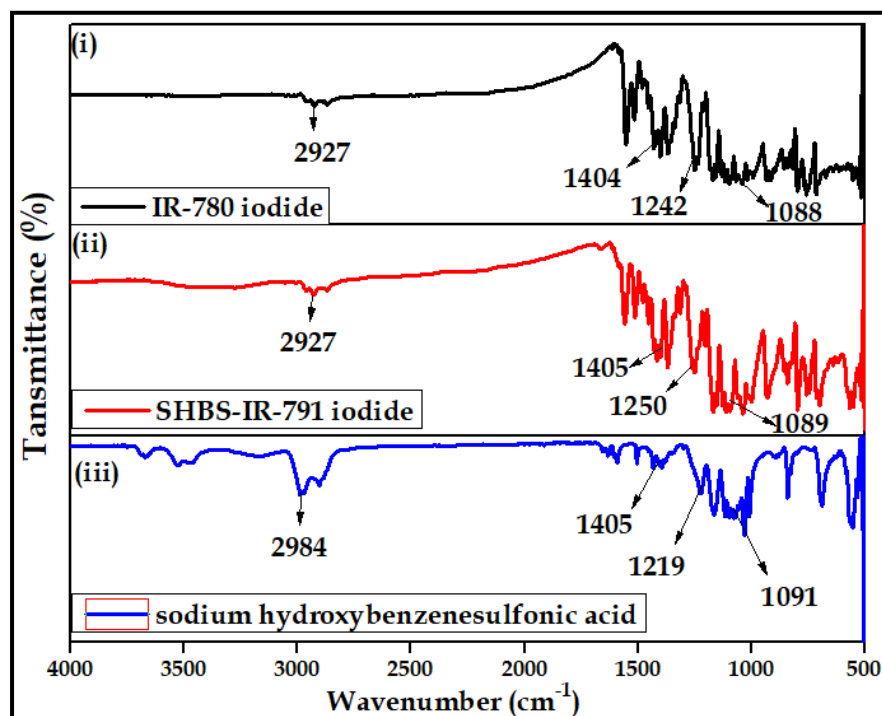
Figure 4.9: Fourier transforms infrared spectra of IR-780 iodide, SHBS-IR-791 iodide, and 4-hydroxybenzenesulfonic acid sodium salt modified IR-780 iodide (SHBS-IR-791 iodide).

The FTIR spectrum of 4-hydroxybenzenesulfonic acid sodium shows the vibrational stretches of the hydroxyl groups between 3400 and 3700 cm^{-1}. Compared to the FTIR spectrum of IR-780 iodide, which does not have the hydroxyl group, such vibrational stretches were not observed. However, a broad but very weak vibrational stretch between 3200 cm^{-1} and 3500 cm^{-1} was observed for SHBS-IR-791 iodide, which can be attributed to the new structure of SHBS-IR-791 iodide which now is a conjugated benzene ring containing group. In general, these changes in the FTIR spectrum of

SHBS-IR-791 iodide confirm the successful attachment of the benzoxasulfonic acid sodium. In IR-780 iodide and SHBS-IR-791 iodide, the FTIR spectra displayed several bands at 1505 cm-1, 1404 cm-1, 1240-1250 cm-1, and 1088–500 cm-1, which are indicative of –NH, C-H, -C=N, -C-H, and C-C of the carbocyanine structure.

4.4. Scanning electron microscope and Energy Dispersive Spectroscopy

4.4.1. Scanning electron microscope of ZnO-NPs and ZnO-NFs

The general morphologies of as-synthesized ZnO-NPs and ZnO-NFs were examined using SEM, and EDX was used to establish the presence of elements in the materials. Images in **Figure 4.10 (a)** and **(b)** depict the morphology of ZnO-NFs at 20, 00 KX and 50, 00 KX magnifications, respectively, while **Figure 4.10 (c)** shows the obtained EDX spectrum of ZnO-NFs. Images in **Figure 4.10 (d)** and **(e)** show the morphology of ZnO-NPs at x11 000 and x18 000 magnifications, respectively, while **Figure 4.10 (f)** shows the obtained EDX spectrum of ZnO-NPs. The samples in powder form were attached to carbon tape, and coated with gold before the morphological study was conducted.
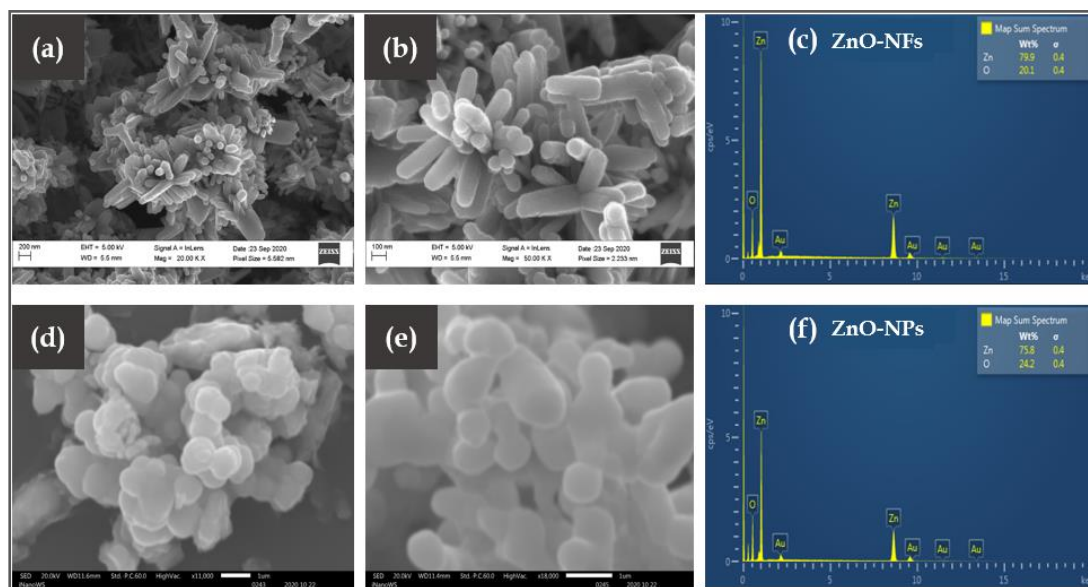
Figure 4.10: Scanning electron microscope and Energy Dispersive Spectra of ZnO-NFs and ZnO-NPs. **(a)** and **(b)** shows the images of ZnO-NFs at different magnifications, while (**c**) represents the EDX spectrum of ZnO-NFs of ZnO-NFs. **(d)**

and **(e)** shows the images of ZnO-NPs at different magnifications, while **(f)** represents the EDX spectrum of ZnO-NPs.

Images **(a)** and **(b)** show flower-like shapes made of nanorods. The nanorods lined up in a circular pattern from the centre outward to form a flower-like shape. The tips of the nanorods appear to be smoothly curved. Image **(c)** presents the EDX of ZnO-NFs that shows the presence of zinc (Zn) and oxygen (O), which leads to the conclusion that the zinc oxide nanoflowers were successfully synthesized and obtained.

Images **(d)** and **(e)** show well-formed agglomerated particles; Aggregation may have happened as a result of charge screening and cation bridging effects. Electrostatic and London attractive forces act on nanoparticles when they approach one other (181). Image **(f)** presents the EDX of ZnO-NPs that shows the presence of zinc (Zn) and oxygen (O). Image **(f)** also shows the presence of Au, which shows the presence of gold. Referring to the presence of gold, it could be attributed to the coating process, as the samples were coated with gold before examination using SEM. Nonetheless, it is conclusive that the ZnO-NPs were successfully synthesized.

4.4.2. Scanning electron microscope of GSH-ZnO-NPs and GSH-ZnO-NFs

The GSH-ZnO-NPs and GSH-ZnO-NFs samples were also analysed using the low-resolution SEM, and the images are shown in **Figure 4.11**. To reduce the agglomeration, the samples were dispersed on the glass slide. The morphology of both GSH-ZnO-NPs and GSH-ZnO-NFs was observed using JEOL SEM IT 300 operated between 15 kV and 20 kV. Methanol was used to disperse samples of GSH-ZnO-NPs and GSH-ZnO-NFs, and each sample was attached to the glass slide in drops. The samples were allowed to dry before being gold-plated. Images **(a)** and **(b)** depict the morphology of GSH-ZnO-NFs at x4, 000 and x22, 000 magnifications, respectively, while image **(c)** shows the obtained EDX spectrum of GSH-ZnO-NFs. Images **(d)** and **(e)** show the morphology of GSH-ZnO-NPs at x4, 300 and x22, 000 magnifications,

while image **(f)** shows the obtained EDX spectrum of GSH-ZnO-NPs. Lastly, images **(g)** and **(h)** are of the used glass slide.
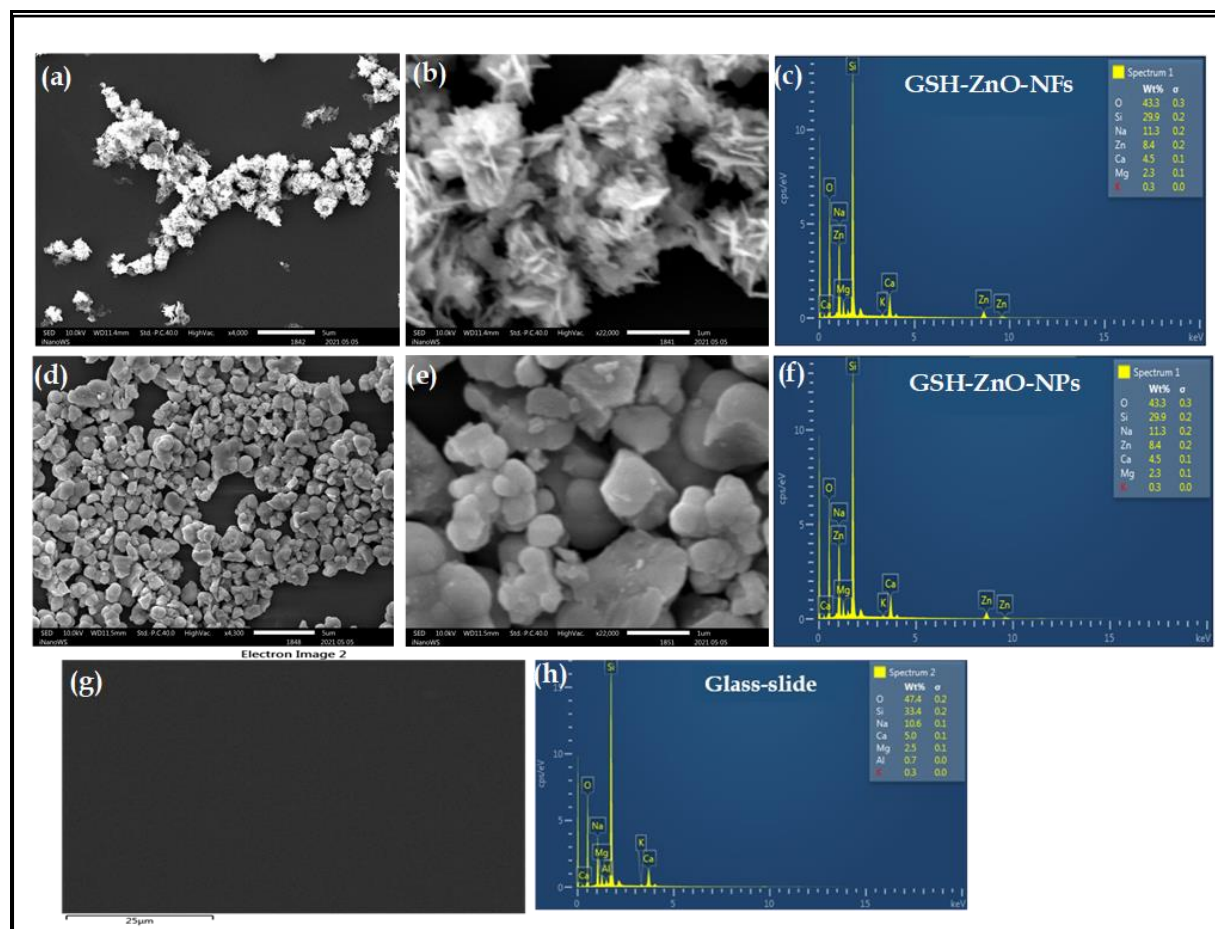
Figure 4.11: Scanning electron microscope and Energy Dispersive Spectroscopy results of GSH-ZnO-NFs, GSH-ZnO-NPs, and glass-slide. **(a)** and **(b)** depict different magnifications of GSH-ZnO-NFs and **(c)** shows EDX spectrums of GSH-ZnO-NFs. **(d)** and **(e)** depict different magnifications of GSH-ZnO-NPs and **(f)** shows EDX spectrum of GSH-ZnO-NPs.

The flower-like morphology is still visible in images **(a)** and **(b)**. Furthermore, images **(d)** and **(e)** show particle morphology, indicating that the morphology of the samples did not change. The new elemental compositions are shown in images **(c)** and **(f)**, which are EDX spectra of GSH-ZnO-NFs and GSH-ZnO-NPs. The unexpected elemental composition monitored in images **(c)** and **(f)** can be concluded that they are

from the glass slide, as the clean glass slide was analysed, and the outcomes are shown in the image **(h)**. Also, the literature (150) reports that the observed extra elemental composition is most commonly found on the glass surface.

4.4.3. Scanning electron microscope of GSH-ZnO-NMs-SHBS-IR-791 iodide

The general morphologies of GSH-ZnO-NPs-SHBS-IR-791 iodide and GSH-ZnO-NFs-SHBS-IR-791 iodide were examined using the JEOL FE-SEM. All the samples were carried out in powder form. The goal was to observe if the morphology would change or remain the same. **Figure 4.12** Images **(a)** and **(b)** present the GSH-ZnO-NFs-SHBS-IR-791 iodide at magnifications at x10, 000 and x30, 000, respectively, while images **(c)** and **(d)** depict the GSH-ZnO-NPs-SHBS-IR-791 iodide at magnifications at x20, 000 and x30, 000, respectively.
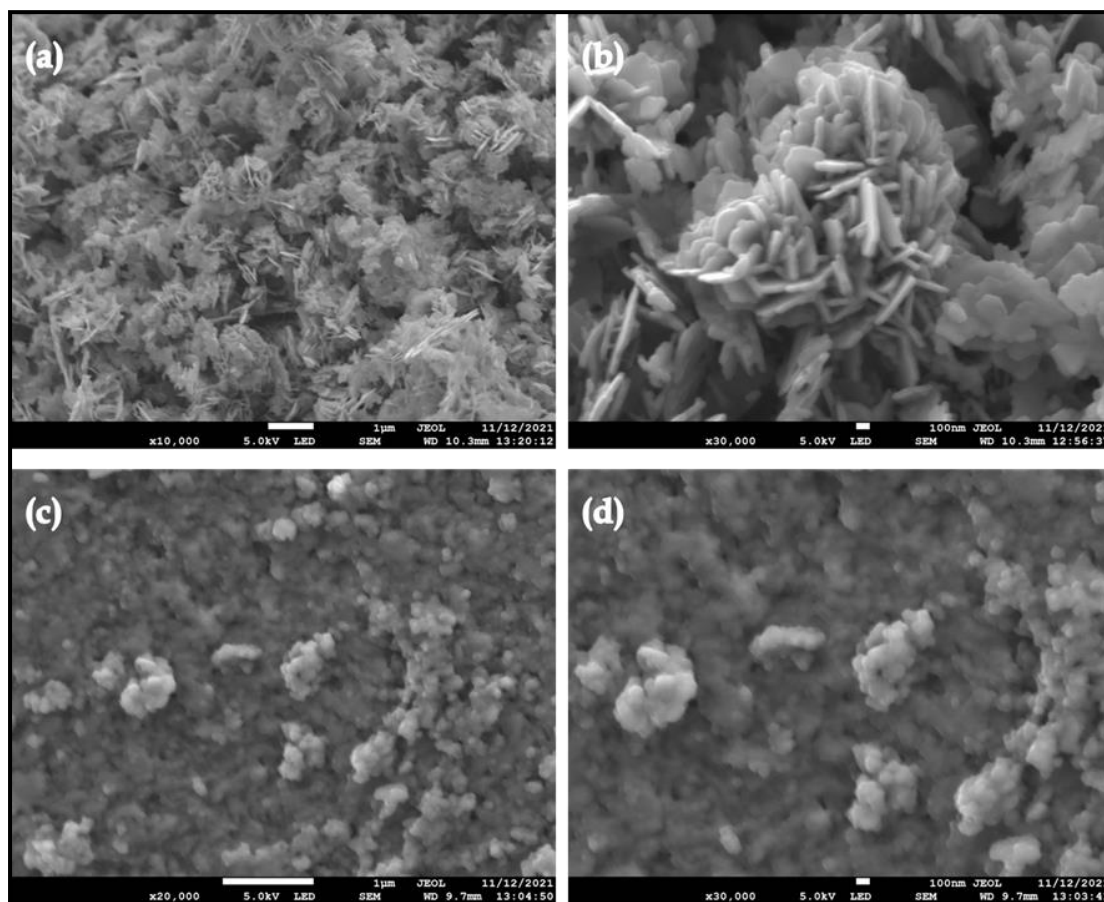
Figure 4.12: Scanning electron microscope images GSH-ZnO-NFs-SHBS-IR-791 iodide and GSH-ZnO-NPs-SHBS-IR-791 iodide. **(a)** and **(b)** show the images of GSH-ZnO-

NFs-SHBS-IR-791 iodide at different magnifications while **(c)** and **(d)** depict the images of GSH-ZnO-NPs-SHBS-IR-791 iodide also at different magnifications.

Images in **Figure 4.12 (a)** and **(b)** show that the morphology still depicts the nanoflowers. However, the flower shapes differ from those presented in **Figure 4.10 and Figure 4.11**. Images in **Figure 4.12 (a)** and **(b)** show the flower-like shapes made up of plate-like structures (nanoplates). The changes are a result of the conjugation of SHBS-IR-791 iodide in the nanocomposites. Images in **Figure 4.12 (c)** and (**d**) indicate agglomeration in GSH-ZnO-NFs-SHBS-IR-791 iodide at different magnifications. According to the literature (182), nanoparticles have a strong, attractive interaction with one another due to their high surface area per unit volume, resulting in a high aggregation or agglomeration tendency. Furthermore, agglomeration might be linked to the surface tautness of the solvent employed, which draws the particles composed through the drying course (183).

4.5. X-ray diffraction (XRD) analysis

4.5.1. X-ray diffraction spectra of ZnO-NPs and ZnO-NFs

The XRD patterns of the ZnO-NPs, ZnO-NFs, GSH-ZnO-NPs and GSH-ZnO-NFs are shown below in **Figure 4.13**. Using monochromatic X-rays, X-ray powder diffraction patterns were acquired in the angular range of 20°-80° with a step size of 0.01°. All reflections in the XRD patterns indicate that ZnO-NPs, ZnO-NFs, GSH-ZnO-NPs and GSH-ZnO-NFs possessed the zinc oxide blend structural patterns, and they matched well with PDXL.
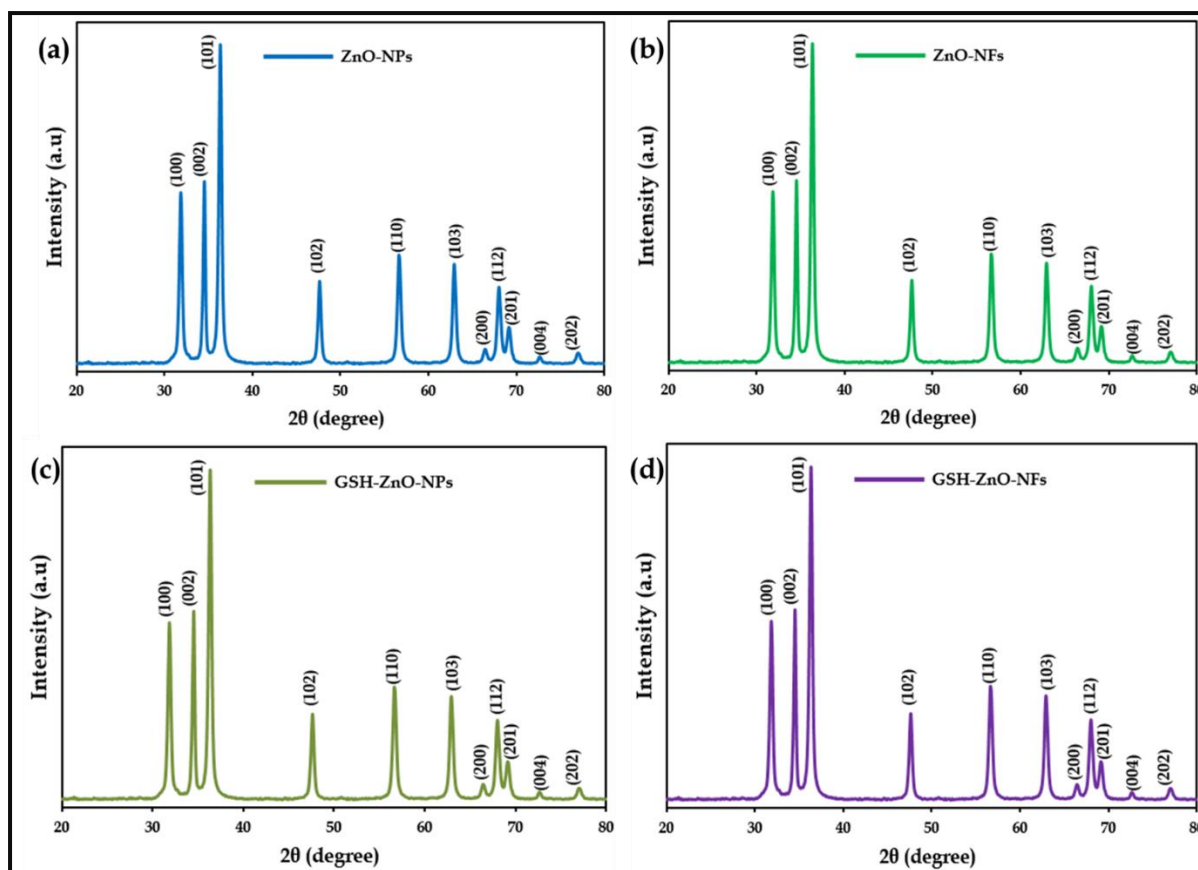
Figure 4.13: X-ray diffractogram **(a)** X-ray diffractogram of ZnO-NPs, **(b)** X-ray diffractogram of ZnO-NFs, **(c)** X-ray diffractogram of GSH-ZnO-NPs and **(d)** X-ray diffractogram of GSH-ZnO-NFs.

All the diffraction peaks of the samples displayed structural patterns nature with 2θ peaks at (100), (002), (101), (102), (110), (103), (200), (112), (201), (004) and (202) planes of the hexagonal ZnO structure. No other peaks were observed in all the functionalized and un-functionalized ZnO-NPs and ZnO-NFs samples. As evident from **Figure 4.1**, all the observed diffractions are well matched with the Wurtzite hexagonal phase of ZnO (Zincite; space group P63mc), and the obtained spectra are aligned with the reported JCPDS data file of 79-0208 (184).

4.5.2. X-ray diffraction spectra of GSH-ZnO-NPs-SHBS-IR-791 iodide and GSH-ZnO-NFs-SHBS-IR-791 iodide

XRD was also used to study the structural patterns of the GSH-ZnO-NFs-SHBS-IR-791 iodide, and GSH-ZnO-NPs-SHBS-IR-791 iodide are presented in **Figure 4.14** below. The X-ray diffractograms were recorded in the angular range of 25°–80° with a step size of 0.01° using monochromatic X-rays.
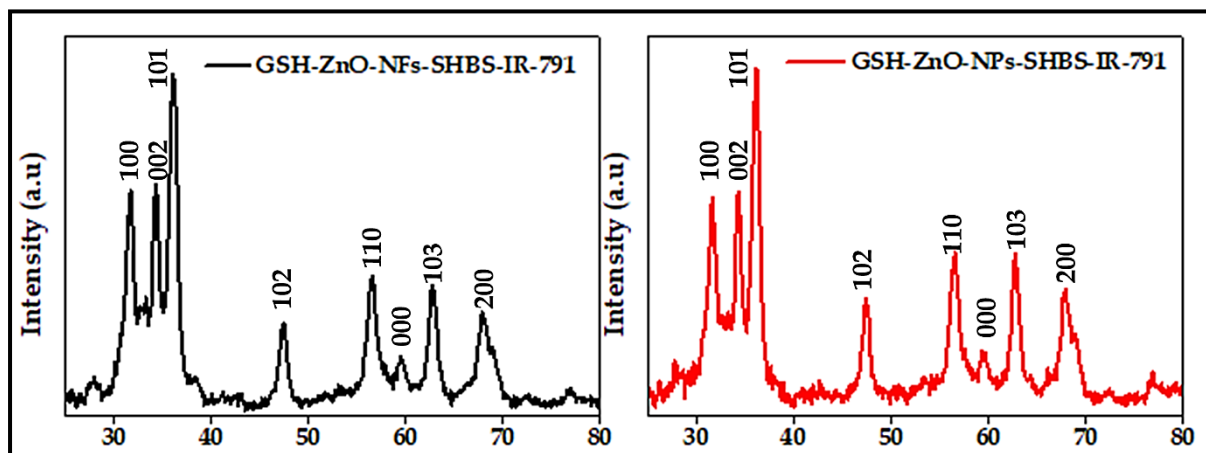
Figure 4.14: X-ray diffractogram of **(a)** GSH-ZnO-NFs-SHBS-IR-791 iodide and **(b)** GSH-ZnO-NPs-SHBS-IR-791 iodide.

The reflection GSH-ZnO-NFs-SHBS-IR-791 iodide and GSH-ZnO-NPs-SHBS-IR-791 iodide in XRD readings display patterns nature with 2θ peaks at (100), (002), (101), (102), (110), (103), and (200), GSH-ZnO-NPs-SHBS-IR-791 iodide and GSH-ZnO-NFs-SHBS-IR-791 iodide present slight differences; the slight change can be attributed to the presence of SHBS-IR-791 iodide in a GSH-ZnO-NPs-SHBS-IR-791 iodide and GSH-ZnO-NFs-SHBS-IR-791 iodide complexes. Most of the observed intensity peaks are well matched with the Wurtzite hexagonal phase of ZnO, which proves that ZnO can be detected in the complex.

Chapter 5

5. Photodynamic antimicrobial chemotherapy (PACT) studies

PACT, as indicated in the introduction, is mechanistically similar to photodynamic therapy (PDT), which uses singlet oxygen and photon (light at a certain wavelength). (93,94). Singlet oxygen has been shown to react with intercellular molecules such as peptides, DNA, and proteins, causing oxidative damage to the cell wall and membrane and ultimately leading to cell death (185). The literature has also reported that Gram-negative bacteria are more drug-resistant than Gram-positive bacteria (185,186). This is because the cell walls of Gram-negative bacteria, such as *E.coli*, consist of an outer membrane with a size-selective porin, an inner phospholipid, an outer negatively charged lipopolysaccharide (LPS), and a thin peptidoglycan layer (12).

The cationic complexes such as carbocyanines may electrostatically interact with the Gram-negative bacteria layer (LPS layer) (187). In this study, IR-780 iodide nanoconjugates (GSH-ZnO-NPs-SHBS-IR-791 iodide, GSH-ZnO-NFs-SHBS-IR-791 iodide) together with their modified complexes (GSH-ZnO-NFs, GSH-ZnO-NPs, and SHBS-IR-791 iodide) were studied against *E. coli*. There are two commonly used methods for calculating bacterial populations: the standard (viable plate count) and spectrophotometric (turbidimetric) methods. Because the technique includes diluting a sample with phosphate buffer diluent until the bacteria are dilute enough to count effectively, the cell biomass can be reliably measured.

5.1. Antimicrobial studies

PACT studies were performed in water and 2% DMF, whereby all the samples were fully soluble after the sonication. The *E. coli* cells were pre-treated using Ethylenediaminetetraacetic acid (EDTA) to prevent biofilms. The reported procedure includes the use of 96 well-plate and the lightbox. The cell survival of the microbes was subjected to a dark and light environment. The following equation (**Eq-1**) was employed to quantify the percentage of cell viability.

$$\text{Cell viability (\%)} = \frac{\text{absorbance of sample}}{\text{absorbance of control}} \times 100 \qquad\qquad \textbf{Eq-1}$$

Cell viability is measured by the proportion of live, healthy cells within a population. This method is commonly employed to determine the overall health of cells, optimize culture or experimental conditions, and measure cell survival following treatment with compounds, such as during a drug screen (188). In this study, the photodynamic antimicrobial activities of modified carbocyanine (SHBS-IR-791 iodide), functionalized zinc oxide-based nanomaterials (GSH-ZnO-NFs, GSH-ZnO-NPs), and carbocyanine nanoconjugates (GSH-ZnO-NPs-SHBS-IR-791 iodide and GSH-ZnO-NFs-SHBS-IR-791 iodide) are studied against *E. coli*, and the obtained outcomes are expressed in details below.
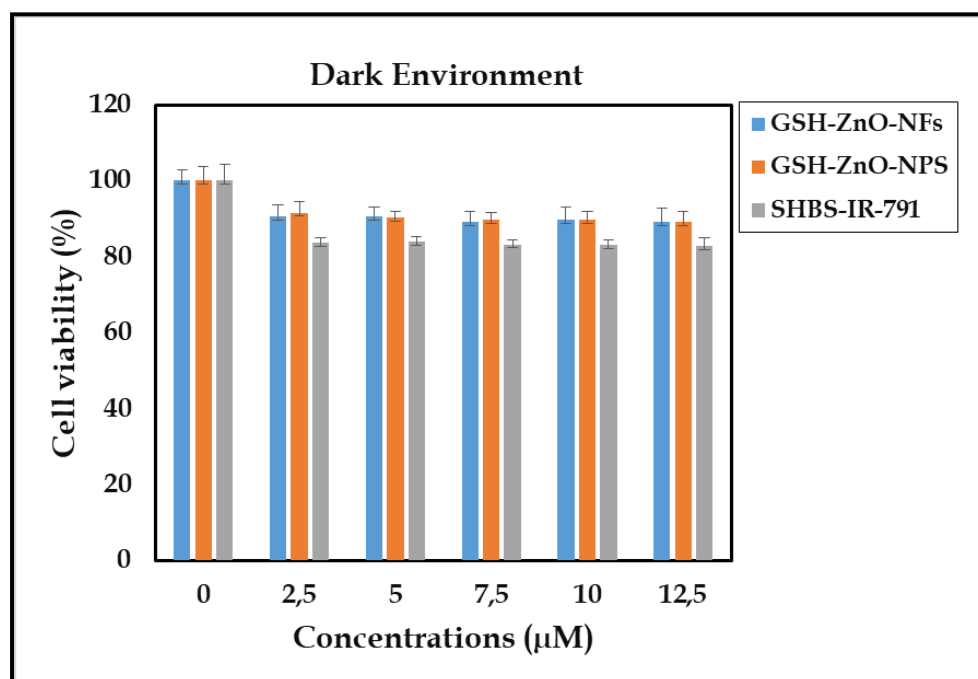
Figure 5.1: Photodynamic inactivation efficiency of various materials (GSH-ZnO-NFs, GSH-ZnO-NPs and SHBS-IR-791 iodide) against *E. coli* in a dark environment over 5 minutes.

The inactivation of *E. coli* with the above-mentioned materials was carried out at various concentrations (0µM, 2.5µM, 5µM, 7.5µM, 10µM, 12.5 µM) at similar irradiance

times. To ensure that the inactivation of *E. coli* was caused exclusively by the introduction of light in the PACT investigation, the experiment was also conducted in the dark to monitor the complexes' dark toxicity. **Figures 5.1** and **5.2** indicate that the complexes had very little effect on *E. coli* denaturation. **Figure 5.1** depicts the dark toxicity studies of GSH-ZnO-NFs, GSH-ZnO-NPs, and SHBS-IR-791 iodide, while **Figure 5.2** depicts the dark toxicity studies of GSH-ZnO-NPs-SHBS-IR-791 iodide and GSH-ZnO-NPs-SHBS-IR-791 iodide against **E. coli**.
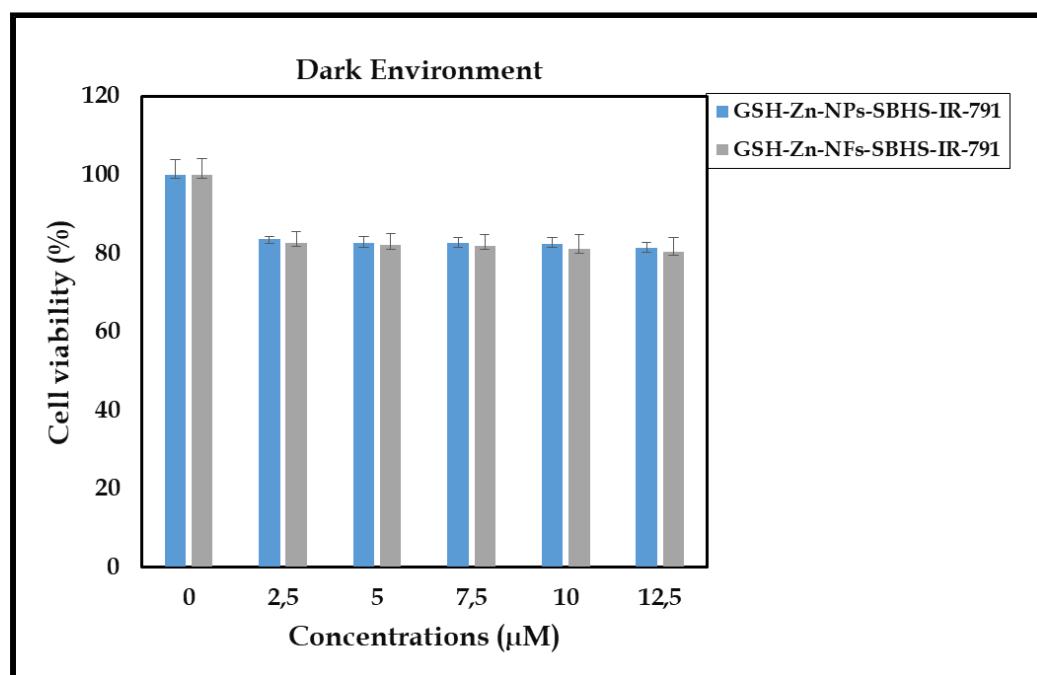
Figure 5.2: Photodynamic inactivation efficiency of GSH-ZnO-NPs-SHBS-IR-791 iodide and GSH-ZnO-NFs-SHBS-IR-791 iodide against *E. coli* in a dark environment over 5 minutes.

In the first PACT experiment under light exposure, modified materials (GSH-ZnO-NFs, GSH-ZnO-NPs, and SHBS-IR-791 iodide) were studied to observe their toxicity and compared with their nanoconjugates (GSH-ZnO-NPs-SHBS-IR-791 iodide and GSH-ZnO-NPs-SHBS-IR-791 iodide). **Figure 5.3** presents the PACT activity of GSH-ZnO-NFs, GSH-ZnO-NPs and SHBS-IR-791 iodide, whereas **Figure 5.4** presents the PACT activity of GSH-ZnO-NPs-SHBS-IR-791 iodide and GSH-ZnO-NPs-SHBS-IR-791 iodide against *E. coli* in a light exposure over 5 minutes.
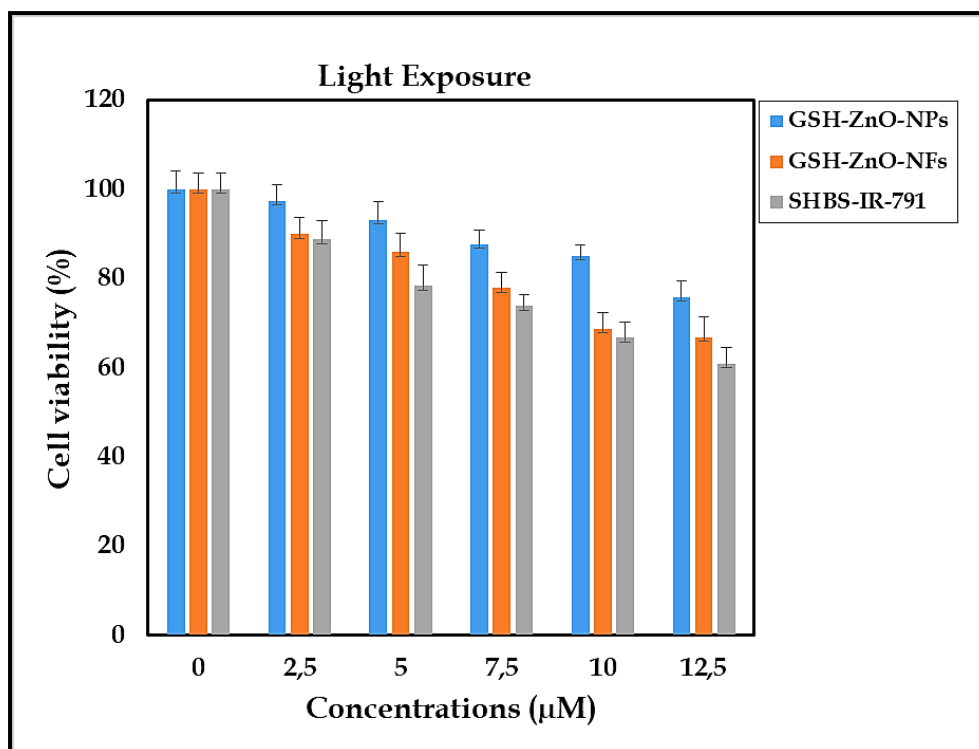
Figure 5.3: Photodynamic inactivation efficiency of GSH-ZnO-NPs, GSH-ZnO-NFs, and SHBS-IR-791 iodide against *E. coli* at different concentrations in a light exposure over a period of 5 minutes.

The outcomes show that cell reduction occurs, and the rate of cell reduction increases as complex concentrations increase in all samples. **Figure 5.3** shows that SHBS-IR-791 iodide has higher toxicity as compared to GSH-ZnO-NPs and GSH-ZnO-NFs. According to the literature, an ideal photosensitizer should have a high absorption coefficient and be able to reach a high quantum yield of triplet formation. Thus, in this comparison, SHBS-IR-791 iodide has a high absorption coefficient and can reach a high quantum yield of triplet formation compared to GSH-ZnO-NPs and GSH-ZnO-NFs. Nonetheless, GSH-ZnO-NPs and GSH-ZnO-NFs also showed phototoxicity against *E. coli*, which was consistent with the literature, which stated that ZnO-based materials have a high potential for inducing the generation of reactive oxygen species (ROS) when exposed to light (189).
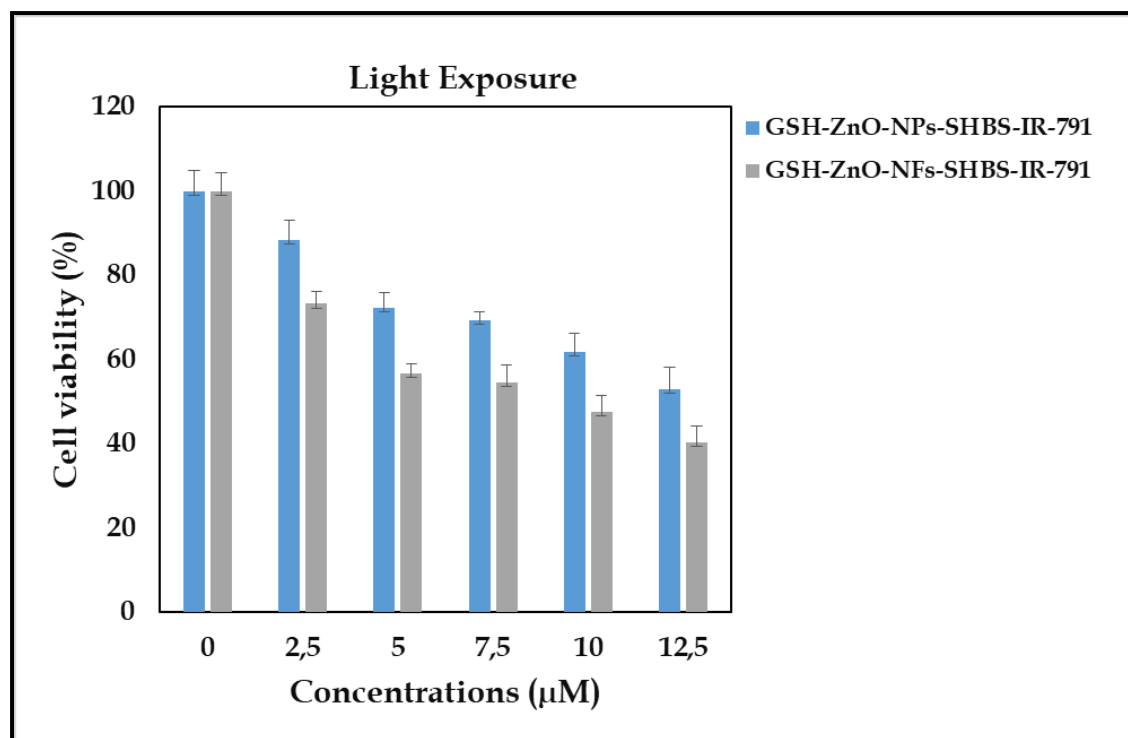
Figure 5.4: PACT PSs concentration optimization for complexes of GSH-ZnO-NPs-SHBS-IR-791 iodide and GSH-ZnO-NPs-SHBS-IR-791 iodide against *E. coli* in a light exposure over 5 minutes.

Figure 5.4 shows that GSH-ZnO-NFs-SHBS-IR-791 iodide has higher phototoxicity than GSH-ZnO-NPs-SHBS-IR-791 iodide, which tells that GSH-ZnO-NFs-SHBS-IR-791 iodide generated more reactive oxygen species than GSH-ZnO-NPs-SHBS-IR-791 iodide. The distinction between GSH-ZnO-NFs-SHBS-IR-791 iodide and GSH-ZnO-NPs-SHBS-IR-791 iodide is that the former is composed of nanoflowers, whereas the latter is composed of nanoparticles.

According to the literature (190), nanoflowers are made up of several layers of petals to cover a larger surface area in a small structure. Also, the zinc oxide nanoflowers (ZnO-NFs) revealed a greater number of adsorption sites, which can help with drug delivery by transporting a large number of drug samples. Thus, GSH-ZnO-NFs-SHBS-IR-791 iodide carries a larger number of SHBS-IR-791 iodide molecules and results in the better production of ROS. Hence the observed difference in photo-inactivation efficiency of GSH-ZnO-NFs-SHBS-IR-791 iodide and GSH-ZnO-NPs-SHBS-IR-791 iodide.

GSH-ZnO-NFs-SHBS-IR-791 iodide and GSH-ZnO-NPs-SHBS-IR-791 iodide are more effective against *E. coli* than SHBS-IR-791 iodide alone. According to the literature (191), the presence of nanomaterials in photosensitizers improves the efficiency of ROS production. As a result, the presence of ZnO-nanostructured materials conjugated with SHBS-IR-791 iodide may have improved the efficiency of SHBS-IR-791 iodide in producing ROS when exposed to light.

Chapter 6

6.   Conclusions and future recommendations

This study focused on microbial treatment using an emerging method, namely photodynamic antimicrobial chemotherapy (PACT). The mentioned method was chosen due to its promising characteristics, such as denaturing the cell without inducing resistance to the method. The study also describes the successful synthesis of ZnO-NPs and ZnO-NPs, the functionalization of ZnO-NPs and ZnO-NPs to form GSH-ZnO-NPs and GSH-ZnO-NFs, respectively, the modification of IR-780 iodide to form SHBS-IR-791 iodide, and finally the conjugation of GSH-ZnO-NPs and GSH-ZnO-NFs with SHBS-IR-791 iodide complex. All the as-prepared samples were characterised using various instruments. The structural and compositional properties of GSH-ZnO-NPs-SHBS-IR-791 iodide, GSH-ZnO-NFs-SHBS-IR-791 iodide, GSH-ZnO-NFs, GSH-ZnO-NPs, and SHBS-IR-791 iodide show that the expected results were successfully obtained. FT-IR shows the nanomaterials' expected chemical compositions and the optical properties obtained in UV-Vis spectroscopy. The XRD diffractograms of the analysed samples show the structural pattern characteristics of zinc oxide, which was also expected due to the presence of zinc oxide in the nanoconjugates. Based on the obtained data, it can be inferred that all of the predicted materials were effectively synthesized. The project aimed to study the PACT activities of the above-mentioned complexes against *E. coli* and all the obtained results are presented in this paper. The obtained results show that all the complexes have a toxicity effect in the presence of light. However, referring to the literature review, the phototoxicity effects vary among the complexes. The results show that the GSH-ZnO-NFs-SHBS-IR-791 iodide sample was more toxic, followed by ZnO-NPs-SHBS-IR-791 iodide and SHBS-IR-791 iodide.

Future recommendations. Silver oxide is one of the compounds recognized to have exceptional antibacterial capabilities. The research can be broadened to investigate the efficacy of silver oxide nanoparticles when combined with modified carbocyanine to generate nanoconjugates. The microbiological toxicity of the generated nanoconjugates can then be investigated using the PACT technique against E. coli.

7.   References

1.   Sattley WM, Madigan MT. Microbiology. Res Gate. 2015;(August):1–10.

2.   Zion National Park. What is a Microorganism? Introduction to Microorganisms. Zion Natl Park [Internet]. 2014;8. Available from: https://www.nps.gov/common/uploads/teachers/lessonplans/WhatisaMicroorganismActivityGuide.pdf

3.   Anjum N, Maqsood S, Masud T, Ahmad A, Sohail A, Momin A. Lactobacillus acidophilus: Characterization of the Species and Application in Food Production. Crit Rev Food Sci Nutr. 2014;54(9):1241–51.

4.   Bull M, Plummer S, Marchesi J, Mahenthiralingam E. The life history of Lactobacillus acidophilus as a probiotic: A tale of revisionary taxonomy, misidentification and commercial success. FEMS Microbiol Lett. 2013;349(2):77–87.

5.   Mohanna MT. Morphology and Classification of Bacteria. ResearchGate. 2016;(April):225–38.

6.   Investigations US for M. Identification of Campylobacter species. Public Heal Engl. 2018;(3.1):1–24.

7.   Yulo PRJ, Hendrickson HL. The evolution of spherical cell shape; progress and perspective. Biochem Soc Trans. 2019;47(6):1621–34.

8.   Lakna. Difference Between Gram Positive and Gram Negative Bacteria Stunning images of cells Discover how scientists use Main Difference – Gram Positive vs Gram Negative Bacteria. Pediaa. 2017;(April):13.

9.   Mai-Prochnow A, Clauson M, Hong J, Murphy AB. Gram positive and Gram negative bacteria differ in their sensitivity to cold plasma. Sci Rep [Internet]. 2016;6(December):1–11. Available from: http://dx.doi.org/10.1038/srep38610

10.   Liu Y, Qin R, Zaat SAJ, Breukink E, Heger M. Antibacterial photodynamic therapy: overview of a promising approach to fight antibiotic-resistant

References

bacterial infections. J Clin Transl Res. 2015;1(03):140–67.

11.   Yamasaki. 基因的改变NIH Public Access. Bone [Internet]. 2014;23(1):1–7. Available from: https://www.ncbi.nlm.nih.gov/pmc/articles/PMC3624763/pdf/nihms41272 8.pdf

12.   Silhavy TJ, Kahne D, Walker S. The Bacterial Cell Envelope. Cold Spring Harb Perspect Biol [Internet]. 2010;2(5):1–16. Available from: https://www.ncbi.nlm.nih.gov/pmc/articles/PMC2857177/pdf/cshperspect-PRK-a000414.pdf

13.   Bintsis T. Foodborne pathogens. AIMS Microbiol. 2017;3(3):529–63.

14.   Ramírez-Castillo FY, Loera-Muro A, Jacques M, Garneau P, Avelar-González FJ, Harel J, et al. Waterborne pathogens: Detection methods and challenges. Pathogens. 2015;4(2):307–34.

15.   Kaye KS, Pogue JM. Infections Caused by Resistant Gram-Negative Bacteria: Epidemiology and Management. Pharmacotherapy. 2015;35(10):949–62.

16.   Al Bshabshe A, Al-Hakami A, Alshehri B, Al-Shahrani KA, Alshehri AA, Al Shahrani MB, et al. Rising Klebsiella pneumoniae Infections and Its Expanding Drug Resistance in the Intensive Care Unit of a Tertiary Healthcare Hospital, Saudi Arabia. Cureus. 2020;12(8).

17.   Braz VS, Melchior K, Moreira CG. Escherichia coli as a Multifaceted Pathogenic and Versatile Bacterium. Front Cell Infect Microbiol. 2020;10(December):1–9.

18.   Maloy SR. E. coli: Good, bad, & deadly. Research Gate. 2011;(November 2011):1–17.

19.   Katouli M. Population structure of gut Escherichia coli and its role in development of extra-intestinal infections. Iran J Microbiol. 2010;2(2):59–72.

20.   Caselli E. Hygiene : microbial strategies to reduce pathogens and drug

resistance in clinical settings. John Wiley Sons Ltd Soc Appl Microbiol. 2017;10:1079–83.

21.　Wilson APR, Livermore DM, Otter JA, Warren RE, Jenks P, Enoch DA, et al. Prevention and control of multi-drug-resistant Gram-negative bacteria: Recommendations from a Joint Working Party. J Hosp Infect [Internet]. 2016;92(March 2015):S1–44. Available from: http://dx.doi.org/10.1016/j.jhin.2015.08.007

22.　Kirchman DL, Malmstrom RR, Cottrell MT. Control of bacterial growth by temperature and organic matter in the Western Arctic. Deep Res Part II Top Stud Oceanogr. 2005;52(24–26):3386–95.

23.　Francy DS, Stelzer EA, Brady AMG, Huitger C, Bushon RN, Ip HS, et al. Comparison of Filters for Concentrating Microbial Indicators and Pathogens in Lake Water Samples. J Am Soc Microbiol. 2013;79(4):1342–52.

24.　Munir MT. Control of Foodborne Biological Hazards by Ionizing Radiations. Multidiscip Digit Publ Inst. 2020;878(9):1–23.

25.　Russell AD. Mechanisms of antimicrobial action of antiseptics and disinfectants: An increasingly important area of investigation. J Antimicrob Chemother. 2002;49(4):597–9.

26.　Hutchings M, Truman A, Wilkinson B. Antibiotics: past, present and future. Curr Opin Microbiol [Internet]. 2019;51(Figure 1):72–80. Available from: https://doi.org/10.1016/j.mib.2019.10.008

27.　PORRITT AE. The discovery and development of penicillin. In: Royal society of chemistry. 1999. p. 1–10.

28.　Russell AD. Lethal effects of heat on bacterial physiology and structure. SAGE journals. 2003;86(05):115–37.

29.　Lumen. Using Physical Methods to Control Microorganisms | Microbiology [Internet]. Microbiology. 2020. Available from: https://courses.lumenlearning.com/microbiology/chapter/using-physical-

References

methods-to-control-microorganisms/

30. Shafiei Y, Razavilar V, Javadi A. Thermal death time of Staphylococcus aureus (PTCC=29213) and Staphylococcus epidermidis (PTCC=1435) in distilled water. Aust J Basic Appl Sci. 2011;5(11):1551–4.

31. Phillips KN, Godwin CM, Cotner JB. The Effects of Nutrient Imbalances and Temperature on the Biomass Stoichiometry of Freshwater Bacteria. Front Microbiol. 2017;8(SEP):1–11.

32. Gounot A -M. Bacterial life at low temperature: physiological aspects and biotechnological implications. J Appl Bacteriol. 1991;71(5):386–97.

33. Panikov NS, Flanagan PW, Oechel WC, Mastepanov MA, Christensen TR. Microbial activity in soils frozen to below -39°c. Soil Biol Biochem. 2006;38(4):785–94.

34. Shapiro RS, Cowen LE. Thermal control of microbial development and virulence: Molecular mechanisms of microbial temperature sensing. MBio. 2012;3(5):1–6.

35. Msarah MJ, Yusoff MFM, Samion SNS, Prabhakaran P, Ibrahim I, Aqma WS. Extreme environment: Biofilms and microbial diversity. Malays J Microbiol. 2018;14(5):435–43.

36. Ebrahimi A, Csonka LN, Alam MA. Analyzing Thermal Stability of Cell Membrane of Salmonella Using Time-Multiplexed Impedance Sensing. Biophys J [Internet]. 2018;114(3):609–18. Available from: https://doi.org/10.1016/j.bpj.2017.10.032

37. Gorji M, Bagherzadeh R, Fashandi H. Electrospun nanofibers in protective clothing [Internet]. Electrospun Nanofibers. Elsevier Ltd.; 2017. 571–598 p. Available from: http://dx.doi.org/10.1016/B978-0-08-100907-9.00021-0

38. ARE JAHW. P Articulate a Ir P Ollution and M Ortality — C Learing the a Ir. N Engl J Med. 2000;343:24.

References

39. Wu CC, Ghosh S, Martin KJ, Pinto AJ, Denef VJ, Olson TM, et al. The microbial colonization of activated carbon block point-of-use (PoU) filters with and without chlorinated phenol disinfection by-products. Environ Sci Water Res Technol [Internet]. 2017;3(5):830–43. Available from: http://dx.doi.org/10.1039/C7EW00134G

40. Wu CC, Love NG, Olson TM. Bacterial transmission and colonization in activated carbon block (ACB) point-of-use (PoU) filters. Environ Sci Water Res Technol. 2021;7(6):1114–24.

41. Konradt N, Kuhlen JG, Hobby R, Rohns H. Removal of Organic Contaminants by Reverse Osmosis and Granular Activated Removal of Organic Contaminants by Reverse Osmosis and Granular Activated Carbon in Drinking Water Treatment. Res Gate. 2018;(May):1–5.

42. GERALD MCDONNELL, RUSSELL AAD. Antiseptics and Disinfectants: Activity, Action, and Resistance. Clin Microbiol Rev. 1999;12(1):147–79.

43. Potts M. Desiccation tolerance : a simple process ? TRENDSin Microbiol. 2001;9(11):553–9.

44. Bordoloi R. Freeze-drying technique and its wide application in biomedical and pharmaceutical sciences. Res J Chem Environ Sci. 2014;2(06):1–5.

45. Soltani A, Sinclair TR. Soil water. Model Physiol Crop Dev growth yield. 2012;161–9.

46. Blair JMA, Webber MA, Baylay AJ, Ogbolu DO, Piddock LJ V. Molecular mechanisms of antibiotic resistance. Nat Rev Microbiol [Internet]. 2015;13(1):42–51. Available from: http://dx.doi.org/10.1038/nrmicro3380

47. Thomann WR. Chemical Safety in Animal Care, Use, and Research. ILAR J. 2003;44(1):13–9.

48. Ingraham A, Fleischer TM. Disinfectants in Laboratory Animal Science : What Are They and Who Says They Work ? Pharmacal Res Lab. 2003;32(1):36–40.

References

49. Skelley J. Open source tactics: Bargaining Power for strategic litigation. J Intellect Prop. 2016;16(1):1–35.

50. Lumen. Physical Antimicrobial Control | Boundless Microbiology [Internet]. courses.lumenlearning.com. 2016. Available from: https://courses.lumenlearning.com/boundless-microbiology/chapter/physical-antimicrobial-control/

51. Organization WH. WHO Report on Surveillance of Antibiotic Consumption [Internet]. Who. 2016. 128 p. Available from: https://apps.who.int/iris/bitstream/handle/10665/277359/9789241514880-eng.pdf

52. Gaynes R. The discovery of penicillin—new insights after more than 75 years of clinical use. Emerg Infect Dis. 2017;23(5):849–53.

53. Aminov RI. A brief history of the antibiotic era: Lessons learned and challenges for the future. Front Microbiol. 2010;1(DEC):1–7.

54. Rajeev L. Antibiotic Discovery. Vol. 8, Materials and Methods. 2018.

55. Norton L, Myers A. The treatment of streptococcal tonsillitis/pharyngitis in young children. World J Otorhinolaryngol - Head Neck Surg [Internet]. 2021;7(3):161–5. Available from: https://doi.org/10.1016/j.wjorl.2021.05.005

56. Ong DSY, Kuyvenhoven MM, Van dijk L, Verheij TJM. Antibiotics for respiratory, ear and urinary tract disorders and consistency among GPs. J Antimicrob Chemother. 2008;62(3):587–92.

57. Davoudi-Kiakalayeh A, Mohammadi R, Pourfathollah AA, Siery Z, Davoudi-Kiakalayeh S. Alloimmunization in thalassemia patients: New insight for healthcare. Int J Prev Med. 2017;8:1–16.

58. Prestinaci F, Pezzotti P, Pantosti A. Antimicrobial resistance: A global multifaceted phenomenon. Pathog Glob Health [Internet]. 2015;109(7):309–18. Available from: http://dx.doi.org/10.1179/2047773215Y.0000000030

References

59. Byrne MK, Miellet S, McGlinn A, Fish J, Meedya S, Reynolds N, et al. The drivers of antibiotic use and misuse: The development and investigation of a theory driven community measure. BMC Public Health. 2019;19(1):1–11.

60. C Reygaert W. An overview of the antimicrobial resistance mechanisms of bacteria. AIMS Microbiol. 2018;4(3):482–501.

61. Alarcon A, Omenaca F. Antimicrobial Resistance in Escherichia coli Sepsis. Pediatr Infect Dis J. 2004;23(10):979–80.

62. Davies J. Origins and evolution of antibiotic resistance. Microbiologia. 1996;12(1):9–16.

63. Ayukekbong JA, Ntemgwa M, Atabe AN. The threat of antimicrobial resistance in developing countries: Causes and control strategies. Antimicrob Resist Infect Control. 2017;6(1):1–8.

64. Llor C, Bjerrum L. Antimicrobial resistance: Risk associated with antibiotic overuse and initiatives to reduce the problem. Ther Adv Drug Saf. 2014;5(6):229–41.

65. Shih MH, Huang FC. Repetitive methylene blue-mediated photoantimicrobial chemotherapy changes the susceptibility and expression of the outer membrane proteins of Pseudomonas aeruginosa. Photodiagnosis Photodyn Ther [Internet]. 2013;10(4):664–71. Available from: http://dx.doi.org/10.1016/j.pdpdt.2013.07.003

66. Cassidy CM, Donnelly RF, Tunney MM. Effect of sub-lethal challenge with Photodynamic Antimicrobial Chemotherapy (PACT) on the antibiotic susceptibility of clinical bacterial isolates. J Photochem Photobiol B Biol [Internet]. 2010;99(1):62–6. Available from: http://dx.doi.org/10.1016/j.jphotobiol.2010.02.004

67. Bartolomeu M, Rocha S, Cunha Â, Neves MGPMS, Faustino MAF, Almeida A. Effect of photodynamic therapy on the virulence factors of Staphylococcus aureus. Front Microbiol. 2016;7(MAR):1–11.

References

68. Urrutia MN, Alovero FL, Ortiz CS. New azine compounds as photoantimicrobial agents against Staphylococcus aureus. Dye Pigment [Internet]. 2015;116:27–35. Available from: http://dx.doi.org/10.1016/j.dyepig.2014.12.021

69. Managa ME. Photodynamic antimicrobial chemotherapy activities of porphyrin- and phthalocyanine-platinum nanoparticle conjugates. 2014.

70. Rajesh S, Koshi E, Philip K, Mohan A. Antimicrobial photodynamic therapy: An overview. J Indian Soc Periodontol. 2011;15(4):323–7.

71. Polat E, Kang K. Natural photosensitizers in antimicrobial photodynamic therapy. Biomedicines. 2021;9(6):1–30.

72. Nastri L, Donnarummal G, Porzio C, Gregorioi VDE, Tufano MAI, Caruso F, et al. EFFECTS OF TOLUIDINE BLUE-MEDIATED PHOTODYNAMIC THERAPY ON PERIOPATHOGENS AND PERIODONTAL BIOFILM : IN VITRO EVALUATION Department ofStomatologic Orthodontic and Surgical Sciences , Second University ofNaples , Naples ; ' Department ofExperimental Medicin. Int J Immunopathol Pharmacol. 2010;23(4):1125–32.

73. Yoon I, Li JZ, Shim YK. Advance in photosensitizers and light delivery for photodynamic therapy. Clin Endosc. 2013;46(1):7–23.

74. Paul DSK. Physical and Chemical Agents for Microbial Control. 2013. p. 1–64.

75. Zhao J, Wu W, Sun J, Guo S. Triplet photosensitizers: From molecular design to applications. Chem Soc Rev. 2013;42(12):5323–51.

76. Berg K, Selbo PK, Weyergang A, Dietze A, Prasmickaite L, Bonsted A, et al. Porphyrin-related photosensitizers for cancer imaging and therapeutic applications. J Microsc. 2005;218(2):133–47.

77. Dube E, Nwaji N, Oluwole DO, Mack J, Nyokong T. Journal of Photochemistry and Photobiology A : Chemistry Investigation of photophysicochemical properties of zinc phthalocyanines conjugated to metallic nanoparticles. "Journal Photochem Photobiol A Chem [Internet]. 2017;349:148–61. Available

References

from: https://doi.org/10.1016/j.jphotochem.2017.09.020

78. Dube E, Oluwole DO, Nwaji N, Nyokong T. Spectrochimica Acta Part A : Molecular and Biomolecular Spectroscopy Glycosylated zinc phthalocyanine-gold nanoparticle conjugates for photodynamic therapy : Effect of nanoparticle shape. Spectrochim Acta Part A Mol Biomol Spectrosc [Internet]. 2018;203:85–95. Available from: https://doi.org/10.1016/j.saa.2018.05.081

79. Cho JJ, Stewart JM, Drashansky TT, Brusko MA, Zuniga AN, Lorentsen KJ, Keselowsky BG ADA antigen-specific semi-therapeutic treatment with local delivery of tolerogenic factors through a dual-sized microparticle system blocks experimental autoimmune encephalomyelitis. B 2017 O-92. doi: 10. 1016/j. biomaterials. 2. 乳鼠心肌提取 HHS Public Access. Physiol Behav. 2016;176(1):139–48.

80. Tada DB, Baptista MS. Photosensitizing nanoparticles and the modulation of ROS generation. Front Chem. 2015;3(MAY):1–14.

81. Lin S, Liu C, Han X, Zhong H, Cheng C. Viral nanoparticle system: An effective platform for photodynamic therapy. Int J Mol Sci. 2021;22(4):1–15.

82. Qi M, Chi M, Sun X, Xie X, Weir MD, Oates TW, et al. Novel nanomaterial-based antibacterial photodynamic therapies to combat oral bacterial biofilms and infectious diseases. Int J Nanomedicine. 2019;14:6937–56.

83. Escudero A, Carrillo-Carrión C, Castillejos MC, Romero-Ben E, Rosales-Barrios C, Khiar N. Photodynamic therapy: Photosensitizers and nanostructures. Mater Chem Front. 2021;5(10):3788–812.

84. Stasheuski AS, Galievsky VA, Stupak AP, Dzhagarov BM, Choi MJ, Chung BH, et al. Photophysical Properties and Singlet Oxygen Generation Efficiencies of Water-Soluble Fullerene Nanoparticles. Photochem Photobiol. 2014;90(5):997–1003.

85. De Simone BC, Mazzone G, Russo N, Sicilia E, Toscano M. Metal atom effect on the photophysical properties of Mg(II), Zn(II), Cd(II), and Pd(II)

tetraphenylporphyrin complexes proposed as possible drugs in photodynamic therapy. Multidiscip Digit Publ Inst. 2017;22(7):1–10.

86.   Samanta PK, Kim D, Coropceanu V, Brédas JL. Up-Conversion Intersystem Crossing Rates in Organic Emitters for Thermally Activated Delayed Fluorescence: Impact of the Nature of Singlet vs Triplet Excited States. J Am Chem Soc. 2017;139(11):4042–51.

87.   Arja K. Multimodal Porphyrin-Based Conjugates: Synthesis and characterization for applications as amyloid ligands, photodynamic therapy agents and chiroptical materials. Vol. 5. 2018.

88.   Maldonado-Carmona N, Ouk TS, Calvete MJF, Pereira MM, Villandier N, Leroy-Lhez S. Conjugating biomaterials with photosensitizers: Advances and perspectives for photodynamic antimicrobial chemotherapy. Photochem Photobiol Sci. 2020;19(4):445–61.

89.   Anas A, Sobhanan J, Sulfiya KM, Jasmin C, Sreelakshmi PK, Biju V. Advances in photodynamic antimicrobial chemotherapy. J Photochem Photobiol C Photochem Rev [Internet]. 2021;49(August):100452. Available from: https://doi.org/10.1016/j.jphotochemrev.2021.100452

90.   Wainwright M, Maisch T, Nonell S, Plaetzer K, Almeida A, Tegos GP, et al. Photoantimicrobials—are we afraid of the light? Lancet Infect Dis. 2017;17(2):49–55.

91.   Daniell MD, Hill J. A HISTORY OF PHOTODYNAMIC THERAPY. AustNZ J Surg. 1991;61:340–8.

92.   Kessel D. Photodynamic therapy: A brief history. J Clin Med. 2019;8(10).

93.   Spikes JD. The origin and meaning of the term "photodynamic" (as used in "photodynamic therapy", for example). J Photochem Photobiol B Biol. 1991;9(3–4):369–71.

94.   Williams KJ. The introduction of "chemotherapy" using arsphenamine - The first magic bullet. J R Soc Med. 2009;102(8):343–8.

References

95. K. Sharma S, Dai T, B. Kharkwal G, Huang Y-Y, Huang L, J. Bil De Arce V, et al. Drug Discovery of Antimicrobial Photosensitizers Using Animal Models. Curr Pharm Des. 2012;17(13):1303–19.

96. Dhingra S, Rahman NAA, Peile E, Rahman M, Sartelli M, Hassali MA, et al. Microbial Resistance Movements: An Overview of Global Public Health Threats Posed by Antimicrobial Resistance, and How Best to Counter. Front Public Heal. 2020;8(November):1–22.

97. Felipe F Sperandio, Ying-Ying Huang and MRH. Antimicrobial Photodynamic Therapy to Kill Gram-negative Bacteria. Recent patents Antiinfect Drug Discov. 2013;8(2):108–120.

98. Gottenbos B, Grijpma DW, Van Der Mei HC, Feijen J, Busscher HJ. Antimicrobial effects of positively charged surfaces on adhering Gram-positive and Gram-negative bacteria. J Antimicrob Chemother. 2001;48(1):7–13.

99. Tedesco AC, Primo FL, de Jesus P da CC. Antimicrobial Photodynamic Therapy (APDT) Action Based on Nanostructured Photosensitizers [Internet]. Multifunctional Systems for Combined Delivery, Biosensing and Diagnostics. Elsevier Inc.; 2017. 9–29 p. Available from: http://dx.doi.org/10.1016/B978-0-323-52725-5/00002-2

100. Ghorbani J, Rahban D, Aghamiri S, Teymouri A, Bahador A. Photosensitizers in antibacterial photodynamic therapy: An overview. Laser Ther. 2018;27(4):293–302.

101. Skwor TA, Klemm S, Zhang H, Schardt B, Blaszczyk S, Bork MA. Photodynamic inactivation of methicillin-resistant Staphylococcus aureus and Escherichia coli: A metalloporphyrin comparison. J Photochem Photobiol B Biol [Internet]. 2016;165:51–7. Available from: http://dx.doi.org/10.1016/j.jphotobiol.2016.10.016

102. Scholz E, Heinrich M, Hunkler D. and their Antimicrobial Activity. Planta Med. 1990;56(06):648–648.

References

103. Ion R-M. Porphyrins and Phthalocyanines: Photosensitizers and Photocatalysts. In: Phthalocyanines and Some Current Applications. 2017. p. 189–221.

104. Marmarchi F. The Utilization of Alternative Synthetic Methods for Further Optimization of Cyanine Dyes and their Potential Use in Imaging and Photodynamic Therapy. Sch @ Georg State Univ. 2018;1–189.

105. Levitz A, Holder C, Soriano E, Henary M. "Turn on" fluorescence response of monomethine cyanines caused by noncovalent binding to ct-DNA. Dye Pigment [Internet]. 2017;145:202–7. Available from: http://dx.doi.org/10.1016/j.dyepig.2017.05.051

106. Gragg JL. Synthesis of Near-Infrared Heptamethine Cyanine Dyes. Sch @ Georg State Univ Chem. 2010;1–119.

107. Ptaszek M. Rational design of fluorophores for in vivo applications [Internet]. 1st ed. Vol. 113, Progress in Molecular Biology and Translational Science. Elsevier Inc.; 2013. 59–108 p. Available from: http://dx.doi.org/10.1016/B978-0-12-386932-6.00003-X

108. Simpson WT. Electronic states of organic molecules. J Chem Phys. 1948;16(12):1124–36.

109. Thavornpradit S, Usama SM, Park GK, Shrestha JP, Nomura S, Baek Y, et al. QuatCy: A heptamethine cyanine modification with improved characteristics. Theranostics. 2019;9(10):2856–67.

110. Meggers WF, Stimson FJ. Dyes for Photographic Sensitizing. J Opt Soc Am. 1920;4(3):91.

111. Sun C, Du W, Wang B, Dong B, Wang B. Research progress of near - infrared fluorescence probes based on indole heptamethine cyanine dyes in vivo and in vitro. BMC Chem [Internet]. 2020;14(21):1–28. Available from: https://doi.org/10.1186/s13065-020-00677-3

112. Xu Y, Liu Y, Qian X. Novel cyanine dyes as fluorescent pH sensors: PET, ICT

mechanism or resonance effect? J Photochem Photobiol A Chem. 2007;190(1):1–8.

113. Levitz A, Ladani ST, Hamelberg D, Henary M. Synthesis and effect of heterocycle modification on the spectroscopic properties of a series of unsymmetrical trimethine cyanine dyes. Dye Pigment. 2014;105:238–49.

114. Henary M, Levitz A. Synthesis and applications of unsymmetrical carbocyanine dyes. Dye Pigment [Internet]. 2013;99(3):1107–16. Available from: http://dx.doi.org/10.1016/j.dyepig.2013.08.001

115. Yin CX. Fluorescent Probes for Reactive Oxygen Species [Internet]. Second Edi. Vol. 8, Comprehensive Supramolecular Chemistry II. Elsevier; 2017. 401–421 p. Available from: http://dx.doi.org/10.1016/B978-0-12-803198-8.12620-3

116. Lange N, Szlasa W, Saczko J, Chwiłkowska A. Potential of cyanine derived dyes in photodynamic therapy. Pharmaceutics. 2021;13(6):1–17.

117. Semenova O, Kobzev D, Yazbak F, Nakonechny F, Kolosova O, Tatarets A, et al. Unexpected effect of iodine atoms in heptamethine cyanine dyes on the photodynamic eradication of Gram-positive and Gram-negative pathogens. Dye Pigment [Internet]. 2021;195(July):109745. Available from: https://doi.org/10.1016/j.dyepig.2021.109745

118. Semenova O, Kobzev D, Yazbak F, Nakonechny F, Kolosova O, Tatarets A, et al. Unexpected effect of iodine atoms in heptamethine cyanine dyes on the photodynamic eradication of Gram-positive and Gram-negative pathogens. Dye Pigment [Internet]. 2021;195(July):1–11. Available from: https://doi.org/10.1016/j.dyepig.2021.109745

119. Cooper E, Choi PJ, Denny WA, Jose J, Dragunow M, Park TI. The Use of Heptamethine Cyanine Dyes as Drug-Conjugate Systems in the Treatment of Primary and Metastatic Brain Tumors. Front Oncol. 2021;11(June):1–16.

120. Gowsalya K, Yasothamani V, Vivek R. Nanoscale Advances nanocarriers for multimodal cancer therapy : R Soc Chem. 2021;3:3332–52.

References

121. Ara ES, Noghreiyan AV, Sazgarnia A. Photodiagnosis and Photodynamic Therapy Evaluation of photodynamic effect of Indocyanine green (ICG) on the colon and glioblastoma cancer cell lines pretreated by cold atmospheric plasma. Photodiagnosis Photodyn Ther [Internet]. 2021;35(April):102408. Available from: https://doi.org/10.1016/j.pdpdt.2021.102408

122. Semenova O, Kobzev D, Yazbak F, Nakonechny F, Kolosova O, Tatarets A, et al. Unexpected effect of iodine atoms in heptamethine cyanine dyes on the photodynamic eradication of Gram-positive and Gram-negative pathogens. Dye Pigment [Internet]. 2021;195(August):109745. Available from: https://doi.org/10.1016/j.dyepig.2021.109745

123. Huang B, Wang L, Tang K, Chen S, Xu Y, Liao H, et al. IR780 Based Sonotherapeutic Nanoparticles to Combat Multidrug-Resistant Bacterial Infections. Front Chem. 2022;10(January):1–10.

124. Guan M, Chu G, Jin J, Liu C, Cheng L, Guo Y, et al. A Combined Cyanine/Carbomer Gel Enhanced Photodynamic Antimicrobial Activity and Wound Healing. Nanomaterials. 2022;12(13):1–14.

125. Prakash AV, Yazabak F, Hovor I, Nakonechny F, Kulyk O, Semenova O, et al. Highly efficient near-IR cyclohexene cyanine photosensitizers for antibacterial photodynamic therapy. Dye Pigment [Internet]. 2023;211(December 2022):111053. Available from: https://doi.org/10.1016/j.dyepig.2022.111053

126. Ilina K, Henary M. Cyanine Dyes Containing Quinoline Moieties: History, Synthesis, Optical Properties, and Applications. Chem - A Eur J. 2021;27(13):4230–48.

127. Levitz A, Marmarchi F, Henary M. Introduction of various substitutions to the methine bridge of heptamethine cyanine dyes: Via substituted dianil linkers. Photochem Photobiol Sci. 2018;17(10):1409–16.

128. Yadav Y, Levitz A, Dharma S, Aneja R, Henary M. Effects of heterocyclic N-alkyl chain length on cancer cell uptake of near infrared heptamethine cyanine dyes. Dye Pigment [Internet]. 2017;145:307–14. Available from:

References

http://dx.doi.org/10.1016/j.dyepig.2017.06.016

129. Khan I, Saeed K, Khan I. Nanoparticles: Properties, applications and toxicities. Arab J Chem [Internet]. 2019;12(7):908–31. Available from: https://doi.org/10.1016/j.arabjc.2017.05.011

130. Dowling a, Clift R, Grobert N, Hutton D, Oliver R, O'neill O, et al. Nanoscience and nanotechnologies : opportunities and uncertainties. London R Soc R Acad Eng Rep [Internet]. 2004;46(July):618–618. Available from: http://scholar.google.com/scholar?hl=en&btnG=Search&q=intitle:Nanoscience+and+nanotechnologies+:+opportunities+and+uncertainties#0

131. Carvalho APA, Conte-Junior CA. Recent Advances on Nanomaterials to COVID-19 Management: A Systematic Review on Antiviral/Virucidal Agents and Mechanisms of SARS-CoV-2 Inhibition/Inactivation. Glob Challenges. 2021;5(5):2000115.

132. Yoon Y, Truong PL, Lee D, Ko SH. Metal-Oxide Nanomaterials Synthesis and Applications in Flexible and Wearable Sensors. Am Chem Soc Nanosci. 2021;1–29.

133. Chavali MS, Nikolova MP, Silver A. Metal oxide nanoparticles and their applications in nanotechnology. SN Appl Sci [Internet]. 2019;1(6):1–30. Available from: https://doi.org/10.1007/s42452-019-0592-3

134. Fontecha-Umaña F, Ríos-Castillo AG, Ripolles-Avila C, Rodríguez-Jerez JJ. Antimicrobial activity and prevention of bacterial biofilm formation of silver and zinc oxide nanoparticle-containing polyester surfaces at various concentrations for use. Foods. 2020;9(4).

135. Chen L, Huang J, Li X, Huang M, Zeng S, Zheng J, et al. Progress of Nanomaterials in Photodynamic Therapy Against Tumor. Front Bioeng Biotechnol. 2022;10(May):1–28.

136. Yi C, Yu Z, Ren Q, Liu X, Wang Y, Sun X, et al. Nanoscale ZnO-based photosensitizers for photodynamic therapy. Photodiagnosis Photodyn Ther

[Internet]. 2020;30(December 2019):101694. Available from: https://doi.org/10.1016/j.pdpdt.2020.101694

137. Naveed A, Haq U, Nadhman A, Ullah I, Mustafa G, Yasinzai M, et al. Synthesis Approaches of Zinc Oxide Nanoparticles : The Dilemma of Ecotoxicity. Hindawi J Nanomater. 2017;2017:1–14.

138. Sabir S, Arshad M, Chaudhari SK. Zinc oxide nanoparticles for revolutionizing agriculture: Synthesis and applications. Sci World J. 2014;2014:1–8.

139. Bououdina M, Rashdan S, Bobet JL, Ichiyanagi Y. Nanomaterials for Biomedical Applications : Synthesis , Characterization , and Applications. J Nanomater. 2013;2013:1–4.

140. Suri SS, Fenniri H, Singh B. Nanotechnology-based drug delivery systems. J Occup Med Toxicol. 2007;6:1–6.

141. Prabu SL. Medicated Nanoparticle for Gene Delivery Medicated Nanoparticle for Gene Delivery. In: Advanced Technology for Delivering Therapeutics. 2017. p. 15–29.

142. Yin Zhang1, Tapas R. Nayak2, Hao Hong2 and WC. Biomedical Applications of Zinc Oxide Nanomaterials. NIH Public Access. 2014;13(10):1633–45.

143. Reuge N, Bacsa R, Serp P, Caussat B. Chemical Vapor Synthesis of Zinc Oxide Nanoparticles : Experimental and Preliminary Modeling Studies. J phys, Chem C. 2009;113(25):19845–52.

144. Chen D, Jiao X, Cheng G. Hydrothermal synthesis of zinc oxide powders with different morphologies. Solid State Commun. 1999;113(6):363–6.

145. Tseng Y, Chuang M, Chen Y, Wu C. Synthesis of 1D, 2D, and 3D ZnO Polycrystalline Nanostructures Using the Sol-Gel Method. J Nanobiotechnology. 2012;2012:1–8.

146. Jen-Chieh Lin a C-PL and K-CH. Zinc oxide synthesis via a microemulsion technique : morphology control with. j mater.chem. 2012;22:1270–3.

References

147. Kołodziejczak-radzimska A, Jesionowski T. Zinc Oxide — From Synthesis to Application: A Review. MDPI. 2014;7:2833–81.

148. Dimitriev Y, Gancheva M, Iordanova R. Synthesis of zno by mechanochemical decomposition of zinc carbonate hydroxide. J Univ Chem Technol Metall. 2011;46(3):243–8.

149. Ao W, Li J, Yang H, Zeng X, Ma X. Mechanochemical synthesis of zinc oxide nanocrystalline. Powder Technol. 2006;168(3):148–51.

150. Stanković A, Veselinović L, Škapin SD, Marković S, Uskoković D. Controlled mechanochemically assisted synthesis of ZnO nanopowders in the presence of oxalic acid. J Mater Sci. 2011;46(11):3716–24.

151. Mohan Kumar K, Mandal BK, Appala Naidu E, Sinha M, Siva Kumar K, Sreedhara Reddy P. Synthesis and characterisation of flower shaped Zinc Oxide nanostructures and its antimicrobial activity. Spectrochim Acta - Part A Mol Biomol Spectrosc [Internet]. 2013;104:171–4. Available from: http://dx.doi.org/10.1016/j.saa.2012.11.025

152. Mahato TH, Prasad GK, Singh B, Acharya J, Srivastava AR, Vijayaraghavan R. Nanocrystalline zinc oxide for the decontamination of sarin. J Hazard Mater. 2009;165(1–3):928–32.

153. Benhebal H, Chaib M, Salmon T, Geens J, Leonard A, Lambert SD, et al. Photocatalytic degradation of phenol and benzoic acid using zinc oxide powders prepared by the sol-gel process. Alexandria Eng J. 2013;52(3):517–23.

154. Vorobyova SA, Lesnikovich AI, Mushinskii V V. Interphase synthesis and characterization of zinc oxide. Mater Lett. 2004;58(6):863–6.

155. Aarthye P, Sureshkumar M. Green synthesis of nanomaterials: An overview. Mater Today Proc. 2021;47:907–13.

156. Guo W, Xu Z, Li T. Metal-based semiconductor nanomaterials for thin-film solar cells [Internet]. Multifunctional Photocatalytic Materials for Energy. Elsevier Ltd.; 2018. 153–185 p. Available from: https://doi.org/10.1016/B978-

References

0-08-101977-1.00009-0

157. Świątkowski A. Industrial carbon adsorbents. Stud Surf Sci Catal. 1999;120 A:69–94.

158. Haitham Ali Kadhem, Sumayah Abdulhussien Ibraheem, Majid Sakhi Jabir, Zainab Jihad Taqi, Mihailescu Dan Florin AAK. Nano Biomed Eng Zinc Oxide Nanoparticles Induces Apoptosis in Pathway. Nano Biomed Eng. 2019;11(1):35–43.

159. Ahmad F, Salem-bekhit MM, Khan F, Alshehri S, Khan A. Unique Properties of Surface-Functionalized Nanoparticles for Bio-Application : Functionalization Mechanisms and Importance in Application. MDPI. 2022;12:1–23.

160. Kuila T, Bose S, Mishra AK, Khanra P, Kim NH, Lee JH. Chemical functionalization of graphene and its applications. Prog Mater Sci [Internet]. 2012;57(7):1061–105. Available from: http://dx.doi.org/10.1016/j.pmatsci.2012.03.002

161. Thiruppathi R, Mishra S, Ganapathy M, Padmanabhan P, Gulyás B. Nanoparticle functionalization and its potentials for molecular imaging. Adv Sci. 2017;4(3).

162. Kanth PC, Verma SK, Gour N. Functionalized nanomaterials for biomedical and agriculture industries [Internet]. Handbook of Functionalized Nanomaterials for Industrial Applications. INC; 2020. 231–265 p. Available from: http://dx.doi.org/10.1016/B978-0-12-816787-8.00010-7

163. Li W, Li M, Qi J. Nano-drug design based on the physiological properties of glutathione. Molecules. 2021;26(18).

164. Arocikia Jency D, Parimaladevi R, Vasant Sathe G, Umadevi M. Glutathione Functionalized Gold Nanoparticles as Efficient Surface Enhanced Raman Scattering Substrate for Poly Chlorinated Biphenyl Detection. J Clust Sci [Internet]. 2018;29(2):281–7. Available from: https://doi.org/10.1007/s10876-

References

017-1323-9

165. Zhao C, Rehman FU, Jiang H, Selke M, Wang X, Liu C. Titanium dioxide-tetra sulphonatophenyl porphyrin nanocomposites for target cellular bio-imaging and treatment of rheumatoid arthritis. Sci China Chem. 2016;59(5):637–42.

166. Oyim J, Omolo CA, Amuhaya EK. Photodynamic Antimicrobial Chemotherapy: Advancements in Porphyrin-Based Photosensitize Development. Front Chem. 2021;9(April):1–15.

167. Cheng Y, Burda C. Nanoparticles for Photodynamic Therapy. Compr Nanosci Technol. 2011;1–5:1–28.

168. Shrestha A, Kishen A. Antibacterial Efficacy of Photosensitizer Functionalized Biopolymeric Nanoparticles in the Presence of Tissue Inhibitors in Root Canal. J Endod [Internet]. 2014;40(4):566–70. Available from: http://dx.doi.org/10.1016/j.joen.2013.09.013

169. Fekrazad R, Nejat AH, Kalhori KAM. Antimicrobial Photodynamic Therapy With Nanoparticles Versus Conventional Photosensitizer in Oral Diseases [Internet]. Vol. 4, Nanostructures for Antimicrobial Therapy: Nanostructures in Therapeutic Medicine Series. Elsevier Inc.; 2017. 237–259 p. Available from: http://dx.doi.org/10.1016/B978-0-323-46152-8.00010-X

170. Ma J, Ren W, Zhao J, Yang H. Growth of TiO 2 nano fl owers photoanode for dye-sensitized solar cells. J Alloy Compd J. 2017;692:1004–9.

171. Sun W, Yu H, Wang D, Li Y, Tian B, Zhu S. MnO2 nanoflowers as a multifunctional nano-plat- form for enhanced photothermal/photodynamic therapy and MR imaging†. R Soc Chem. 2021;(05):1–13.

172. Singh P, Kim YJ, Wang C, Mathiyalagan R, Yang DC. Microbial synthesis of Flower-shaped gold nanoparticles. Artif Cells, Nanomedicine, Biotechnol [Internet]. 2015;(04):1–6. Available from: http://dx.doi.org/10.3109/21691401.2015.1041640

173. Saif MS, Zafar A, Waqas M, Hassan SG, Haq A ul, Tariq T, et al. Phyto-

References

reflexive Zinc Oxide Nano-Flowers synthesis: An advanced photocatalytic degradation and infectious therapy. J Mater Res Technol [Internet]. 2021;13:2375–91. Available from: https://doi.org/10.1016/j.jmrt.2021.05.107

174. Joseph A, Praveen GL, Abha K, Lekha GM, George S. Photoluminescence study on amino functionalized dysprosium oxide – zinc oxide composite bifunctional nanoparticles. J Lumin [Internet]. 2012;132(8):1999–2004. Available from: http://dx.doi.org/10.1016/j.jlumin.2012.03.023

175. Kumar A, Arora S, Mogha N, Al-Deyab SS, Ansari ZA, Ansari SG. Glutathione Coated Zinc Oxide Nanoparticles: A Promising Material for Pesticide Detection. Energy Environ Focus. 2013;2(2):101–7.

176. Sekhosana KE, Amuhaya E, Nyokong T. Nonlinear optical behavior of neodymium mono- and bi-nuclear phthalocyanines linked to zinc oxide nanoparticles and incorporated into poly acrylic acid. Polyhedron [Internet]. 2016;105:159–69. Available from: http://dx.doi.org/10.1016/j.poly.2015.12.045

177. Pudukudy M, Yaakob Z. Facile Synthesis of Quasi Spherical ZnO Nanoparticles with Excellent Photocatalytic Activity. J Clust Sci. 2015;26(4):1187–201.

178. Kumar A, Rahman S, Kazim SN, Ansari ZA, Ansari SG. Application of Glutathione Coated ZnO Nanoparticles to Study the Oxidative Stress in Bacterial Cells. Mater Focus. 2013;2(2):148–54.

179. Kavita, Singh K, Kumar S, Bhatti HS. Glutathione-assisted synthesis of star-shaped zinc oxide nanostructures and their photoluminescence behavior. J Lumin [Internet]. 2014;149:112–7. Available from: http://dx.doi.org/10.1016/j.jlumin.2014.01.001

180. Poole LB. The Basics of Thiols and Cysteines in Redox Biology and Chemistry. Free Radic Biol Med [Internet]. 2015;80:148–57. Available from: http://dx.doi.org/10.1016/j.freeradbiomed.2014.11.013

181. Ul A, Khan H, Liu Y, Naidu R, Fang C. Environmental Technology &

References

Innovation Interactions between zinc oxide nanoparticles and hexabromocyclododecane in simulated waters. Environ Technol Innov [Internet]. 2021;24:1–14. Available from: https://doi.org/10.1016/j.eti.2021.102078

182. Zare Y, Yop K, Hui D. In fl uences of nanoparticles aggregation / agglomeration on the interfacial / interphase and tensile properties of nanocomposites. Compos Part B [Internet]. 2017;122:41–6. Available from: http://dx.doi.org/10.1016/j.compositesb.2017.04.008

183. Baruah S, Dutta ÆJ. Effect of seeded substrates on hydrothermally grown ZnO nanorods. J Sol-Gel Sci Technol. 2009;50:456–64.

184. Swanson H., Fuyat R. Standard X-ray Diffraction Powder Patterns UNITED STATES DEPARTMENT OF COMMERCE NATIONAL BUREAU OF STANDARDS. United states Dep Commer. 1953;Volume II:1–65.

185. Pizzino G, Irrera N, Cucinotta M, Pallio G, Mannino F, Arcoraci V, et al. Oxidative Stress: Harms and Benefits for Human Health. Oxid Med Cell Longev. 2017;2017.

186. Maisch T, Bosl C, Szeimies RM, Lehn N, Abels C. Photodynamic effects of novel XF porphyrin derivatives on prokaryotic and eukaryotic cells. Antimicrob Agents Chemother. 2005;49(4):1542–52.

187. Saji George†, a, Michael R. Hamblinb, c, d and AK. Uptake pathways of anionic and cationic photosensitizers into bacteria. Photochem Photobiol Sci. 2009;8(6):788–95.

188. Stoddart MJ. Mammalian Cell Viability: Methods and Protocols - Cell Viability Assays. In: Methods in Molecular Biology [Internet]. 2011. p. 1–6. Available from: http://link.springer.com/10.1007/978-1-61779-108-6

189. Yi C, Yu Z, Ren Q, Liu X, Wang Y, Sun X, et al. Nanoscale ZnO-based photosensitizers for photodynamic therapy. Photodiagnosis Photodyn Ther [Internet]. 2020;30:1–22. Available from:

References

https://doi.org/10.1016/j.pdpdt.2020.101694

190. Shende P, Kasture P, Gaud RS. Nanoflowers: the future trend of nanotechnology for multi-applications. Artif Cells, Nanomedicine Biotechnol [Internet]. 2018;46(1):413–22. Available from: https://doi.org/10.1080/21691401.2018.1428812

191. Tavakkoli Yaraki M, Liu B, Tan YN. Emerging Strategies in Enhancing Singlet Oxygen Generation of Nano-Photosensitizers Toward Advanced Phototherapy [Internet]. Vol. 14, Nano-Micro Letters. Springer Nature Singapore; 2022. 1–49 p. Available from: https://doi.org/10.1007/s40820-022-00856-y